Diss. ETH No. 21865

CONTRIBUTIONS TO MODEL-BASED CONTROL OF DIESEL ENGINES

A dissertation submitted to
ETH Zurich

to attain the degree of
Doctor of Sciences of ETH Zurich
(Dr. sc. ETH Zurich)

presented by

Stephan Zentner

MSc ETH in Mechanical Engineering
born on January 10, 1983
citizen of Germany

accepted on the recommendation of
Prof. Dr. Lino Guzzella, examiner
Prof. Dr. Rolf Johansson, co-examiner
Dr. Christoph Teetz, co-examiner

2014

Stephan Zentner
stephan.zentner@alumni.ethz.ch

ETH Zurich
Institute for Dynamic Systems and Control
Sonneggstrasse 3
8092 Zurich, Switzerland

Institute for Dynamic Systems and Control
IDSC
Institut für Dynamische Systeme und Regelungstechnik

Till min älskade Sara

Preface

This thesis is the result of the successful collaboration between the engine manufacturer MTU Friedrichshafen GmbH and the Institute for Dynamic Systems and Control (IDSC) at ETH Zurich. This was the first time our institutions joined forces, and I am grateful to Dr. Gerald Fast for seeking this collaboration. I would also like to thank him and Dr. Erika Schäfer for supporting the project both organizationally and technically, and for their company during numerous days at the test bench and the ensuing evenings. Moreover, I would like to thank Dr. Christoph Teetz (MTU) and Prof. Rolf Johansson (Lund University) for agreeing to be my co-examiners.

I would like to express my gratitude to Prof. Lino Guzzella for first sparking my interest in control systems and then giving me the opportunity to write this thesis under his supervision. His consistent encouragement to work harder and to focus my efforts helped me develop the skills necessary to conduct relevant research and to finish this project successfully.

Furthermore, I would like to thank Dr. Christoph Onder for his invaluable technical advice and for his support whenever the project didn't go according to plan. I also want to thank my colleagues from the IDSC. Their companionship and the countless breaks and team events were a refreshing relief from the hard work which more than once sparked a breakthrough idea. In particular, I would like to thank my former office mates and fellow members of the diesel team Jonas Asprion and Frédéric Tschanz for hours of sometimes meaningful, albeit always entertaining discussion.

Finally, I want to express my gratitude to my family and my fiancée Sara, who have supported me throughout the entire time. Without their backing I would not have succeeded.

February 2014

Stephan Zentner

Contents

Abstract

Due to their high fuel efficiency, diesel engines are used in a wide range of applications. However, they emit large amounts of harmful pollutants, such as nitrogen oxide (NO_x) and particulate matter (PM). In order to comply with increasingly stringent diesel-engine emission legislation while satisfying the customer demands for power, fuel efficiency, and comfort, the hardware used in diesel engines is becoming increasingly complex. This complexity introduces additional degrees of freedom, which create opportunities for optimization. Model-based strategies are necessary to control these degrees of freedom and to unlock the potential of complex hardware. This thesis contributes to the research field of model-based control of diesel engines by analyzing three different control problems.

In the first part of the thesis, air-path control is considered. The turbo charger(s) and the exhaust-gas recirculation (EGR) are responsible for supplying the gas mixture which is aspirated by the cylinders. Therefore they have a strong influence on the fuel consumption and the pollutant emissions. However, from a control point of view, they introduce disadvantageous plant properties, such as nonlinearities, cross-couplings and a sensitivity to disturbances. The air-path controller has to handle these problems while being applicable to a wide range of air-path configurations. A system analysis of the models of two engines of different size and air-path configuration is used to derive a generic control structure designed specifically to handle these problems. Its advantage compared to a conventional control structure is demonstrated in test bench experiments using these two engines.

In the second part of the thesis, the pollutant emissions (NO_x and PM) generated during transients are considered. During transients, the air-path controller cannot perfectly follow the reference trajectory, which can lead to the emission of significant amounts of pollutants. In order to influence these transient emissions, a model-based controller is developed, which adapts the fuel injection and the EGR during transients. It is shown

experimentally that there exists a trade-off between the transient pollutant emissions and the drivability of the engine. The proposed controller can be used to adjust this trade-off and to realize various transient operating strategies.
In the last part of the thesis, online optimal control of diesel engines is considered. The goal is to minimize the fuel consumption (i.e. the CO_2 emissions) while not exceeding an upper limit for the cumulated pollutant emissions (e.g. NO_x and PM) at the end of the cycle. In order to obtain the optimal solution, knowledge of the future operating conditions is required. However, such information is not available when carrying out an online optimization. In this thesis, a suboptimal causal approach to solve this inherently non-causal problem is proposed. A case study shows that the performance of the proposed causal approach is only marginally inferior to that of the non-causal optimal solution obtained by dynamic programming, while being applicable to online control.

Zusammenfassung

Aufgrund ihres hohen Wirkungsgrads werden Dieselmotoren in einer Vielzahl von Anwendungen eingesetzt. Sie stoßen aber große Mengen an Schadstoffen wie Stickstoffoxid (NO_x) und Partikel aus. Um stetig sinkende Grenzwerte für die Schadstoffemissionen einzuhalten und dem Kundenwunsch nach Leistung, Wirtschaftlichkeit und Komfort nachzukommen, wird der mechanische Aufbau von Dieselmotoren immer komplexer. Dadurch werden zusätzliche Freiheitsgrade, welche Optimierungspotenzial mit sich bringen, geschaffen. Es werden modellbasierte Regelungsstrategien benötigt, um diese Freiheitsgrade zu regeln und das Potenzial der komplexen Mechanik auszuschöpfen. Diese Arbeit trägt zum Forschungsgebiet der modellbasierten Regelung von Dieselmotoren bei, indem sie drei verschiedene Regelprobleme analysiert.
Der erste Teil der Arbeit befasst sich mit Luftpfadregelung. Die Aufgabe der Turbolader und der Abgasrückführung (AGR) ist es, das vom Zylinder angesaugte Gasgemisch bereitzustellen. Sie haben deswegen einen großen Einfluss auf den Kraftstoffverbrauch und die Emissionen des Motors. Sie bringen jedoch einige für die Regelung nachteilige Eigenschaften wie Nichtlinearität, Kreuzkopplungen und eine Empfindlichkeit auf Störungen mit sich. Der Luftpfadregler muss mit diesen Problemen umgehen können und gleichzeitig für viele verschiedene Luftpfadkonfigurationen einsetzbar sein. Aus einer Systemanalyse der Modelle von zwei verschieden großen Motoren mit verschiedenen Luftpfadkonfigurationen wird eine generische Reglerstruktur abgeleitet, welche gezielt mit diesen Problemen umgehen kann. Ihr Vorteil gegenüber einer gewöhnlichen Regelstruktur wird anhand dieser zwei Motoren am Prüfstand experimentell aufgezeigt.
Der zweite Teil der Arbeit befasst sich mit transienten Schadstoffemissionen (NO_x und Partikel). Während Transienten kann der Luftpfadregler dem Sollwert nicht perfekt folgen, was zum Ausstoß großer Mengen an Schadstoffen führen kann. Um diese transienten Emissionen beeinflussen zu können, wird ein modellbasierter Regler, welcher die Kraftstoffeinsprit-

zung und das AGR anpasst, entwickelt. Es wird in Experimenten gezeigt, daß ein Zielkonflikt zwischen den transienten Emissionen und der Fahrbarkeit des Motors besteht. Der hier vorgeschlagene Regler kann benutzt werden, um diesen Zielkonflikt einzustellen und verschiedene transiente Betriebsstrategien umzusetzen.

Der letzte Teil der Arbeit befasst sich mit der optimalen Regelung von Dieselmotoren in Echtzeit. Das Ziel hierbei ist die Minimierung des Kraftstoffverbrauchs (bzw. der CO_2 Emissionen) unter Einhaltung eines Grenzwertes für die kumulierten Schadstoffemissionen (z.B. NO_x und Partikel) am Ende des Zyklus. Um die optimale Lösung zu ermitteln, benötigt man Informationen über die zukünftigen Betriebszustände. Bei einer Optimierung in Echtzeit sind solche Informationen jedoch nicht verfügbar. In dieser Arbeit wird ein suboptimaler kausaler Ansatz für die Lösung dieses inhärent akausalen Problems vorgeschlagen. In einer Fallstudie wird aufgezeigt, daß dieser kausale Ansatz nur geringfügig schlechtere Resultate liefert als eine akausale Optimierung mit Dynamic Programming und daß er gleichzeitig für eine Optimierung in Echtzeit geeignet ist.

Nomenclature

List of symbols

C	Controller
H	Hamiltonian
$\widehat{H}$	Hamiltonian of the extended problem
J	Performance criterion
$\widetilde{J}$	Performance criterion of the (partially) dual formulation
$\widehat{J}$	Performance criterion of the extended problem
$\widehat{\mathcal{J}}$	Cost-to-go of the extended problem
K	Average CO_2 penalty for a given saving of a pollutant
K_{egr}	Proportional gain (EGR reduction)
K_I	Integral gain (input estimator)
K_P	Proportional gain (input estimator)
KS	Series compensator
L	Gain of error correction term (burnt-gas estimator)
L	Integrand of the performance criterion
$\widehat{L}$	Integrand of the extended performance criterion
L_e	Loop gain
N	Rotational speed
N	Total number of samples
P	Plant
P	Power
R	Ideal gas constant
S_e	Sensitivity of the loop gain
T	Final time
T	Torque

T_e	Complementary sensitivity of the loop gain
T_h	Time horizon for elimination of the emission-control error
T_{int}	Integration time
V	Volume
W	Work
a	Polynomial coefficient
$\boldsymbol{f}$	Function vector
m	Mass
$\overline{m}$	Brake-specific mass
$\overline{\boldsymbol{m}}$	Brake-specific mass vector
n	Number of emission species
n	Index of discrete-time model
p	Pressure
q	Order of the emission penalty
$\widehat{p}$	Calculated pressure (input estimator)
r	Reference value
t	Time
u	Input
$\boldsymbol{u}$	Input vector
x	Burnt-gas fraction
x	State variable
$\boldsymbol{x}$	State vector
$\widehat{x}$	Calculated burnt-gas fraction (estimator)
y	Output
Δ	Difference, error
α	Weighting parameter
$\widetilde{\alpha}$	EEMS tuning parameter
δ	Difference
η	Efficiency
ϑ	Temperature
λ	Normalized air-to-fuel ratio
λ	Co-state

$\boldsymbol{\lambda}$	Co-state vector
$\boldsymbol{\xi}$	State vector
σ_0	Stoichiometric air-to-fuel ratio
τ	Time
φ	Crank angle of injection
ω	Rotational speed, frequency

List of subscripts

ac	After combustion
bg	Burnt gas
bt	Between the turbines
c	Compressor
comb	Combustion
cyl	Cylinder
des	Desired
dp	Dynamic programming
e	Engine
egr	Exhaust-gas recirculation
em	Exhaust manifold
emis	Emission
eng	Engine
est	Estimated
ffw	Feed-forward
fut	Future
hp	High pressure
i	Index
im	Intake manifold
in	Inner loop
inj	Injected
lim	Limited
lp	Low pressure

max	Maximum
nom	Nominal
norm	Normalization
out	Outer loop
pen	Penalty
pred	Predicted
ref	Reference
ss	Steady-state
t	Turbine
tc	Turbo charger
vgt	Variable-geometry turbine
vol	Volumetric
wg	Waste gate
0	Initial condition
φ	Fuel

List of superscripts

o	Optimal

List of acronyms and abbreviations

AFR	Air-to-fuel ratio
AGR	Abgasrückführung
BSconst	Constant brake-specific reference emissions
CAD	Computer-aided design
CEF	Constant equivalent factor
CO_2	Carbon dioxide
Comp	Compressor(s)
Cyl	Cylinders
DP	Dynamic programming

DPF	Diesel particulate filter
ECU	Engine control unit
ECMS	Equivalent consumption minimization strategy
EEMS	Equivalent emission minimization strategy
EGA	Exhaust-gas aftertreatment
EGR	Exhaust-gas recirculation
EM	Exhaust manifold
FFW	Feed-forward
HCCI	Homogeneous charge compression ignition
HFM	Hot-film air-mass meter
HJB	Hamilton-Jacobi-Bellman
HP	High pressure
IM	Intake manifold
LNT	Lean NO_x trap
LP	Low pressure
LPV	Linear parameter-varying
LQR	Linear quadratic regulator
LTR	Loop-transfer recovery
MIMO	Multiple-input, multiple-output
MPC	Model-predictive control
NO_x	Nitrogen oxide
OPdep	Operating-point dependent reference emissions
PID	Proportional integral derivative (controller)
PI	Proportional integral (controller)
PM	Particulate matter
Pos.	Position
RGA	Relative gain array
SCR	Selective catalytic reduction
SISO	Single-input, single-output
S/KS/T	H_∞ design scheme
SOI	Start of injection
SSVGT	Single-stage, variable-geometry turbine

TC	Turbo charger(s)
TC Rot	Rotational dynamics of the turbo charger(s)
TSWG	Two-stage, waste gate
Turb	Turbine(s)
VGT	Variable-geometry turbine
WG	Waste gate
WHTC	World harmonized transient cycle
ic	Intercooler
inj	Fuel injection

Mathematical notation

$\dot{(\ )}$	Time derivative
$\overset{*}{(\ )}$	Flow
$(\ )^T$	Transposed
$(\ )_{\vert o}$	Evaluated using optimal inputs
$\nabla_{\boldsymbol{x}} f$	Standing gradient vector: $[\frac{\partial f}{\partial x_1} \dots \frac{\partial f}{\partial x_n}]^T$
$\frac{\partial f}{\partial \boldsymbol{x}}$	Lying gradient vector: $[\frac{\partial f}{\partial x_1} \dots \frac{\partial f}{\partial x_n}]$
$\min\limits_{\boldsymbol{u}(\cdot)}$	Optimization over the entire input trajectory

Chapter 1

Introduction

Today, almost 17% of the carbon dioxide (CO_2) emissions are caused by road transportation [1]. By 2035, the global number of road transport vehicles is expected to have almost doubled compared to 2009 [2]. Given the impact of carbon dioxide emissions on the climate [3] and the limited crude-oil resources [2], the fuel efficiency of engines has become more important than ever. Consequently, because of their high fuel efficiency, diesel engines are used in a wide range of applications.
The compliance with emission legislation while satisfying the customer demand for power, fuel efficiency, and comfort is one of the main challenges during the development of a diesel engine. It is achieved by a combination of advanced hardware and sophisticated control systems. The research presented in this thesis contributes to the development of the control systems which enable the operation of state-of-the-art diesel engines with low pollutant emissions. This chapter serves as an introduction to this topic. Section 1.1 provides an introduction to the hardware and the control systems of diesel engines. Sec. 1.2 summarizes the contribution, while Sec. 1.3 provides an outline of this thesis.

1.1 Introduction to diesel engines

Rudolf Diesel (1858-1913) presented the first working compression ignition engine in 1892. In contrast to previous engine technology, a liquid fuel was injected directly into the combustion chamber and ignited by the heat of the compressed air. This novel method avoided knock and was able to realize unprecedentedly high compression ratios, resulting in a doubling of the combustion efficiency compared to previous combustion engines [4].
Still today, the high combustion efficiency of diesel engines causes them to

be a popular choice for both stationary and mobile applications. More than a century of development has considerably increased their power output and their combustion efficiency. However, because of their lean combustion they cannot be equipped with a three-way catalyst to reduce the nitrogen oxide (NO_x) emissions, such as is the common practice with spark ignition engines. Furthermore, a large part of the combustion is diffusion combustion, which leads to the formation of particulate matter (PM). Because of the harmful effect of these pollutants on humans [5] and the environment [6], diesel-engine emission legislation has been introduced and then tightened steadily [7].
The improvements in performance and the compliance with constantly tightening pollutant emission limits are enabled by the introduction of ever more advanced engine hardware. However, this increasing complexity of the hardware necessitates a simultaneous evolution of the control systems used to control that hardware. The following sections introduce the hardware (Sec. 1.1.1) and the control systems (Sec. 1.1.2) used in a modern diesel engine.

1.1.1 Common hardware components

Without claiming the list to be complete, this section provides an overview of the engine components which, from a control point of view, have the largest impact on the performance and the pollutant emissions.

Turbo charging

Turbo chargers are used to increase the fresh-air charge of the engine [8]. They consist of two turbo-dynamic components, namely the turbine and the compressor. The turbine converts the exhaust-gas enthalpy to mechanical energy, thus driving the turbo-charger shaft. The compressor is driven by this shaft and it compresses the fresh air. This increase in available fresh air allows for the injection of increased amounts of fuel, which results in higher power outputs. The effect of a turbo charger can be augmented by installing several turbo chargers in series.
The turbo chargers are usually controlled either by using bypass valves or a variable geometry. Variable-geometry turbines are state-of-the-art [7], whereas variable-geometry compressors have only recently come into the focus of research [9]. The rotational dynamics of the turbo charger, which

are in the order of seconds, introduce some very relevant dynamics to the system.

Exhaust-gas recirculation

An exhaust-gas recirculation (EGR) takes exhaust gas from the exhaust manifold and feeds it into the intake manifold, where it is mixed with the fresh air supplied by the turbo charger(s). EGR decreases the oxygen concentration of the aspirated gas mixture. At the same time it increases the thermal mass of the cylinder content, thereby reducing the combustion temperatures. Since high combustion temperatures and high oxygen concentrations are the main conditions for the production of NO_x [4], the use of EGR decreases the amount of NO_x emitted.
The EGR is usually controlled by a valve in the EGR path. Additionally, a throttle can be used to increase the pressure difference over the EGR path and thus to increase the EGR mass flows achievable. The relevant dynamic of the EGR is the mixing of the EGR with the fresh air in the intake manifold, which is in the order of less than a second.

Common-rail injection

Common-rail injection-systems can inject fuel at very high pressures [10]. High injection pressures generally lead to an improved spray formation and a decreased formation of particulate matter. Furthermore, common-rail systems allow for multiple injections. Pilot injections can be used to decrease the share of premixed combustion, thus reducing the combustion noise. Post injections can be used to improve the combustion of unburnt hydro-carbons, thus reducing the emission of particulate matter.
The main degrees of freedom of the fuel injection are the injection pressure and the timing and the quantity of the respective injections. The fuel injection has a virtually instantaneous influence on the combustion and the resulting torque and pollutant emissions. The fuel injection thus does not introduce any relevant dynamics to the system.

Exhaust-gas aftertreatment

Exhaust-gas aftertreatment (EGA) is used to lower the tailpipe pollutant emissions. Selective catalytic reduction (SCR) uses urea to form ammonia, which then reduces the NO_x in the exhaust gas [11]. Lean NO_x traps

(LNT) absorb NO_x emissions [12]. However, they require regular regeneration periods using rich exhaust gas to reduce the absorbed NO_x. Diesel particulate filters (DPF) mechanically filter out the particulate matter in the exhaust gas [13]. They also require regular regeneration periods using hot exhaust gas to burn off the trapped PM.
The operation of the SCR catalyst is controlled by the amount of urea that is injected. The main dynamics of the SCR are the temperature and the concentration of the ammonia absorbed on the catalyst surface. Both dynamics are in the order of minutes. The LNT and the DPF are both passive devices. The degree of freedom is the scheduling of the respective regeneration periods. The relevant dynamics are the filling state of the device. They usually are in the order of hours.

1.1.2 Control of diesel engines

Although the components described in Sec. 1.1.1 allow the engine to be operated with low pollutant emissions, they also introduce additional degrees of freedom to the engine. Every degree of freedom can be optimized and needs to be controlled. Furthermore, these components add dynamics, nonlinearities, and cross-couplings to the system, thus complicating the control task even further. A good introduction to the main control systems in a diesel engine can be found in [14, 10]. From a control point of view, the engine can be divided into the subsystems air-path, combustion, and exhaust-gas aftertreatment. The following sections provide an overview of the respective control systems. Furthermore, some general information about the interaction, the design, and the optimization of these control systems is offered as well.

Air-path control

The fuel consumption and the pollutant emissions of a diesel engine strongly depend on the cylinder content. The air path controller controls the turbo charger(s) and the EGR in order to supply the desired aspirated gas mixture for the combustion. The air-path is usually controlled using a feedback of the intake manifold pressure and of a second signal, such as the intake burnt-gas fraction, the air-to-fuel ratio or the fresh-air mass flow. Often the control of the turbo charger(s) and the EGR is coordinated because the two systems are coupled strongly. The control problem is complicated further by the nonlinearities and a sensitivity to disturbances which are introduced by the turbo charger(s) and the EGR. A thorough discussion of this topic can be found in chapter 2.

Combustion control

The combustion controller uses the fuel injection to control the combustion in order to provide the desired torque while keeping the emissions within certain limits. Usually the combustion is controlled using a feedforward controller and the injection parameters are calibrated during the development of the engine. If cylinder pressure sensors are available, possible control objectives could be to track a reference for the center of combustion or the ignition delay. Feedback control of the combustion is especially relevant for advanced combustion modes, such as homogeneous charge compression ignition (HCCI) [15] and dual fuel combustion [16]. It is also advantageous in the context of feedback control of the pollutant emissions [17, 18].

Aftertreatment control

In the case of an SCR, the aftertreatment controller uses the urea injection upstream of the SCR catalyst to control the tailpipe NO_x emissions [19]. The control performance can be improved by estimating the surface concentration of the ammonia absorbed. In the case of the DPF and the LNT, the regeneration has to be scheduled based on their loading. Using the measured pressure difference over the DPF, its loading can be estimated using a DPF model and the regeneration can be triggered accordingly [13]. In the case of the LNT, the loading can be estimated using an LNT model and a NO_x sensor downstream of the LNT [20].

Interaction among the control systems

The subsystems of a diesel engine influence each other. For example, the air path supplies the boundary condition for the combustion, whereas the combustion influences the exhaust-gas temperature and the enthalpy available for the turbine(s). Together, the air path and the combustion determine the pollutant emissions and exhaust flow, which are the input to the EGA.

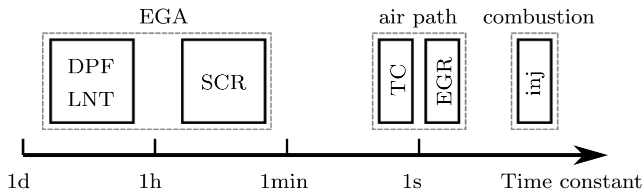

Figure 1.1: Relevant time constants of the most common components and subsystems of an engine, namely the EGA consisting of the DPF, the LNT, and the SCR, the turbo charger(s) (TC), the EGR, and the fuel injection (inj).

However, the subsystems EGA, air path, and combustion operate on different time scales. Figure 1.1 shows an overview of the time scales of the relevant dynamics of the components which constitute these subsystems. This time-scale separation decouples the plants and allows them to be controlled separately. According to [21], the stability and the performance of a fast control loop is not influenced much by the presence of a slower control loop. The operation of the slower control loop acts as a slow disturbance on the fast control loop. Because it acts within the bandwidth of the fast controller, this disturbance is rejected. On the other hand, the operation of the fast control loop has little influence on the stability and the performance of the slow control loop. Since the high-frequency behavior of the fast control loop occurs outside the bandwidth of the slower control loop, it is attenuated. In practice this decoupling means that despite the interaction of the subsystems, no centralized controller is required in order to achieve stability and a good performance[1] for all subsystems. Only the control of processes on similar time scales, such as the turbo charging and the EGR, has to be coordinated using a multivariable controller.

Model-based design of control systems

Although the major control systems of a modern diesel engine can be designed separately, the respective control problems are still challenging. The underlying plants are often highly nonlinear and coupled. A way to handle the complexity of a modern diesel engine is to apply model-based

[1] Here, the term "performance" refers to the ability to follow the reference trajectory. The performance of the overall system, such as the torque or the pollutant emissions, also strongly depends on the reference values of the subsystems.

control [22]. In a first step, a system analysis of an engine model can indicate how a suitable control system has to be structured. Once a suitable control structure has been determined, the engine model can be used to design the control loops. One possibility is to use model-based controllers which directly incorporate the model equations in the design process, such as H_∞ control [23] and linear quadratic regulators (LQR) [24]. Alternatively, simpler controllers such as PID controllers can be used. Regardless of the controller type used, the properties of the resulting control loop can be analyzed and the controllers can be tuned such that the desired specifications are met. The combination of advanced control structures and model-based control design and tuning results in a significant simplification of the control-system design process.

Optimization

A further simplification can be achieved by using the engine model for optimization. For example in [25], an offline optimization is carried out to determine the optimal set point values for the engine, such that the fuel consumption and the pollutant emissions are minimized for a given driving cycle. In [26], an offline optimization is applied to determine the optimal tuning parameters for the air-path controller. Recent research has shown that it is even possible to determine the optimal actuator trajectories for entire driving cycles by applying optimal control [27]. The application of such offline optimizations greatly reduces the amount of time necessary for calibration and tuning.

Furthermore, it is possible to carry out an online optimization to determine the optimal actuator settings during the operation. However, unlike for an offline calculation, the future driving conditions are not known when an online optimization is carried out. This problem of causality is especially critical when the final values of some state variables are constrained. This situation occurs when upper limits for the cumulated pollutant emissions are given, as is often the case with legislative limits. This problem is discussed in detail in chapter 4.

1.2 Scientific contribution

The control systems of a modern diesel engine play a significant role in meeting the demands of customers and legislation. They have to cope with the steadily increasing complexity of the engine hardware while remaining transparent enough to allow tuning and calibration. Optimization methods and model-based approaches for the design of the control structure and the control loops can render this task feasible.

This thesis contributes to the research field of model-based control of diesel engines by discussing three different control problems. All three are related to the overall objective of operating a diesel engine with low pollutant emissions and a low fuel consumption. They consider the air path, the combustion, and the optimal operation during a driving cycle, respectively. Since the dynamics which are relevant for the respective control problems are on three different time scales, the control problems can be treated separately. For each of them a controller is proposed to aid in achieving low pollutant emissions and fuel consumption.

The first contribution of this thesis is the development of the air-path controller published in [28, 29, 30]. It is the first air-path controller designed specifically to handle the disadvantageous properties of the plant (nonlinearities, cross-couplings, and a sensitivity to fast changes of the operating point), while being applicable to a wide range of engines. In [28] the control structure is derived and validated. The control structure is patented [29], and some early results are published in [30].

[28] S. Zentner, E. Schäfer, G. Fast, C. H. Onder, and L. Guzzella, "A cascaded control structure for air-path control of diesel engines," *Proceedings of the Institution of Mechanical Engineers, Part D: Journal of Automobile Engineering, available online*, 2014

[29] E. Schäfer, T. Kreissig, G. Fast, S. Zentner, L. Guzzella, and C. Onder, "Method and device for operating an internal combustion engine with supercharging and exhaust-gas recirculation," Patent Nr. WO/2013/159899, October 2013

[30] E. Schäfer, S. Zentner, and G. Fast, "Model-based development of a multi-variable control strategy for large diesel engines," in *Proceedings of the 6th Emission Control Conference, Dresden, Germany*, 2012

The second contribution is the development of the model-based method to adapt the fuel injection and the EGR during transients which is published in [31]. It is the first model-based controller which allows the adjustment of the trade-off between the transient pollutant emissions and the drivability using two simple parameters.

[31] S. Zentner, E. Schäfer, C. Onder, and L. Guzzella, "Model-based injection and EGR adaptation and its impact on transient emissions and drivability of a diesel engine," in *Proceedings of the 7th IFAC Symposium on Advances in Automotive Control, Tokyo, Japan*, 2013, pp. 89–94

The third contribution is the development of the framework for causal optimal control of diesel engines published in [32]. It is the first causal approach to the solution of the optimal control problem of minimizing the CO_2 emissions while not exceeding an upper limit for the cumulated pollutant emissions at the end of the driving cycle.

[32] S. Zentner, J. Asprion, C. Onder, and L. Guzzella, "An equivalent emission minimization strategy for causal optimal control of diesel engines," *Energies*, vol. 7, no. 3, pp. 1230–1250, March 2014

In addition to the contributions presented in this thesis, the collaboration with colleagues has led to the publication of two papers on the cascaded feedback control of the combustion and the pollutant emissions [17, 33] and one paper on the iterative optimization of diesel engines [34].

[17] F. Tschanz, S. Zentner, C. H. Onder, and L. Guzzella, "Cascaded control of combustion and pollutant emissions in diesel engines," *Control Engineering Practice, available online*, 2014

[33] F. Tschanz, S. Zentner, E. Özatay, C. H. Onder, and L. Guzzella, "Cascaded multivariable control of the combustion in diesel engines," in *Proceedings of the 2012 IFAC Workshop on Engine and Powertrain Control, Simulation and Modeling, Paris, France*, 2012, pp. 25–32

[34] J. Asprion, G. Mancini, S. Zentner, C. H. Onder, N. Cavina, and L. Guzzella, "A framework for the iterative dynamic optimisation of diesel engines: numerical methods, experimental setup, and first results," in *WIT Transactions on Ecology and the Environment*, C. Brebbia, E. Magaril, and M. Khodorovsky, Eds. WIT Press, Southampton, 2014, vol. 190

1.3 Outline

The next three chapters are dedicated to the three main contributions of the thesis. Chapter 2 describes the cascaded control structure for air-path control. Chapter 3 describes the model-based adaptation of the fuel injection and the EGR during transients. Chapter 4 describes the framework for causal optimal control of diesel engines. These three chapters are self-contained and can be read independently. Chapter 5 offers some concluding remarks and presents an outlook to future fields of research.

Chapter 2

Cascaded Air-Path Control

In order to comply with increasingly stringent diesel-engine emission legislation, the fast and precise control of the turbochargers and the exhaust-gas recirculation is necessary. The difficulties lie in certain disadvantageous plant properties such as cross-couplings and nonlinearities, the disturbance of the air path by fast operating-point changes, and the multitude of air-path configurations that are available. In this chapter, a novel, model-based approach for air-path control based on cascaded control is proposed. The resulting multivariable controller has a low sensitivity to the nonlinearity of the plant and the disturbances caused by sudden changes of the operating point. Furthermore, the controller is applicable to various types of air-path configurations. This flexibility is demonstrated by a system analysis of the models of two engines that span a broad range of air-path configurations. The performance of the proposed controller is compared experimentally with that of a conventional, model-based, multivariable controller, by implementing both on two engines, each of them running on a test bench. This comparison confirms that the cascaded controller presented herein can handle the cross-couplings of the system and that it exhibits a lower sensitivity to the nonlinearity and the disturbances than the conventional controller.
The content of this chapter is based on [28]. Two figures based on additional measurements (Figs. 2.17 and 2.19) and two sections discussing them have been added.

2.1 Introduction

Due to their high fuel efficiency, diesel engines are used in a wide range of applications. However, because of their lean combustion they cannot be equipped with a three-way catalyst to reduce the nitrogen oxide (NO_x) emissions, such as is the common practice with spark ignition engines. Furthermore, a large part of the combustion is diffusion combustion, which leads to the formation of particulate matter (PM). Since these emissions are harmful to both humans and the environment, emission legislation is becoming increasingly stringent with the introduction of transient test cycles and ever lower emission limits. State-of-the-art technologies, such as variable-geometry turbochargers (VGT), exhaust-gas recirculation (EGR), two-stage turbocharging, common-rail injection and exhaust-gas aftertreatment enable manufacturers to comply with the tightening emission regulations.

A widely used technology for reducing NO_x emissions is the exhaust-gas recirculation. Since it increases the mass of the cylinder content and thereby its heat capacity, it lowers the combustion temperatures. It also decreases the oxygen concentration of the aspirated gas mixture. Since high combustion temperatures and high oxygen concentrations are the main conditions for the production of NO_x [4], the introduction of EGR decreases the NO_x emissions. On the other hand, the reduction of the oxygen concentration is beneficial for the formation of particulate matter in the diffusion flame. To compensate for this effect, turbocharging is used to increase the fresh-air charge and the oxygen concentration. However, the turbochargers and the EGR introduce noticeable dynamics to the air path, thereby complicating the task of the air-path controller.

During a driving cycle a considerable portion of the emissions is generated during fast operating-point[1] changes when the air path cannot supply the cylinder charge that is desired for the current operating point. Improvements in the transient behavior of the air path are therefore crucial for the reduction of the emissions on a given driving cycle. However, several problems arise. The plant is afflicted with nonlinearities and cross-couplings. The transient operation of the engine poses additional difficulties. First, the rapidly changing cylinder mass-flows and temperatures act as disturbances on the air path. Second, the engine is frequently operating far from the design point of the controller, which makes the effect of the plant nonlinearities more severe.

Given the diversity of applications and legal limits, an engine manufacturer may implement several different air-path configurations. Among others,

[1] The term "operating point" refers to the current engine speed and torque.

there exist variable and fixed geometry turbines, turbines with and without waste-gate, and single-stage and two-stage turbochargers. In the development of a control structure, it is therefore highly desirable to ensure that it will be applicable to many different air-path configurations.

The air-path control for diesel engines has been the subject of research for the past two decades. A special focus has been placed on engines equipped with a VGT and an EGR. A good introduction can be found in [35, 14, 36, 37]. However, none of the published approaches can deal with the problems posed by the plant and by transient driving cycles while being generic enough to deal with different engine configurations. Most model-based controllers are restricted to one engine configuration only. Some of them invert the model equations for certain parts of the engine (EGR valve and VGT), such as those proposed in [38, 39, 40]. Some well-known nonlinear approaches [41, 42, 43, 44, 45, 46, 47] are based on nonlinear model equations and thus explicitly assume a certain configuration. In [26], simple single-input single-output (SISO) controllers are used. That approach is generic enough for use with various engine configurations, but the cross-couplings of the system are not taken into account. The same applies to the air-to-fuel ratio based controllers presented in [48, 49] and the approach shown in [50].

In [51], motion planning is used to determine reference values for the fresh-air and the EGR mass flows. These are also controlled using SISO controllers without considering the cross-couplings of the system. In [52], fuzzy control is used to coordinate the EGR valve and the VGT in a certain operating region and to improve the transient response by switching from control of the intake pressure to control of the exhaust pressure. That approach is specifically designed for engines equipped with a VGT and outside of the coordinated operating region it does not take into account the cross-couplings. Approaches based on linear, parameter-varying (LPV) models [53, 54, 55, 56] could work with various air-path configurations and are well-suited to the suppression of the disturbances caused by changes of the operating point. But they depend on the availability of an LPV engine model, an approach that has not yet been shown to be applicable for two-stage configurations. In [57], a controller based on internal model control is presented. In combination with the flatness-based feed-forward described in [58, 59], that approach could be applied to single- and two-stage turbocharged diesel engines with EGR. However, that control strategy has not been validated by experiments as yet. In [60], a linear decoupler is used to decouple the plant at low frequencies. Since the decoupler is based on a linear model of the plant, the controller is sensitive to the nonlinearity of the plant. Another promising approach is model predictive control (MPC) [61, 62, 63, 64]. The main drawback of MPC is its computational load in view of the limited computational power available in current series-production engine control units. The same applies to an even larger extent to nonlinear MPC approaches [65, 66].

In this chapter, a novel control structure for the air path of a diesel engine is proposed. It is designed to deal with the disadvantageous plant properties such as nonlinearities and cross-couplings and with the difficulties that fast operating point changes pose to the air-path controller, namely disturbances. Furthermore, this structure can be applied to a wide range of diesel-engine configurations. Although it is somewhat more complex than a conventional controller, its tuning process remains straightforward. The advantages of the control structure are shown experimentally in a comparison with a conventional controller using two engines, each of them running on a test bench.

The control problem is defined in Sec. 2.2. The engines used for simulation and experimental validation are described in Sec. 2.3. The control structure, including an estimator for the EGR-related signals, is presented in Sec. 2.4. The advantages of the new structure are shown in an experimental comparison with a conventional controller. The results of that comparison are presented in Sec. 2.5, and Sec. 2.6 concludes the chapter.

2.2 Problem formulation

The overall goal of air-path control is the control of the cylinder charge. Together with the injection parameters, the cylinder charge determines the amounts of torque generated and of the pollutants emitted. Considering that neither a variable valve train nor a swirl valve are used, controlling the cylinder charge is equivalent to controlling the intake manifold pressure p_{im} and the burnt-gas fraction x_{im},

$$y = \begin{bmatrix} p_{\mathrm{im}} \\ x_{\mathrm{im}} \end{bmatrix}. \tag{2.1}$$

The latter is defined by

$$x_{\mathrm{im}} = \frac{m_{\mathrm{bg}}}{m_{\mathrm{bg}} + m_{\mathrm{air}}}, \tag{2.2}$$

with the mass of burnt gas m_{bg} and the mass of fresh air m_{air} in the intake manifold.

The control inputs depend on the structure of the air path. Figure 2.1 shows the air-path configurations that are considered here. The turbocharging may be single-staged or two-staged. The control of the turbine load can be achieved by a variable-geometry turbine (VGT) or a waste gate (WG). If the configuration is two-staged, this control input is assumed to act on the high-pressure (HP) turbine, whereas the low-pressure (LP) turbine is assumed to not have any specific control input. All engines are assumed to have HP EGR controlled by a valve. Low-pressure EGR systems have significantly less interaction with the turbocharging system than HP systems [67]. This fact fundamentally changes the requirements for the control system. Control of LP EGR is thus not considered here. The control inputs are the turbocharger control input u_{tc} (VGT or WG position) and the position of the EGR valve u_{egr},

$$u = \begin{bmatrix} u_{\mathrm{tc}} \\ u_{\mathrm{egr}} \end{bmatrix}. \tag{2.3}$$

The control inputs are normalized between 0 and 1, where the value 1 indicates a closed VGT/WG or an opened EGR valve, respectively.

Without claiming the list to be complete, I consider the following issues to pose the most significant problems for the air-path controller on a transient driving cycle:

1. Cross-couplings of the plant: Both inputs influence both outputs. A multivariable (MIMO) controller is necessary to coordinate the control of both outputs.

2. Nonlinearity of the plant: The gains of the plant strongly depend on the operating point and the current states and inputs. During transients on an aggressive driving cycle, the engine is frequently operating far from the design point of the controller, which makes the control system more sensitive to the nonlinearity of the plant.

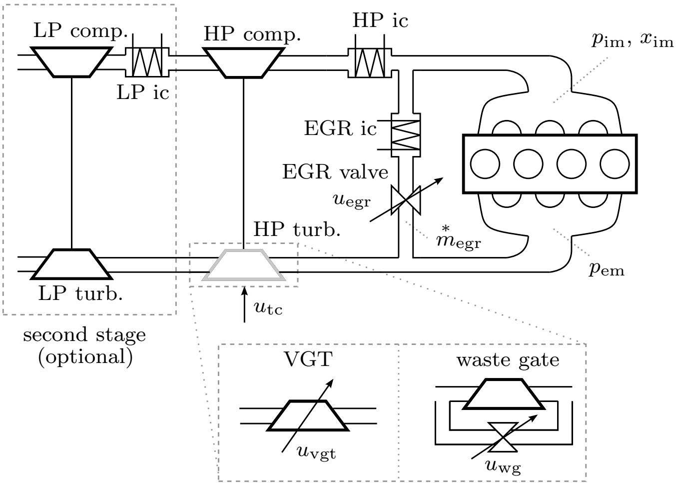

Figure 2.1: Air-path configurations considered for control, where LP = low–pressure, HP = high-pressure, comp. = compressor, turb. = turbine and ic = intercooler.

3. Disturbance by operating-point changes: Operating-point changes cause suddenly changing cylinder mass flows and temperatures. These have a direct impact on the exhaust pressure, which in turn drives both the turbines and the EGR. The entire air path is thus disturbed by the operating-point changes.

The cross-couplings and the nonlinearity have already been reported in [35]. The sensitivity to operating-point changes is a direct consequence of the dependence of the air path on the exhaust pressure. All three problems apply to all the air-path configurations considered. A control structure has to be developed that tackles all three problems while not depending on any configuration-specific assumptions.

2.3 Engines used for simulation and measurement

This section describes the engine models used for the system analysis (2.3.1) and the engine test-benches used for the experimental validation (2.3.2).

2.3.1 Engine models used for the system analysis

In order to show that the proposed control structure is valid and advantageous for engines of different sizes and with various types of air-path configurations, the mean-value models of two different engines have been analyzed. An overview of the specifications of the two engines is given in Table 2.1. The smaller engine is a production-type automotive engine with a single-stage variable-geometry turbine. In the following it will be referred to as the SSVGT engine. The larger engine is an experimental industrial engine with two-stage turbocharging and fixed geometry turbines with a high-pressure waste-gate. In the following it will be referred to as the TSWG engine. These two engines will also be used for the experimental validation of the control approach described in Sec. 2.5. They cover a broad spectrum of sizes and turbocharger configurations. This fact is the basis for the assumption that the proposed control structure will hold for all engines with similar configurations. Both engines have been modeled by zero-dimensional mean-value models. For more information about this modeling approach, see [22]. The parameters have been identified using measurement data or construction data. For example, the parameters of the cylinder model were identified using experimental data, whereas the volumes of the receivers modeling the manifolds were taken from a 3D CAD model and the parameters of the turbocharger model were identified using turbocharger maps. The models have been validated with transient measurement data.

Table 2.1: Specifications of the engines considered

	Engine 1	Engine 2
Number of cylinders	6 cylinders	12 cylinders
Displacement	2,987 cm^3	21,042 cm^3
Power	160 kW	680 kW
turbocharging	Single stage	Two stage
High-pressure Turbine	VGT	Waste gate
EGR	High pressure	High pressure
Abbreviation	SSVGT	TSWG

A comparison of simulated and measured data is shown in Fig. 2.2 (TSWG) and in Fig. 2.3 (SSVGT) for a stepwise manipulation of the input sig-

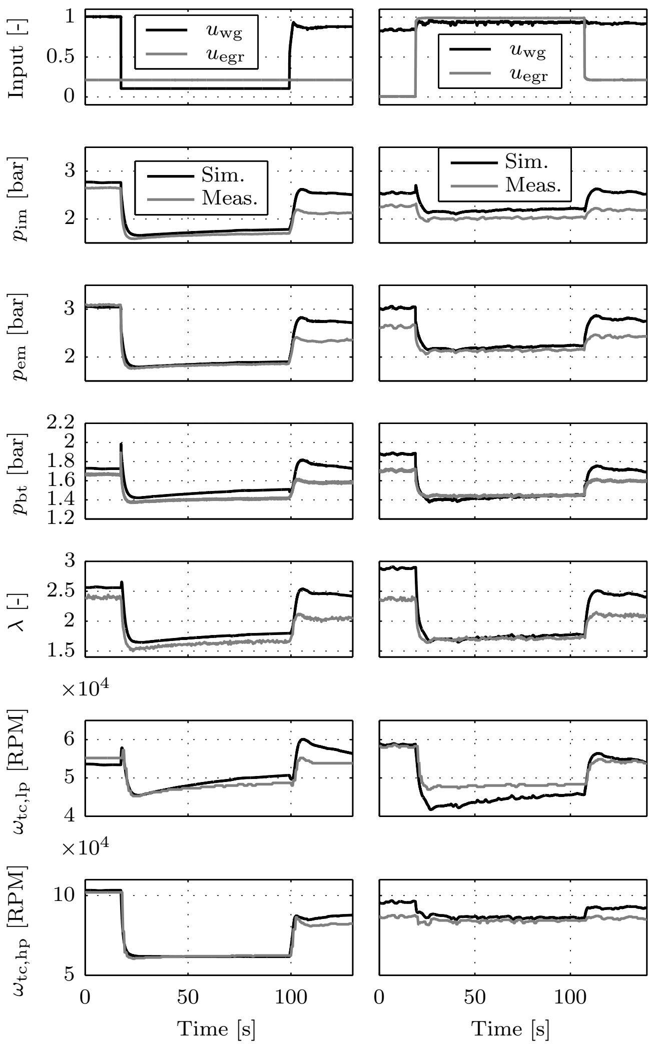

Figure 2.2: Comparison of the measured and simulated responses of the TSWG engine for stepwise manipulation of the air-path actuators u_{wg} and u_{egr}.

nals. Both models capture all relevant dynamics of the respective engines. Important dynamic differences between the single-stage and the two-stage configuration are also captured. One of them is the inverse-response behav-

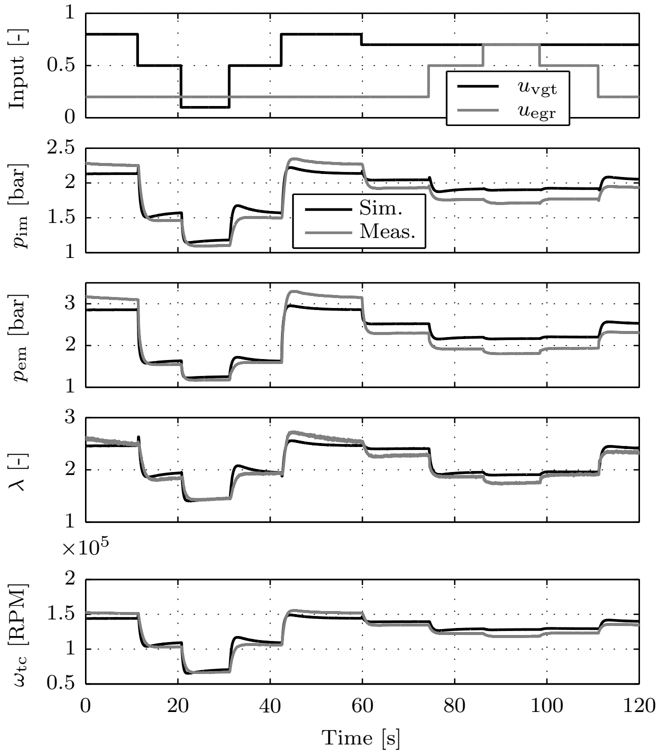

Figure 2.3: Comparison of the measured and simulated responses of the SSVGT engine for stepwise manipulation of the air-path actuators u_{vgt} and u_{egr}.

ior (also known as nonminimum-phase behavior) of the LP turbocharger speed of the TSWG engine with respect to the waste-gate position. This behavior can be explained physically. When the waste gate is opened (t=17 s), more exhaust gas is led directly to the LP turbine (increasing the pressure between the turbines), whereas less exhaust gas remains in the exhaust manifold (decreasing the exhaust pressure). This effect leads to a decrease of the HP turbocharger speed and an increase of the LP turbocharger speed. Because the HP turbine is affected by both pressure changes, the change in HP turbocharger speed is much higher, resulting in an overall decrease in fresh-air mass flow. Eventually, this compensates the gain of exhaust-gas that the opening of the waste gate has caused for

the LP turbine. When this happens, the speed of the LP turbocharger decreases again.
The model of the SSVGT engine shows better accuracy in steady-state conditions. The reason for this observation is the fact that for the TSWG engine, two turbochargers connected in series have to be modeled. Model errors in the upstream block change the operating point of the downstream block. In combination with the model errors of the downstream block, this effect can lead to notable offsets. This problem applies to both the compressors and the turbines. Furthermore, the additional feedback loop introduced by the rotational speed of the LP turbocharger promotes the propagation of model errors even more. But since capturing all relevant dynamics is more important for controller design than the exact representation of the stationary behavior, this model inaccuracy is acceptable.

2.3.2 Engines used for the experimental validation

The experiments have been carried out on both engines. For both engines, the standard engine control unit (ECU) was partly bypassed using an ETAS ES910 rapid control prototyping module. Only the air-path controller of the ECU was bypassed, while all other ECU functionalities remained active.

2.4 Cascaded control of the air path

The three problems described in Sec. 2.2 can be tackled by applying cascaded control. For cascaded control, the control problem is separated into two sub-problems, and additional feedback variables are introduced. The additional information contained in the additional feedback signals and the advantageous properties of the sub-problems are responsible for the improved performance of the cascaded control structure. The structure and its advantages are described in Sec. 2.4.1. The controller requires an estimator for all EGR-related signals. This estimator is described in Sec. 2.4.2. The controllers implemented for the two sub-problems are described in Sec. 2.4.3.

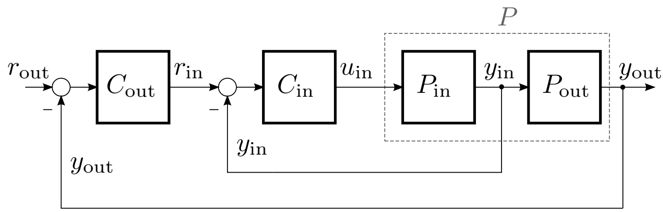

Figure 2.4: Structure of a cascaded control system

2.4.1 Description of the control structure

Introduction to cascaded control systems

In order to apply cascaded control, the plant P has to consist of two processes connected in series. The output of the fast inner plant P_{in} is the input to the slower outer plant P_{out}. Figure 2.4 shows the structure of a cascaded control loop. Two controllers are implemented, namely a fast controller C_{in} for the inner loop and a slower controller C_{out} for the outer loop. The outer loop controls the main feedback variables ($y_{out} = y$), whereas the inner loop controls some additional signals y_{in}. The control input of the outer controller is the reference value of the inner feedback loop ($u_{out} = r_{in}$). Cascaded control systems have the following advantages [21]:

- The nonlinearity of the inner plant and any disturbances acting on the inner plant have less influence on the outputs of the outer plant when the inner loop is closed. This is due to the fact that the high bandwidth of the inner-loop controller allows a fast compensation of the nonlinearity and of the disturbances.

- The phase lag in the inner plant is reduced by closing the inner loop, which improves the achievable performance of the outer loop. This improvement is due to the fact that additional feedback signals are introduced, which are affected by a smaller phase lag.

In order to exploit the advantages of using cascaded control, the feedback signals of the inner loop must have the following properties: First, there must be a time-scale separation between them and the feedback signals of the outer loop, such that the inner loop can be controlled with a higher

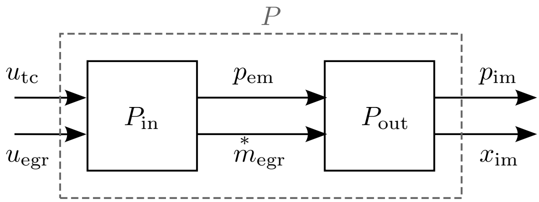

Figure 2.5: Cascaded plant

bandwidth. Second, for the cascaded structure to lead to an improved suppression of the disturbances, they must affect the feedback signals of the inner loop. The disturbances can thus be compensated by the fast inner loop controller before they reach the outer loop. Third, the feedback signals of the inner loop have to be chosen such that the nonlinearity of the plant is included in the inner plant, thus reducing its influence on the control of the feedback signals of the outer loop.
The feedback signals of the inner loop are chosen to be the exhaust manifold pressure p_{em} and the EGR mass flow $\overset{*}{m}_{\mathrm{egr}}$,

$$y_{\mathrm{in}} = \begin{bmatrix} p_{\mathrm{em}} \\ \overset{*}{m}_{\mathrm{egr}} \end{bmatrix}. \tag{2.4}$$

They are the intermediate signals connecting the inner and the outer plant (see Fig. 2.5). The exhaust manifold pressure can be measured directly using a sensor, but that sensor is not standard in all series-production engines. Both engines considered in this chapter are equipped with that sensor, therefore it is assumed to be generally available. If this is not the case, a model-based estimation [68] may be used as an alternative. An analysis of estimator-based feedback control of the exhaust pressure is not described here since it would exceed the scope of this thesis. For the EGR mass flow, no series production sensors are available. An estimator for that signal is described in Sec. 2.4.2. In the following sections, these signals are shown to have the required properties.

Time-scale separation

Both quantities can be controlled with a higher bandwidth than the feedback signals of the outer loop (p_{im} and x_{im}). An analysis of the frequency responses of the various plants shows their achievable bandwidths. The operating points used for the analysis are chosen such that they represent a medium speed and load. All plants considered are 2×2 MIMO plants. For the sake of clarity, only the two dominant channels each are discussed below. Figure 2.6 shows the Bode diagrams of the dominant channels of the following plants:

- Inner plant: It describes the interaction between the air-path actuators (u_{tc}, u_{egr}) and the intermediate signals (p_{em}, $\overset{*}{m}_{\mathrm{egr}}$).

- Idealized outer plant: It describes the interaction between the intermediate signals (p_{em}, $\overset{*}{m}_{\mathrm{egr}}$) and the outputs of the outer plant (p_{im}, x_{im}). This plant is fictitious because it assumes perfect control of the inner loop. It is obtained by assuming steady-state conditions for the exhaust manifold, which allows the physical inputs (u_{tc}, u_{egr}) to be replaced by the fictitious inputs (p_{em}, $\overset{*}{m}_{\mathrm{egr}}$). The steady-state assumption is valid because the dynamics of the exhaust manifold are very fast compared to the dynamics of the outer plant, which is dominated by the rotational dynamics of the turbocharger.

- Real outer plant: It describes the interaction between the reference values of the intermediate signals ($p_{\mathrm{em,ref}}$, $\overset{*}{m}_{\mathrm{egr,ref}}$) and the outputs of the outer plant (p_{im}, x_{im}). For this plant, a realistic inner loop controller with a crossover frequency of $4\,\mathrm{rad/s}$ is assumed. This frequency is indicated by a vertical line. Despite the different sizes of the two engines, the same bandwidth has been used for the inner loop. This is due to the fact that the limiting factors in that loop are the actuator dynamics and the pressure dynamics in the exhaust manifold, which are similar for both engines.

- Full plant: It describes the interaction between the air-path actuators (u_{tc}, u_{egr}) and the outputs of the outer plant (p_{im}, x_{im}). It is the plant that a conventional, non-cascaded controller faces.

The pressure path ($u_{\mathrm{tc}} \to p_{\mathrm{em}} \to p_{\mathrm{im}}$) is analyzed first. In both engines, the magnitude of the real and of the ideal outer plant starts to decrease at approximately $1\,\mathrm{rad/s}$, which is caused by the rotational dynamics of the turbochargers. However, the inner plant differs for the two engines. Both engines show a first drop in magnitude at low frequencies (caused by the rotational dynamics of the turbochargers) and then another drop at higher

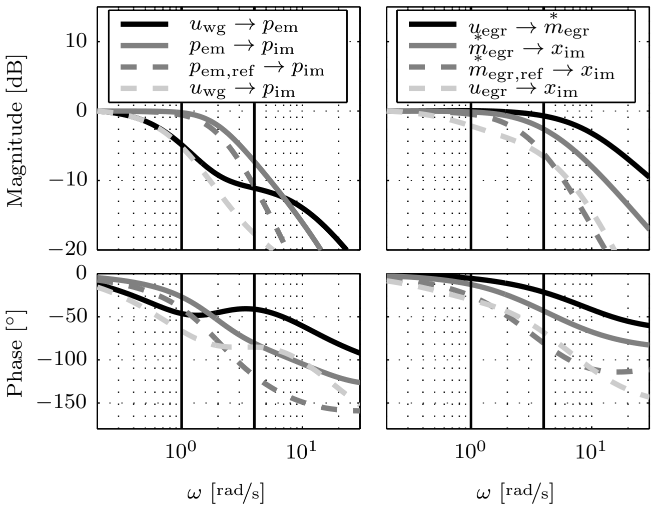

(a) TSWG engine

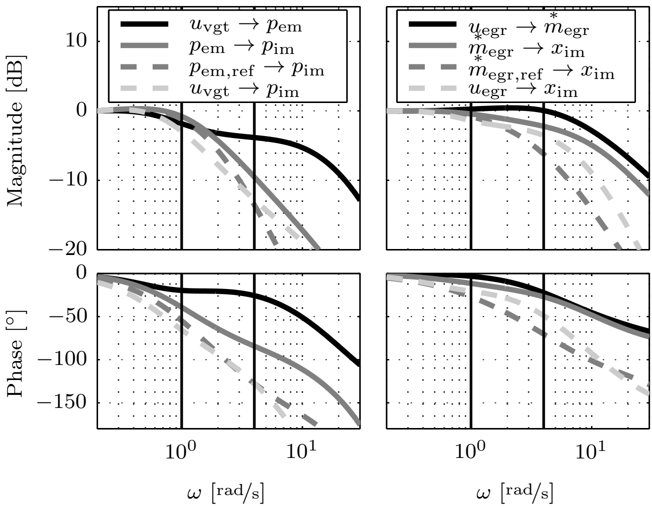

(b) SSVGT engine

Figure 2.6: Frequency responses of the main channels of the inner plant (black), the idealized outer plant (gray), the real outer plant (dashed gray) and the full plant (dashed, light gray). The frequencies 1 rad/s and 4 rad/s are indicated by a vertical line. All systems have been normalized to have a static gain of 0 dB.

frequencies (caused by actuator and exhaust-pressure dynamics). In the SSVGT engine, the low-frequency drop in magnitude is caused by the low-pass behavior introduced by the rotational dynamics of the turbocharger. In the TSWG engine, an additional effect causes the drop to occur at lower frequencies (approximately $0.3\,\mathrm{rad/s}$) and to be more pronounced. This effect can be attributed to the inverse-response behavior of the LP turbocharger speed with respect to the waste-gate position that has been observed in Sec. 2.3.1.

If the waste gate is excited with a frequency that is sufficiently low for the LP turbocharger to react and sufficiently high to prevent the LP turbocharger speed from reverting from its initial inverse response, then it is possible to achieve an oscillation of the two turbocharger speeds with opposite phases[2]. Since their effects on the fresh-air mass-flow cancel each other out, the oscillation of the intake and exhaust pressure has a small magnitude. This effect is responsible for the drop in magnitude and phase at low frequencies and the increase in phase at approximately $1\,\mathrm{rad/s}$. However, this effect (for the TSWG engine) and the low-pass characteristic introduced by the turbocharger (for the SSVGT engine) do not hinder a high-bandwidth control of the inner loop because the exhaust pressure is still mainly influenced directly by the turbocharger actuator, which is evidenced by the low phase lag of the inner loop even at high frequencies. Because the phase lag at high frequencies is much smaller for the inner loop than for the outer loop, a higher bandwidth can be achieved for the inner loop.

Now, the EGR path ($u_{\mathrm{egr}} \rightarrow \overset{*}{m}_{\mathrm{egr}} \rightarrow x_{\mathrm{im}}$) is analyzed. Generally, for the EGR path the time-scale separation is not as distinct as for the pressure path. For both engines, the magnitude and the phase of the outer plant start decreasing at approximately $1\,\mathrm{rad/s}$, whereas for the inner plant this occurs at higher frequencies (approximately $4\,\mathrm{rad/s}$). Thus, the inner loop can be controlled with a higher bandwidth than the outer loop.

Figure 2.6 shows that at low frequencies, i.e. up to a frequency of approximately $1\,\mathrm{rad/s}$, the real outer plant is almost equivalent to the ideal plant. The idealized outer plant may thus be used for further analyses. In addition, the phase enhancing effect of the cascaded controller becomes evident. For both paths of the TSWG engine and the pressure path of

[2]This can be confirmed by analyzing the phase difference between the two systems $u_{\mathrm{wg}} \rightarrow \omega_{\mathrm{tc,lp}}$ and $u_{\mathrm{wg}} \rightarrow \omega_{\mathrm{tc,hp}}$.

the SSVGT engine, the real outer plant shows a smaller phase lag than the non-cascaded plant up to the frequency of $2\,\mathrm{rad/s}$, which is half the crossover frequency of the inner loop. This fact shows that the phase lag in the inner plant is reduced by closing the inner loop. If the bandwidths of the two loops are separated by an octave, the outer loop can benefit from this effect. However, for the EGR path of the SSVGT engine, the cascaded control structure causes a slight increase in phase because the time-scale separation between the loops is rather small. Nonetheless, the other advantages are still present, namely the compensation of disturbances and of the nonlinearity of the inner loop.

Disturbances

The choice of feedback signals of the inner loop described above is suitable for suppressing the disturbances caused by fast operating-point changes. This fact can be verified by analyzing the cause-and-effect diagram of a diesel engine. Figure 2.7 shows such a diagram that applies to all the air-path configurations considered. For a single-stage engine, the blocks representing the turbochargers are static because they only represent the turbocharger maps. For a two-stage engine, they are dynamic because they represent the maps of both stages and the receivers between the compressors and turbines, respectively. A sudden change in engine speed and load changes the cylinder mass flow and temperature. The resulting change in exhaust pressure influences the EGR mass flow, which in turn disturbs the intake burnt-gas fraction. The change in exhaust pressure also has an effect on the speed of the turbocharger(s), whereas the resulting change in fresh-air mass flow disturbs the intake pressure. When the exhaust pressure and the EGR mass flow are measured and controlled with a high bandwidth, the effect of those disturbances can be compensated quickly before they affect the outer loop.

Nonlinearity

This choice of feedback signals of the inner loop ensures that the nonlinearity of the actuators is contained in the inner loop. The functions describing the VGT and EGR mass flows are highly nonlinear, and this nonlinearity is largely responsible for the nonlinearity of the overall system. Figure 2.8 shows the steady-state values of the most important signals of the inner

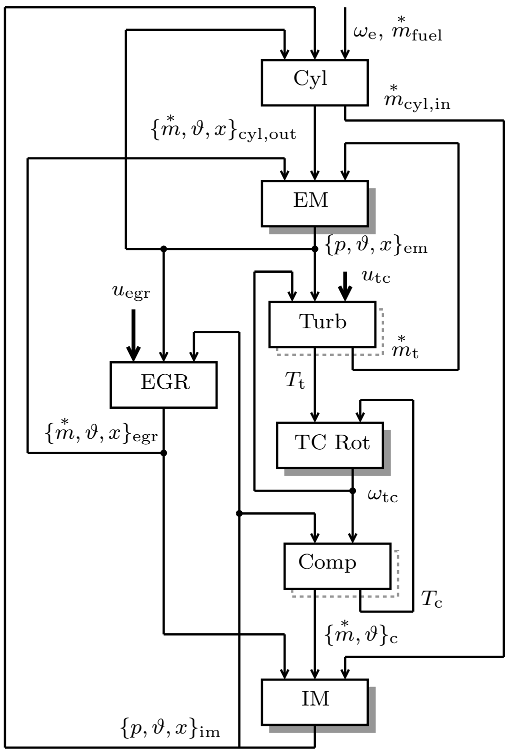

Figure 2.7: Cause-and-effect diagram of a diesel engine including blocks for the cylinder process (Cyl), the exhaust manifold (EM), the turbine(s) (Turb), the exhaust-gas recirculation (EGR), the rotational dynamics of the turbocharger(s) (TC Rot), the compressor(s) (Comp) and the intake manifold (IM). Dynamic blocks are indicated by a shadow.

and the outer plant for a constant operating point. This data was obtained by simulation of the nonlinear engine models for various actuator positions. The operating points have been chosen such that they represent a medium speed and load. For both engines, the EGR valve has almost no influence on the EGR mass flow at large openings. However, the effect of the EGR mass flow on the intake burnt-gas fraction is almost linear. The same applies to the turbocharger actuators. For large openings, their effect on the exhaust pressure is minimal, whereas the effect of the exhaust pressure on the intake pressure is almost linear.

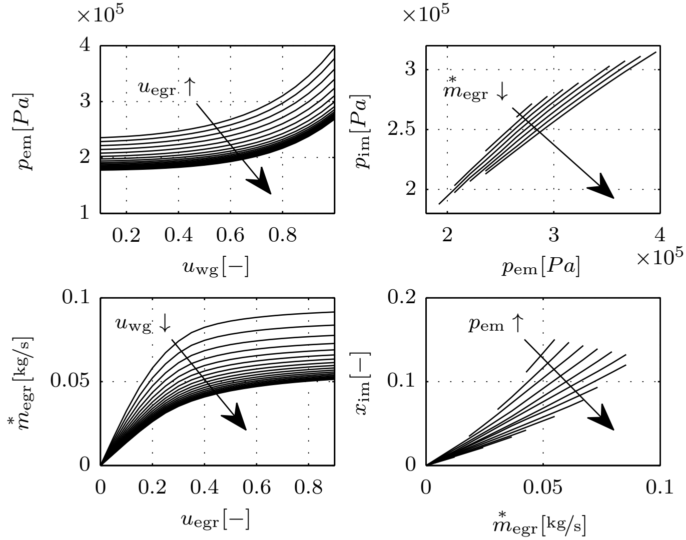

(a) TSWG engine

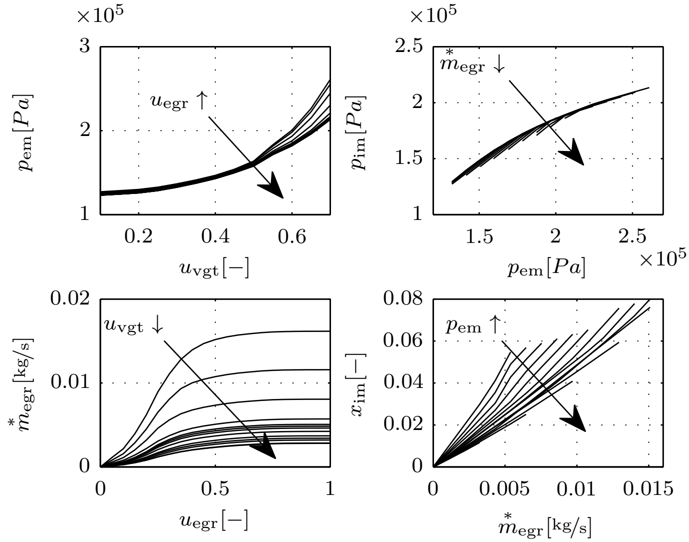

(b) SSVGT engine

Figure 2.8: Steady-state values of the air path illustrating the nonlinearities with which the actuators are afflicted.

The loss of control authority of the physical actuators is caused by two phenomena. First, there is the nonlinearity between the control input and the flow area of a valve, which is caused by the geometry of the valve and its actuator. Second, the flow properties of a valve cause a decrease in sensitivity of the mass flow to the valve area for large openings. The EGR valve and the waste gate can be modeled as a valve. Although it is more complicated, the fundamental behavior of a VGT is very similar to that of a valve. As the valve area increases, the mass flow increases as well causing the pressure ratio over the valve to decrease. This decrease in pressure ratio reduces the mass flow, which counteracts the effect of the larger valve area. For pressure ratios approaching one, the effect of the pressure ratio on the mass flow becomes stronger, up to the point where both effects are equally strong and an increase in valve area loses its effect on the mass flow or on the pressure ratio. Both effects are present for both actuators, and the effect of this nonlinearity can be detected by measuring the exhaust pressure and the EGR mass flow.

Further properties of the new subsystems

In the previous sections it was shown that if the exhaust pressure and EGR mass flow are used as feedback signals for the inner loop, the preconditions for cascaded control are fulfilled and the general advantages of that control strategy can be exploited. However, there are additional advantages that are unique to the air path of a diesel engine. First, a large number of the cross-couplings of the system are contained in the inner plant. The exhaust gas can either be recirculated (EGR mass flow) or used to drive the turbine by increasing the exhaust pressure. The former increases the intake burnt-gas fraction, whereas the latter increases the turbocharger speed and the intake pressure. This trade-off between EGR mass flow and exhaust pressure is largely responsible for the cross-couplings in the system. Because the cross-couplings induced by this trade-off are included in the inner plant, the outer plant is almost decoupled.
This statement can be verified by analyzing the relative gain array (RGA). The RGA matrix is a measure for the strength of the cross-couplings among the various control channels and for how well a plant can be controlled using single-input single-output (SISO) controllers. Given the transfer function of the plant $P(s)$, the relative gain array is defined as [21]

$$RGA(P) = P \times (P^{-1})^T, \tag{2.5}$$

where $\times$ denotes an element-by-element multiplication (i.e. a Hadamard or a Schur product). The variable RGA_{11} describes how well the channel $u_1 \rightarrow y_1$ can be controlled by a SISO controller. Values close to unity indicate small cross-couplings and a good performance of a SISO controller. Since it is a structural property of the RGA matrix that every row and every column adds up to one, the diagonal elements of a two-by-two RGA matrix are equal, as are the off-diagonal elements. The analysis of only one element thus suffices since all other elements can be calculated therefrom.

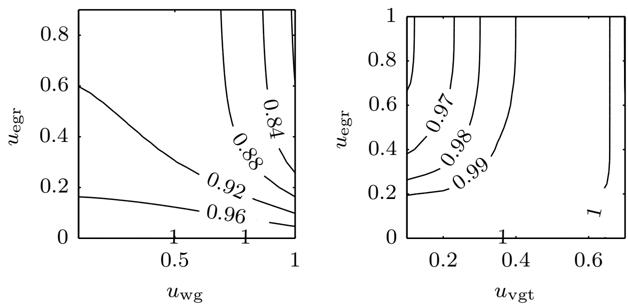

(a) TSWG engine (b) SSVGT engine

Figure 2.9: $|RGA_{11}|$ of the outer plant at $1\,\mathrm{rad/s}$.

Figure 2.9 shows the absolute value of the first diagonal entry of the RGA matrix ($|RGA_{11}|$) for a frequency of $1\,\mathrm{rad/s}$ for both engines at the same operating points as those used in the previous analyses. This data is obtained by linearizing the model of the idealized outer plant, which was already used in the analysis of the time-scale separation in Sec. 2.4.1, for different positions of the air-path actuators. The RGA analysis is then carried out for all linear models. For all actuator positions, the value of $|RGA_{11}|$ is close to one and the outer loop is almost decoupled. For both engines the couplings decrease with a decreasing opening of the EGR valve. In the extreme case of a closed EGR valve, the system is completely decoupled. The TSWG engine shows stronger couplings, the cause being the higher EGR mass flows that the TSWG engine can achieve. This is reflected in the much higher intake burnt-gas fractions of the TSWG

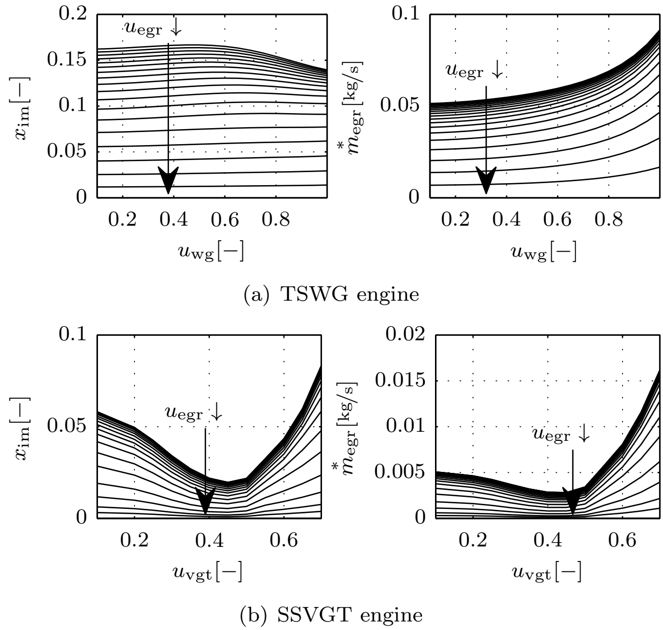

Figure 2.10: Steady-state values of the air path illustrating the sign change of the gain in the channel $u_{\mathrm{tc}} \rightarrow x_{\mathrm{im}}$.

engine (see Fig. 2.8). The fact that the outer loop can be controlled using two separate SISO controllers is a great advantage of the cascaded control structure. Although both an inner and an outer controller are required, one of them is very simple.

Another interesting effect can be observed with the turbocharger control signal, the EGR mass flow and the intake burnt-gas fraction. Figure 2.10 shows these signals for both engines for the same operating points as before. For both engines, the steady-state gain in the channel $u_{\mathrm{tc}} \rightarrow x_{\mathrm{im}}$ changes sign. This behavior has also been described in [35]. It can be explained physically. When the VGT/WG is closed, the exhaust pressure increases. The increase in available enthalpy for the turbocharger(s) increases the fresh-air mass flow. At the same time, the increased exhaust pressure may increase or decrease the EGR mass flow, depending on how the intake pressure has increased along with it. Depending on which effect is dominant, the intake burnt-gas fraction may decrease or increase. For both engines, the inner plant $u_{\mathrm{tc}} \to \overset{*}{m}_{\mathrm{egr}}$ exhibits much less nonlinearity than the full plant $u_{\mathrm{tc}} \to x_{\mathrm{im}}$.

For the TSWG engine the EGR mass flow behaves monotonically with respect to the WG position, and the sign change in the steady-state gain can be eliminated by using the valves to control the EGR mass flow instead of the burnt-gas fraction. For the SSVGT engine the sign change of the gain is also present in the inner loop in the channel $u_{\mathrm{vgt}} \to \overset{*}{m}_{\mathrm{egr}}$. This fact can be explained by the high efficiency of the turbine for medium openings[3]. Beginning at a fully opened VGT, a closing of the VGT brings the turbine into the efficient operating region, such that the pressure difference between the intake and the exhaust decreases. This reduces the EGR mass flow. When the turbine is closed further, the turbine efficiency decreases again, the pressure difference increases, and consequently the EGR mass flow increases. However, since the EGR valve has a much higher influence on the EGR mass flow, the channel $u_{\mathrm{vgt}} \to \overset{*}{m}_{\mathrm{egr}}$ is not very pronounced and the sign change of the gain can be considered a disturbance.

For the TSWG engine, the separation of the plant into an inner and an outer plant removes the sign change in the steady-state gain. For the SSVGT, the sign change is still present, but it is less prominent. For both engines the cascaded control structure reduces the effect of the nonlinearity of the turbocharger control-input on the EGR.

Summary of the properties of the cascaded control structure

Introducing additional feedback variables and reformulating the control problem allows us to tackle all three problems:

1. Cross-couplings in the plant: The inner-loop controller decouples the outer plant.

2. Nonlinearity of the plant: Nonlinearities of the actuators are contained in the inner loop and are overcome by the fast inner loop controller before they can affect the outer loop.

3. Disturbance by operating-point changes: The fast inner loop compensates disturbances caused by operating-point changes before they can affect the outer loop.

[3] For variable geometry turbines, the geometry of the blades is optimized for one blade angle. Deviating from this angle decreases the turbine efficiency. The turbine of the engine used for the analysis was optimized for medium openings.

These properties apply to two engines of different size and turbocharger configuration. The advantages can be generalized to similar engines because they partly are inherent to cascaded control and partly are due to the exploitation of system properties that similar engines share. Figure 2.11 shows the cascaded control structure.

2.4.2 Observer description

The control structure described above uses the EGR mass flow $\overset{*}{m}_{\text{egr}}$ and the intake burnt-gas fraction x_{im} as feedback signals. Since there are no series-production sensors available for these signals, they cannot be measured and thus have to be estimated. The EGR mass flow is estimated using a high-gain input estimator. The estimated EGR mass flow is then used to estimate the intake burnt-gas fraction.

EGR mass flow

The estimation of the EGR mass flow differs from usual estimation problems in the regard that it is not a state variable but an input of a dynamic system that has to be estimated. Assuming an isothermal receiver, the equation governing the dynamics of the intake manifold pressure is

$$\frac{d}{dt}p_{\text{im}} = \frac{R \cdot \vartheta_{\text{im}}}{V_{\text{im}}} \cdot [\overset{*}{m}_{\text{air}} + \overset{*}{m}_{\text{egr}} - \overset{*}{m}_{\text{cyl}}]. \tag{2.6}$$

The EGR mass flow is an input to the system, which can be estimated using an input estimator [69]. The input estimator simulates the intake-pressure dynamics and uses an aggressive PI controller to control the amount of EGR mass flow needed in order match the simulated intake pressure $\widehat{p}_{\text{im}}$ with the measured intake pressure p_{im}:

$$\frac{d}{dt}\widehat{p}_{\text{im}} = \frac{R \cdot \vartheta_{\text{im}}}{V_{\text{im}}} \cdot [\overset{*}{m}_{\text{air}} + \overset{*}{m}_{\text{egr,est}} - \overset{*}{m}_{\text{cyl}}] \tag{2.7}$$

$$\overset{*}{m}_{\text{egr,est}} = K_P \cdot (p_{\text{im}} - \widehat{p}_{\text{im}}) + K_I \cdot \int (p_{\text{im}} - \widehat{p}_{\text{im}}) dt \tag{2.8}$$

The fresh air mass flow $\overset{*}{m}_{\text{air}}$ is measured with a hot-film air-mass meter (HFM) mass-flow sensor. The intake temperature ϑ_{im} is also measured. The cylinder mass flow $\overset{*}{m}_{\text{cyl}}$ can be calculated from the intake density, the volumetric efficiency and the engine speed. The intake volume V_{im} and

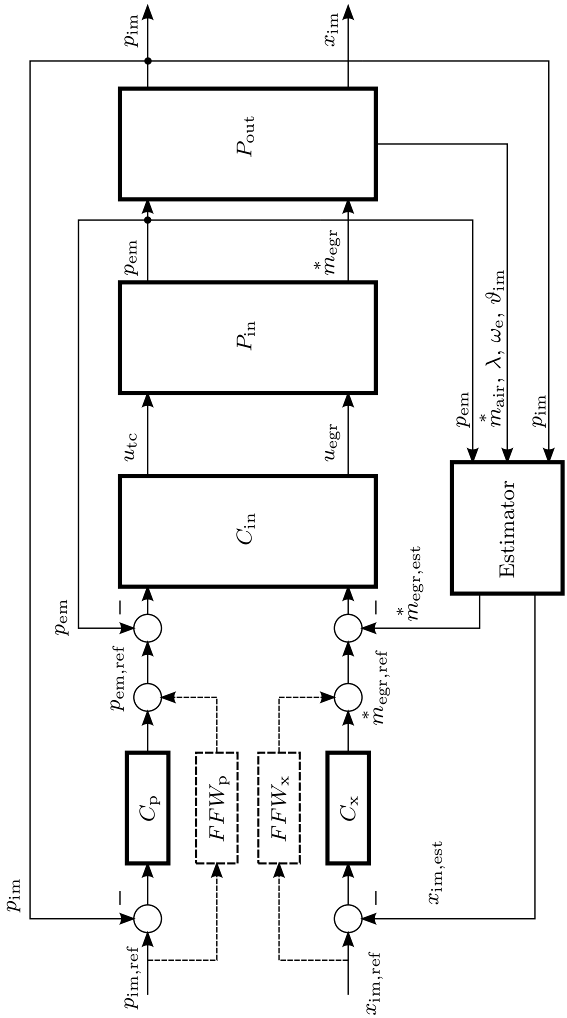

Figure 2.11: Cascaded control structure with the outer loop controllers for the intake pressure (C_{p}) and burnt-gas fraction (C_{x}), an optional feed-forward for these channels (FFW_{p} and FFW_{x}), the inner loop controller (C_{in}) and the estimator for the EGR-related signals.

the ideal gas constant of air R are assumed to be known. The high-gain controller is tuned to a bandwidth of $50\,{}^{\mathrm{rad}}/_{\mathrm{s}}$ for the TSWG engine and to $150\,{}^{\mathrm{rad}}/_{\mathrm{s}}$ for the SSVGT engine.

Intake burnt-gas fraction

The dynamics of the burnt-gas fraction are described by

$$\frac{d}{dt}x_{\mathrm{im}} = \frac{\vartheta_{\mathrm{im}} \cdot R}{p_{\mathrm{im}} \cdot V_{\mathrm{im}}} \cdot [\overset{*}{m}_{\mathrm{egr}} \cdot x_{\mathrm{egr}} - x_{\mathrm{im}} \cdot (\overset{*}{m}_{\mathrm{air}} + \overset{*}{m}_{\mathrm{egr}})], \tag{2.9}$$

with the burnt-gas fraction of the EGR, x_{egr}. Using the estimated EGR mass flow, the dynamics of the estimated burnt-gas fraction $\widehat{x}_{\mathrm{im}}$ can be simulated,

$$\frac{d}{dt}\widehat{x}_{\mathrm{im}} = \frac{\vartheta_{\mathrm{im}} \cdot R}{p_{\mathrm{im}} \cdot V_{\mathrm{im}}} \cdot [\overset{*}{m}_{\mathrm{egr,est}} \cdot x_{\mathrm{egr}} - \widehat{x}_{\mathrm{im}} \cdot (\overset{*}{m}_{\mathrm{air}} + \overset{*}{m}_{\mathrm{egr,est}})]. \tag{2.10}$$

The burnt-gas fraction of the EGR x_{egr} is identical to the one in the exhaust manifold x_{em}. Assuming lean combustion, it can be calculated from the measured air-to-fuel ratio λ_{em} using

$$x_{\mathrm{egr}} \approx x_{\mathrm{em}} = \frac{1 + \sigma_0}{1 + \lambda_{\mathrm{em}} \cdot \sigma_0}. \tag{2.11}$$

Since both estimators are based on the equations governing the dynamics of the intake manifold, they are independent of the turbocharger configuration. They are valid for all engines using only high-pressure EGR.

2.4.3 Controller description

In this section, the controllers for both subsystems (inner and outer loop) are presented. It is not necessary to use the controller types proposed here. The structural advantages of the cascaded controller are independent of the controllers used in the two loops. But the controllers proposed have certain properties that make them especially suitable for the respective problem.

Outer-loop controller

In Sec. 2.4.1 it was shown that the outer plant is almost completely decoupled by the closing of the inner loop. This fact allows the use of two

separate SISO controllers. The SISO controllers are implemented as PI controllers. Tuning of the controller parameters is a straightforward process that can even be carried out online on the engine test-bench.
The response of the control system can be improved by implementing a feed-forward controller for the two channels. For the channel $\overset{*}{m}_{\mathrm{egr}} \rightarrow x_{\mathrm{im}}$ the steady-state solution of the dynamics of the intake burnt-gas fraction can be used,

$$x_{\mathrm{im}} = \frac{\overset{*}{m}_{\mathrm{egr}} \cdot x_{\mathrm{egr}}}{\overset{*}{m}_{\mathrm{egr}} + \overset{*}{m}_{\mathrm{air}}}. \tag{2.12}$$

This leads to

$$\overset{*}{m}_{\mathrm{egr,ffw}} = \overset{*}{m}_{\mathrm{air}} \cdot \frac{x_{\mathrm{im,ref}}}{x_{\mathrm{egr}} - x_{\mathrm{im,ref}}}, \tag{2.13}$$

with the reference value for the intake burnt-gas fraction $x_{\mathrm{im,ref}}$, the burnt-gas fraction of the EGR x_{egr} calculated using Eq. (2.11), and the measured fresh-air mass-flow $\overset{*}{m}_{\mathrm{air}}$. Since this feed-forward controller is solely based on the inversion of the steady-state solution of the mixing dynamics of the intake manifold, it is independent of the turbocharger configuration. It is therefore valid for all engines using only high-pressure EGR.
For the channel $p_{\mathrm{em}} \rightarrow p_{\mathrm{im}}$, no such general feed-forward controller can be found, because it depends on the operating point of the turbochargers. For single-stage turbocharged configurations the torque balance of the shaft of the turbocharger can be used to calculate the necessary exhaust pressure for a given intake pressure and burnt-gas fraction [44]. For a two-stage turbocharged engine the torque balance has to be fulfilled for both turbochargers. To this author's knowledge, an explicit solution to the steady-state equations of such an engine has not been published as yet. However, the necessary exhaust pressure for a given intake pressure and burnt-gas fraction can be determined by measurement or simulation. The results can be stored in a lookup table, which is then used for static feed-forward control of this channel. Alternatively, an approximate feed-forward controller can be used,

$$p_{\mathrm{em,ffw}} = p_{\mathrm{im,ref}}. \tag{2.14}$$

The underlying assumption is that for a reasonably designed turbo charging system the exhaust and intake pressures, at least for part-load conditions, are approximately equal. While this may not be true for the entire operating range, it is a valid assumption that allows the use of feed-forward control even on a two-stage turbocharged engine.

Inner-loop controller

The inner plant contains a large number of the cross-couplings of the system. Therefore, the use of a model-based multiple-input multiple-output (MIMO) controller is the most suitable approach. The underlying model has to represent the influence of the physical actuators (u_{tc}, u_{egr}) on the outputs of the inner plant (p_{em}, $\overset{*}{m}_{\mathrm{egr}}$). To this end, a nonlinear engine model of the type used for the system analysis can be implemented[4]. The requirements for the controller of the inner loop are the following [70]: First, integral action is not necessary because a steady-state offset of the inner loop does not affect the performance of the outer loop. The outer loop has integral action, which compensates the steady-state offset of the inner loop. Integral action in the inner loop is even detrimental to the performance of the outer loop. It increases the phase lag of the inner loop, which leads to a reduction of the achievable bandwidth. Therefore, the controller of the inner loop should not have integral action. Second, the inner control loop has to have a higher bandwidth than the outer control loop. To prevent the necessity to slow down the outer loop, the inner control loop must be as fast as possible. However, it is limited in speed by the dynamics of the plant. Actuator dynamics and the pressure dynamics in the exhaust manifold limit the maximum achievable bandwidth. These specifications leave a narrow window for the crossover frequency of the loop gain. A MIMO controller whose bandwidth can be tuned precisely and directly is thus desirable. An H_∞ controller was chosen here because it can be tuned using frequency-domain specifications.

For the controller design, the plant has been augmented according to the S/KS/T scheme [23]. This scheme allows the specification of an upper bound for the sensitivity S_{e}, the complementary sensitivity T_{e} and the series compensator KS. The upper bounds for the sensitivities allow the bandwidth and the robustness of the control loop to be tuned. The series compensator (KS) is defined by

$$KS(s) = C(s) \cdot S_{\mathrm{e}}(s), \tag{2.15}$$

[4]A full engine model is not assumed to be necessary to represent the inner plant. The use of reduced models could be the topic of future research.

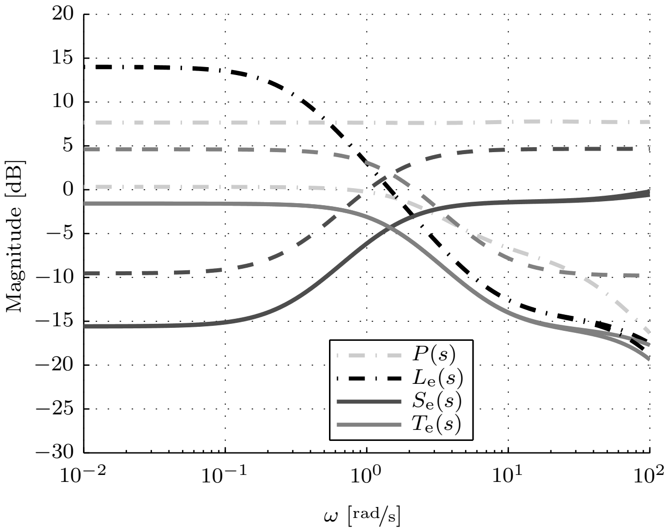

Figure 2.12: Singular values of the inner control loop. The upper bounds for the sensitivity and the complementary sensitivity are indicated by dashed lines, whereas the actual values are indicated by solid lines. The plant $P(s)$ and the loop gain $L_{\mathrm{e}}(s)$ are indicated by dash-dotted lines.

with the controller $C(s)$ and the sensitivity $S_{\mathrm{e}}(s)$. It can be used to limit the controller gain and the control action.

Figure 2.12 shows how the upper bounds for the sensitivities can be used to tune the bandwidth of the inner-loop controller for the SSVGT engine. In this case the desired bandwidth is 2 rad/s. This bandwidth is found to be a good compromise between speed and robustness. Although the linearized plant indicates that higher bandwidths are possible, unmodeled nonlinearities such as an actuator hysteresis caused by backlash limit the achievable bandwidth on the real system. The H_∞ controller automatically brings the maximum and minimum singular values of the loop gain so close together that in the plot they appear as a single line. Even strict specifications can thus be met, such as a narrow band for the crossover frequency of the loop gain. For comparison, a controller designed with the LTR loop-shaping technique [71] exhibits a crossover frequency band. While the width of this frequency band can be adjusted, the tuning parameters are based on the time domain rather than on the frequency domain.

The tuning process thus becomes unintuitive and work-intensive, and the compliance with tight specifications becomes hard or even impossible to achieve.
The tuning of the bandwidth of the H_∞ controller is also very straightforward. The upper limit of the sensitivity can be used to increase the bandwidth, whereas the upper limit of the complementary sensitivity can be used to reduce the bandwidth. If the corner frequencies of both upper bounds are chosen to be close to each other, a window for the crossover frequency of the loop gain can be created. The corner frequencies of the upper bounds thus can be shifted in order to shift the crossover frequency of the loop gain.

2.4.4 Tuning and calibration

Although the cascaded control structure incorporates additional feedback variables, the tuning process does not become more complex. As an alternative to the cascaded structure, the additional feedback signals could have been included by creating one centralized multivariable controller with four measurements and two control inputs. This would considerably increase the complexity of the tuning process because all channels have to be tuned simultaneously. Due to the separation of the cascaded controller into an inner and an outer controller, the tuning process can be carried out sequentially.
First, the controller for the inner loop is designed without taking the outer loop into account. The tuning has to be carried out offline since it involves the solution of the H_∞ control problem. For the inner control loop the focus is on achieving the maximum bandwidth possible. The inner loop can also be tested in isolation by manually supplying reference values. This process is illustrated in Fig. 2.13 where reference steps for the inner loop of the SSVGT engine are shown. The steady-state error that is present for both feedback signals is caused by the lack of integral action of the inner loop. Once the outer loop is added, the reference values are supplied by the outer-loop controller.
In order to tune the outer loop, the inner loop has to be closed. The tuning of the outer-loop controller can be carried out offline. The linear plant considered for controller design has to reflect the behavior of the outer plant given that the inner loop is closed, using the controller designed previously. This can be achieved by considering the series connection of

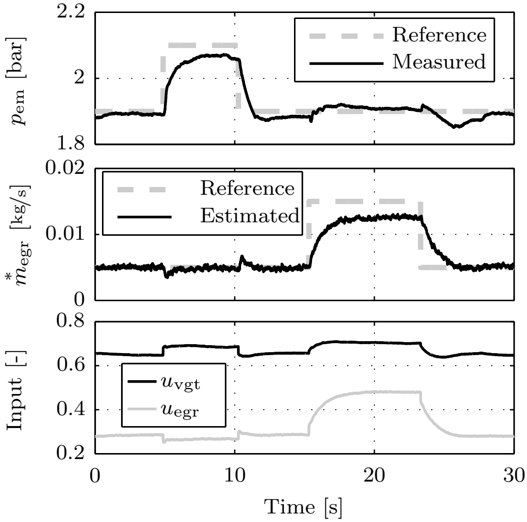

Figure 2.13: Measured step responses of the inner loop used for tuning of the inner-loop controller in isolation.

the linearized model of the idealized outer loop and the complementary sensitivity (i.e. the closed-loop transfer-function) of the inner loop. Using this linear model, loop-shaping techniques can be applied to tune the controllers. The bandwidth of the outer-loop controller should not be higher than half the bandwidth of the inner-loop controller (see Sec. 2.4.1) if the controller is to benefit from the reduction of phase lag that is inherent to cascaded control. As opposed to the inner loop, the outer loop can also be tuned online by adjusting the parameters of the two PI controllers during operation. This allows for a fast and straightforward final tuning of the behavior of the overall control system.

Similarly to other linear controllers, one set of controller parameters cannot be optimal for the entire operating range of the engine. Different operating points yield different mass flows, temperatures and pressures. As a result, the gains and the time constants of the plant change considerably and the controller has to be gain-scheduled. A system analysis for different operating points and a detailed description of gain scheduling techniques are beyond the scope of this thesis. However, the remainder of this section should serve to give a short overview of the most important

system properties and to suggest a way to implement gain scheduling.
While controller gains can vary up to a factor of ten for different operating points, with the exception of one channel, the sign of the gains do not change. The gains of the outer loop ($p_{\mathrm{em}} \rightarrow p_{\mathrm{im}}$, $\overset{*}{m}_{\mathrm{egr}} \rightarrow x_{\mathrm{im}}$) cannot change sign. An increase in exhaust pressure always increases the exhaust-gas enthalpy, the compressor power, and with it, the intake pressure. An increase in EGR mass flow always increases the intake burnt-gas fraction. The gains in the channels $u_{\mathrm{egr}} \rightarrow \{p_{\mathrm{em}}, \overset{*}{m}_{\mathrm{egr}}\}$ cannot change sign either. An opening of the EGR valve always decreases the exhaust pressure, and it always increases the EGR mass flow. The sign of the gain in the channel $u_{\mathrm{tc}} \rightarrow p_{\mathrm{em}}$ cannot change either. A closing of the WG/VGT always increases the exhaust pressure. The only location where a sign change can physically occur is the channel $u_{\mathrm{vgt}} \rightarrow \overset{*}{m}_{\mathrm{egr}}$ for an engine equipped with a VGT. This phenomenon has been discussed in Sec. 2.4.1. Analogously to the case of a constant operating point, the nonlinearity in this channel can be considered a disturbance, because the EGR valve exerts a much higher influence on the EGR mass flow than the VGT.
Gain scheduling of the PI controllers used in the outer loop is straightforward because depending on the operating point, the controller parameters can be interpolated from a lookup table. Gain scheduling of the multivariable controller of the inner loop is more challenging. Generally, the state variables of an H_∞ controller have no physical meaning. Since the state variables of two H_∞ controllers designed at different operating points do not have the same meaning, it is not possible to interpolate between the controller parameters of the two H_∞ controllers. There exist methods to directly design a gain-scheduled H_∞ controller [72]. However, they require that the system matrices of the linearized plant have an affine dependency on the operating point. Alternatively, good results can be obtained by reducing the H_∞ controller to order one. The reduced controller corresponds to a multivariable controller where every channel is a P controller with a roll-off. This step eliminates the ambiguity of the state variables and enables the interpolation of controller parameters from a lookup table.
Gain scheduling can then be implemented by interpolating the controller parameters for both the inner and the outer loop from operating-point dependent lookup tables.

2.5 Experimental results

In order to demonstrate the structural advantages of the cascaded control structure, the controller has been applied to two diesel engines, each of them running on a test bench. The setup of the engines and the test benches are described in Sec. 2.3. The experiments show that all three problems identified in Sec. 2.2 are dealt with successfully by the cascaded control structure:

1. The cascaded controller is a MIMO controller. The inner loop acts as a decoupler to the outer loop.

2. The cascaded controller shows a decreased sensitivity to the nonlinearity of the plant.

3. The cascaded controller shows a decreased sensitivity to the disturbances induced by changes of the operating point.

For a comparison of their performance, a conventional, non-cascaded controller has been implemented on the engines as well. It controls the same feedback variables as the outer loop of the cascaded controller (p_{im}, x_{im}). The term "conventional" refers to the fact that it does not have the key feature of the cascaded controller, which is the inner control loop for the additional feedback variables (p_{em}, $\overset{*}{m}_{\mathrm{egr}}$). The structure of the non-cascaded control loop is shown in Fig. 2.14. Because of the cross-couplings of the plant, the controller used for comparison is also a model-based MIMO controller. Analogously to the controller used in the inner loop, it was designed using the H_∞ method. However, the controller used for comparison has integral action because offset-free control is necessary.
In order to allow a fair comparison, the cascaded controller and the conventional controller have been tuned to have equal linear system properties, namely equal loop gains. First the conventional controller was tuned. Since the same H_∞ approach was used as for the inner loop controller (Sec. 2.4.3), the minimum and maximum singular values of the loop gain are very close together. This frequency response of the minimum and maximum singular values of the loop gain was then used as a reference for the tuning of the cascaded controller. The SISO controllers in the outer loop of the cascaded controller were tuned such that the loop gains of both channels would be equal to the reference furnished by the conventional

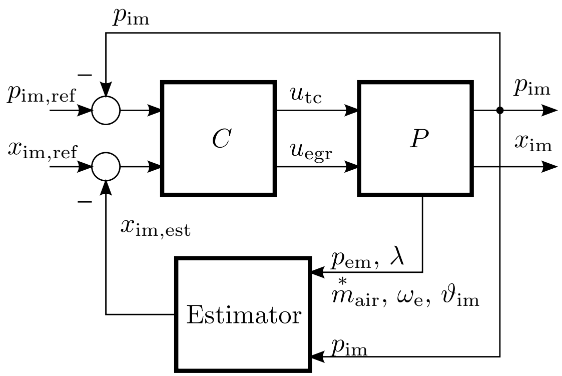

Figure 2.14: Control structure used for comparison.

controller. This tuning method is illustrated in Fig. 2.15, which depicts the loop gains of the resulting controllers for the SSVGT engine. Throughout the entire frequency range of interest the loop gains are equal. This tuning ensures that the comparison is fair and all advantages originate from the cascaded structure rather than from the tuning. For the same reason, feed-forward control and gain scheduling are deliberately omitted. Using both controllers, two types of experiments have been conducted:

- Reference steps for the air path at a constant operating point.
- Operating-point changes, where the reference values for the air path depend on the operating point and are obtained from a lookup table.

The results of these experiments are shown in the following sections.

2.5.1 Results obtained at a constant operating point

The experiments have been carried out with both engines. The following subsections describe the results obtained with the SSVGT engine and the TSWG engine, respectively.

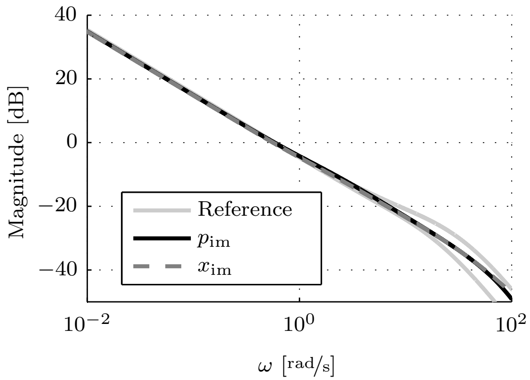

Figure 2.15: Singular values of the loop gain of the reference controller and the two SISO controllers of the outer loop of the cascaded controller for the SSVGT engine.

SSVGT engine

Figure 2.16 shows the experimental results of the SSVGT engine at a constant operating point. Figure 2.16(a) shows both the cascaded controller and the conventional controller for reference steps of the intake pressure at a constant operating point. Figure 2.16(b) shows reference steps of the intake burnt-gas fraction. The reaction of the two control systems to the reference steps shows that both controllers have been tuned equally.

During reference steps of the intake pressure, the intake burnt-gas fraction is disturbed very little for both controllers. The same is true vice versa for steps of the intake burnt-gas fraction, however there the cascaded controller shows a slightly smaller disturbance of the intake pressure than the conventional controller does. Their behavior during the steps shows that both controllers can handle the cross-couplings of the system. The decoupling effect of the inner loop is also evident when the behavior of the feedback variables of the inner loop are compared during reference steps of the outer loop. In Fig. 2.16(b) the reference value of the intake pressure is constant. During reference steps of the burnt-gas fraction, the EGR mass flow changes strongly, whereas the exhaust pressure remains almost constant.

The decreased sensitivity to the nonlinearity of the plant can be observed in the reference steps of the burnt-gas fraction (Fig. 2.16(b)). During the

first small step (t=10 s) both controllers behave similarly. At the second step (t=23 s), the conventional controller shows difficulties reaching the set point. During this step the EGR valve has to move from a position that is almost closed to a position that is almost fully opened. During the opening of the valve, the mass flow increases and the control authority of the valve is reduced. In order to compensate for the loss of control authority, the controller should open the EGR valve more aggressively. The cascaded controller can detect and compensate the effect of this nonlinearity because it is part of the fast inner control loop. The conventional controller can only use integral action to compensate for the nonlinearity of the system. This leads to the slow, almost linear opening of the EGR valve between t=30 s and t=36 s. The same unsatisfactory behavior at high EGR mass flows can be observed at the third reference step (t=36 s).
Figures 2.16(a) and 2.16(b) also show the importance of good actuator dynamics for the cascaded controller. During steady-state conditions (t< 10 s), the position of the VGT oscillates slightly. This behavior is caused by backlash in the VGT actuator. Due to its high bandwidth, the performance of the inner loop is limited by the actuator dynamics. The inner loop has been tuned such that the backlash has no significant influence on the performance of the controller. Improved actuator dynamics would increase the achievable bandwidth of the inner loop, which would improve the performance of the cascaded controller even further. In contrast, the performance of the conventional controller cannot be influenced by improvements of the actuator dynamics, because it is limited in bandwidth mainly by the rotational dynamics of the turbocharger.

TSWG engine

Figure 2.17 shows the experimental results of the TSWG engine at a constant operating point. The results are very similar to those obtained with the SSVGT engine. Due to this similarity, the discussion of the results obtained with the TSWG engine is kept rather short and only the most important aspects are pointed out.
The reaction of the two controllers shows that they have been tuned equally. Both controllers suppress the cross-couplings in the system, such that the channel with a constant reference value is disturbed only marginally during the reference steps of the other channel. However, during the steps of the intake burnt-gas fraction, the cascaded controller shows

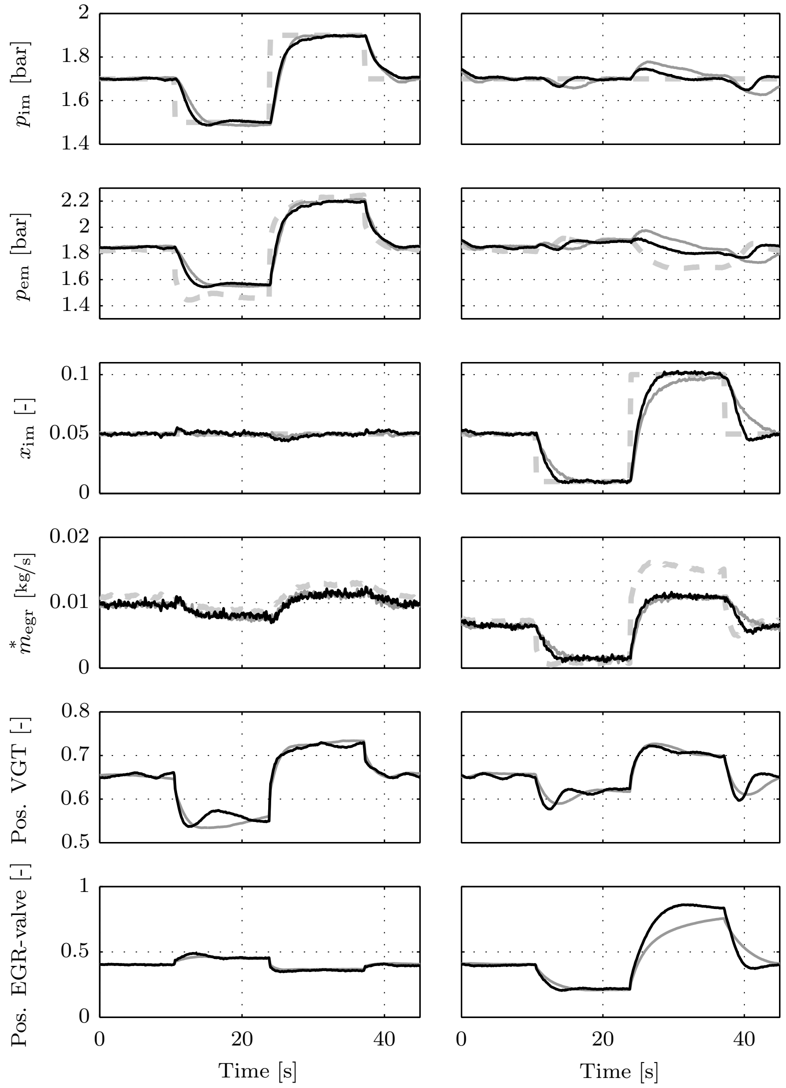

(a) Reference steps of the intake pressure

(b) Reference steps of the intake burnt-gas fraction

Figure 2.16: Comparison of the cascaded controller (black) and the conventional controller (solid gray) for reference steps (dashed gray) of the air path of the SSVGT engine.

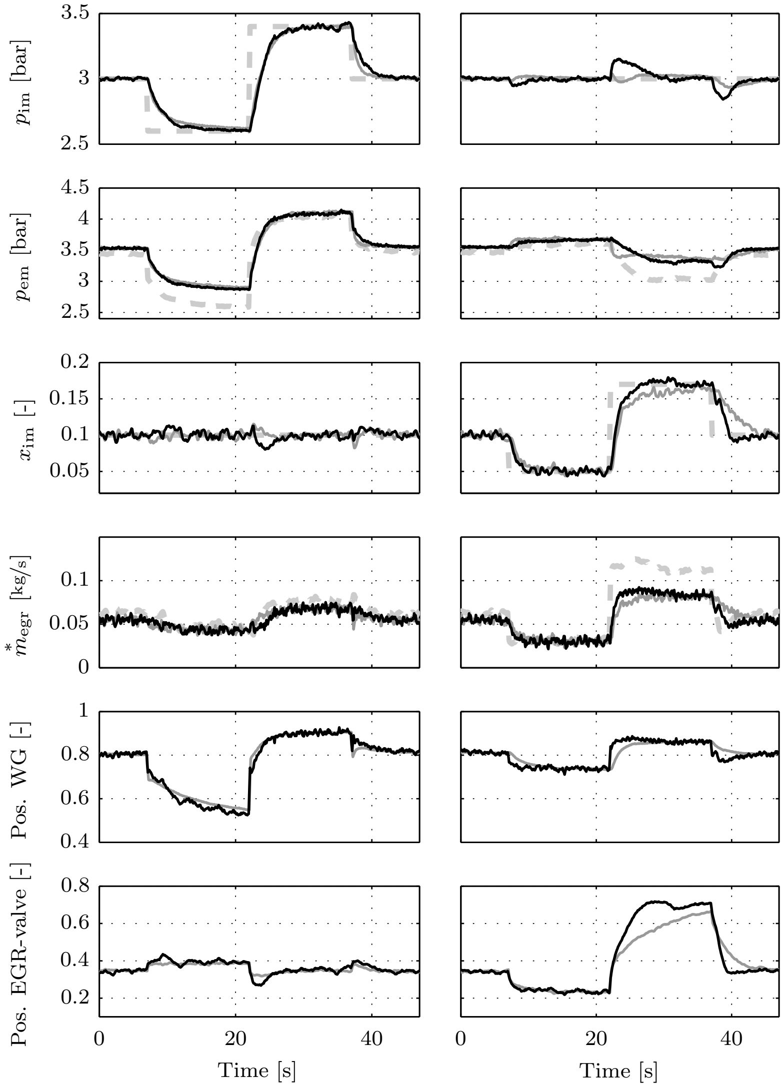

(a) Reference steps of the intake pressure

(b) Reference steps of the intake burnt-gas fraction

Figure 2.17: Comparison of the cascaded controller (black) and the conventional controller (solid gray) for reference steps (dashed gray) of the air path of the TSWG engine.

a slightly larger disturbance of the intake pressure than the conventional controller does. Again, the improved handling of the nonlinearity of the system is evident. For the large reference step of the intake burnt-gas fraction (t=22 s), the cascaded controller detects and compensates for the decreased control authority of the EGR valve at large openings. The conventional controller fails to do so and consequently reaches the set point only very slowly. The same behavior can be observed for the subsequent step decrease of the burnt-gas fraction reference (t=37 s).
There are also differences to the results obtained with the SSVGT engine. The actuator of the waste gate is not afflicted with backlash, as it was the case for the VGT actuator of the SSVGT engine. Therefore, the slight, slow oscillation of the turbo-charger control input, which was observed for the SSVGT engine, does not occur. However, the measurement signals of the TSWG engine are afflicted with considerable noise because they are not processed in a series-production ECU, as it was the case for the SSVGT engine. The EGR-related signals ($\overset{*}{m}_{\mathrm{egr}}$, x_{im}) are affected most by the noise. The noise of the feedback signals causes the slight ripple in the control inputs of both actuators. For a series production engine with state-of-the-art signal processing, this effect is not an issue.

2.5.2 Results for changes of the operating point

The experiments have been carried out with both engines. The following subsections describe the results obtained with the SSVGT engine and the TSWG engine, respectively.

SSVGT engine

Figure 2.18(a) shows a comparison of the cascaded controller and the conventional controller during fast changes of the operating point of the SSVGT engine. Figure 2.18(b) shows an excerpt of that measurement in more detail. The operating point is indicated by the engine speed (N_{e}) and the injected fuel volume per cylinder (V_{inj}). The controllers are the same as those used in the experiments described in Sec. 2.5.1. Both controllers show a similar behavior for the burnt-gas control. The cascaded controller is faster, which is due to its improved handling of the nonlinearity of the system. The performance of the intake pressure control differs strongly for the two controllers. The conventional controller overshoots

for every step. This effect is due to the disturbance of the air path by the sudden change in exhaust-gas mass flow and temperature. The conventional controller can react to the disturbance once it has affected the main feedback variables (p_{im}, x_{im}). The cascaded controller detects the disturbance as soon as it affects the feedback variables of the inner loop (p_{em},$\overset{*}{m}_{\mathrm{egr}}$), and it reacts quickly with the high-bandwidth controller of the inner loop. Due to the faster control of the burnt-gas fraction and the more robust control of the intake pressure, the cumulated control error of the conventional controller is reduced by the cascaded controller by 25% for the intake burnt-gas fraction and by 15% for the intake pressure.
Furthermore, the conventional controller's overshooting of the intake pressure is critical for several reasons. First, an overshoot of the intake pressure leads to an unwanted high cylinder charge. At very high loads this can cause a violation of the maximum allowable cylinder pressure, leading to possibly fatal damage of the engine. Second, a controller should exhibit similar behavior patterns for air-path reference steps in a constant operating point and for operating-point changes. The air-path controller can then be tuned at a constant operating point by applying reference steps for the air path. While the conventional controller shows robust behavior at a constant operating point, it significantly overshoots the intake pressure as soon as the operating point is changed, necessitating further tuning at changes of the operating point. In contrast, the cascaded controller shows the same robust behavior in both cases, which considerably simplifies the tuning process.

TSWG engine

Figure 2.19 shows the experimental results obtained with the TSWG engine. For these experiments, the same controllers as those used in the experiments described in Sec. 2.5.1 have been used. For the TSWG engine, no reference map for the burnt-gas fraction was available. Therefore, a constant reference value was used.
Both controllers show a similar behavior for the burnt-gas control. However, the lack of reference steps limits the advantage that the cascaded controller can have compared to the conventional controller. As for the SSVGT engine, the most significant difference between the controllers can be observed for the intake pressure control. The conventional controller generally overshoots the intake pressure, whereas the cascaded controller

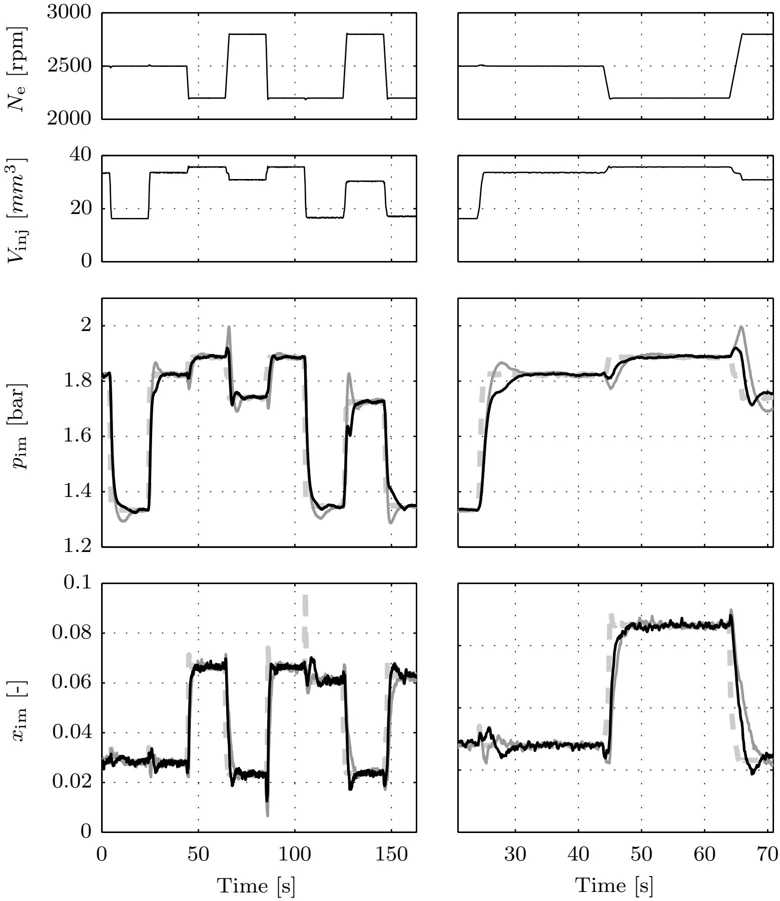

(a) Full view (b) Detailed view

Figure 2.18: Comparison of the cascaded controller (black) and the conventional controller (solid gray) for changes of the operating point of the SSVGT engine. Reference values are shown in dashed gray. Operating point indicated by engine speed (N_e) and injected fuel volume per cylinder (V_{inj}).

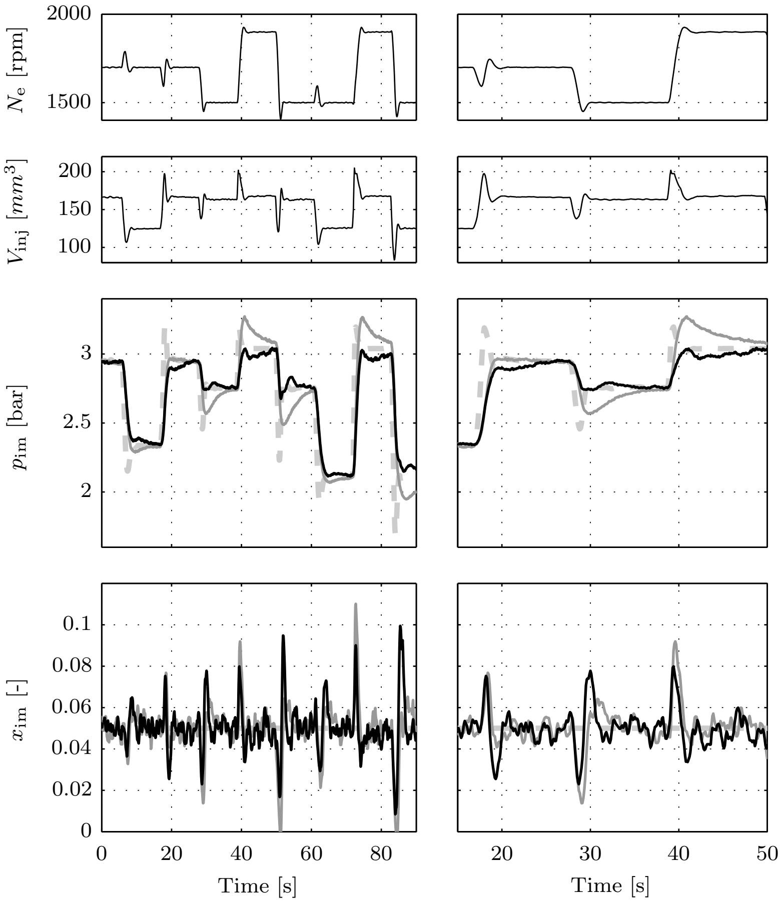

(a) Full view

(b) Detailed view

Figure 2.19: Comparison of the cascaded controller (black) and the conventional controller (solid gray) for changes of the operating point of the TSWG engine. Reference values are shown in dashed gray. Operating point indicated by engine speed (N_e) and injected fuel volume per cylinder (V_{inj}).

does not exhibit this behavior. The advantage which this property brings was already discussed in the context of the results obtained with the SSVGT engine. The cumulated control error of the conventional controller is reduced by the cascaded controller by 25% for the intake pressure and by 3% for the intake burnt-gas fraction.

2.5.3 Discussion

The experimental comparison with a conventional controller of equal tuning shows the advantages of the cascaded approach. The measurements taken at a constant operating point show its improved handling of the nonlinearity of the plant. At changes of the operating point, the measurements taken show its improved suppression of disturbances. The experiments thus confirm the theoretical advantages outlined in Sec. 2.4.1.

These experimental results are significant because both controllers are tested under identical conditions. Both controllers use linear feedback without feed-forward or gain scheduling. The same controller type is used for both multivariable controllers, and the overall control systems are tuned to yield matching frequency responses. Therefore, the measurement results show that the improvements are not caused by detail changes, such as improved tuning or a different controller type. They are caused solely by a control structure that exploits the structure of the plant. The improvements in performance are shown to be inherent to the cascaded control approach. Importantly, these results have been obtained for two engines of different size and air-path configuration, which confirms the claim that the cascaded control structure is beneficial for a wide range of engines.

It might be argued that other measures, such as fine-tuning of the controller or feed-forward could be used to improve the performance of the conventional controller without the need to change the controller structure. However, the time required to fine-tune the conventional controller until it shows a similar performance as the cascaded controller should be taken into account as well. Especially when gain scheduling requires the controller to be tuned at several different operating points, the amount of time required to fine-tune the conventional controller is considerable. The fact that the behavior of the conventional control loop changes whenever the operating point is changed quickly renders the tuning process quite unmanageable. Due to its inherent advantages, the cascaded controller requires less tuning to achieve a good performance. Although two loops have to be tuned, the tuning process is straightforward because the loops can be tuned sequentially. Therefore, the cascaded control structure represents a solid framework for the development of air-path controllers.

2.6 Conclusion and outlook

A novel cascaded control structure for the air path of a diesel engine has been developed. It addresses the difficulties that the plant and aggressive driving cycles impose on the control problem. The control structure can be applied to a wide range of diesel engines. This is shown experimentally and in an analysis of the mean value models of two very different diesel engines. The tuning of the cascaded controller is straightforward because it can be carried out sequentially and the controllers of the main feedback variables can even be tuned online at the test bench.
The control strategy is well suited to handling the cross-couplings of the system. It exhibits a low sensitivity to the nonlinearity of the plant and to disturbances of the air path caused by operating-point changes. These advantages are shown in an experimental comparison with a conventional controller of equal tuning. For the comparison, two engines of different size and air-path configuration were used.
Further research could focus on the possibility of using reduced engine models to derive the model-based inner-loop controller. The fact that the inner plant comprises only a subsystem of the engine suggests that this approach should be possible. Another promising topic is the analysis of engine configurations with LP EGR or two EGR loops (HP and LP). For LP EGR, certain system properties should be similar, such as the time-scale separation and the nonlinearities. However, because the LP EGR is fairly decoupled from the turbocharging system and the exhaust pressure [67], the coupling of the system and the disturbance by changes of the operating point should be less pronounced. A simplified version of the cascaded controller, with SISO control for the inner loop, might be well suited for the control of engines with LP EGR. Furthermore, the fact that the LP EGR loop is fairly decoupled from the rest of the system indicates that the cascaded control strategy, which is designed for HP EGR, could be extended to handle even dual loop EGR. Finally, it could be analyzed whether the cascaded control structure could be used to control air paths with more than two turbo chargers, such as the one presented in [73].

Chapter 3

Model-Based Adaptation of the Fuel Injection and the EGR

The emissions of diesel engines are harmful to both humans and the environment. Especially during load steps, the particulate emissions can be excessive. This effect is due to the lack of fresh air caused by the rotational dynamics of the turbocharger. One way to deal with this problem is to seek improvements in the control of the turbo charger(s) (see chapter 2). When this option has been exhausted, a further possibility is the model-based limitation of the injected fuel mass based on the estimated cylinder charge. However, this method impairs the torque generation and consequently the drivability. Furthermore, the EGR can be reduced in order to supply more exhaust gas to the turbine and to facilitate a faster acceleration of the turbocharger. However, this method leads to increased NO_x emissions. Therefore, there exists a trade-off between the drivability and the pollutants emitted during a load step.

In this chapter, a method for the combined, model-based adaptation of the injection and the EGR is presented. It is based on a dynamic estimation of the cylinder charge. The equations used for the estimator need to be consistent with the ones used for the model-based injection reduction. Otherwise, the injection reduction will not be accurate. An extension to the estimator which resolves that issue is presented. The proposed combined injection and EGR limiter is validated with measurements on a test bench. These measurements show how the tuning parameters of the injection and EGR limiter can be used to influence the trade-off between transient emissions and drivability during a load step.

The content of this chapter is based on [31]. Two figures (Figs. 3.4 and 3.7) and their discussion have been added.

3.1 Introduction

Due to their high fuel efficiency, diesel engines are used in a wide range of applications. However, their emissions (nitrogen oxide (NO_x) and particulate matter (PM)) are harmful to both humans and the environment. Consequently, emission legislation is becoming increasingly stringent with the introduction of transient test cycles and ever lower emission limits.
A widely used technology for reducing NO_x emissions is the exhaust-gas recirculation (EGR). Since it increases the mass of the cylinder content and thereby its heat capacity, it lowers the combustion temperatures. It also decreases the oxygen concentration of the aspirated gas mixture. Since high combustion temperatures and high oxygen concentrations are the main conditions for the production of NO_x [4], the introduction of EGR decreases the NO_x emissions. On the other hand, this reduction of the oxygen concentration and the air-to-fuel ratio (AFR) is beneficial for the formation of particulate matter. To compensate for this effect, turbocharging is used to increase the fresh-air charge and the oxygen concentration. However, the turbochargers and the EGR introduce noticeable dynamics to the air path.
The control of the turbocharger and the EGR is carried out by the air-path controller. The air-path control for diesel engines has been the subject of research for the past two decades. A special focus has been placed on engines equipped with a variable-geometry turbine (VGT) and an EGR. A good introduction can be found in chapter 2 and in [35, 14, 36, 37, 28]. The set points for the air-path controller are chosen such that a compromise between NO_x emissions, PM emissions, and fuel consumption is found for steady-state operation.
Due to the dynamics of the air path, the air-path controller cannot follow the set points perfectly during transients. This deviation will lead to emissions that differ strongly from the emissions occurring during steady-state operation. Most notably, the rotational dynamics of the turbocharger lead to a lack of fresh air during load steps. This lack of fresh air and the resulting low air-to-fuel ratios lead to high PM emissions, unless the fuel injection is limited in order to account for the insufficient amount of fresh air available. The implementation of such so-called "smoke limiters" has been the state of the art for several years [14]. However, the limited fuel quantity leads to a limitation of the torque the engine can deliver. As-

suming that drivability is the possibility to deliver the torque desired by the driver, this limitation causes a reduction of the drivability. Smoke limiters therefore introduce a trade-off between drivability and PM emissions. Limiting the transient fuel injection strongly leads to low PM emissions and bad drivability. The same is true vice versa for no limitation. However, the performance of a smoke limiter is limited by the accuracy of the estimation of the cylinder charge.

The lack of fresh air caused by the rotational dynamics of the turbocharger is increased even more by the use of EGR. The exhaust gas that is recirculated cannot be used to drive the turbine, which leads to an even slower acceleration of the turbocharger and a more severe lack of fresh air. One way to improve the transient response is to reduce the EGR during transients in order to facilitate a faster acceleration of the turbocharger. This behavior can be achieved by controlling the air-to-fuel ratio using the EGR valve [26], such that the low air-to-fuel ratios occurring during a tip-in lead to a closing of the EGR valve. Alternatively, low air-to-fuel ratios can be predicted and the EGR valve can be closed before they occur. However, the reduction of the EGR increases the NO_x emissions, leading to a trade-off between drivability and NO_x emissions.

In this chapter, a novel combined, model-based injection and EGR limiter is presented. It is based on a dynamic estimation of the intake manifold burnt-gas fraction. In order to obtain an estimate of the burnt-gas fraction which can be used for injection control, the estimator has to incorporate the injected fuel mass. An estimator which is based on the measurement of the fresh-air mass-flow and the air-to-fuel ratio is extended in order to take into account the injected fuel mass. The injection and EGR limiter is independent of the air-path controller and can be implemented in addition to an existing air-path control structure. It has two tuning parameters to adjust the level of intervention. The proposed method is validated with measurements on a production-type automotive engine on a test bench. These measurements show the effect that the tuning parameters have on the drivability and the transient emissions.

3.2 Problem formulation

The system assumed here is a turbocharged diesel engine equipped with high pressure EGR. The turbine load may be controlled using a waste gate

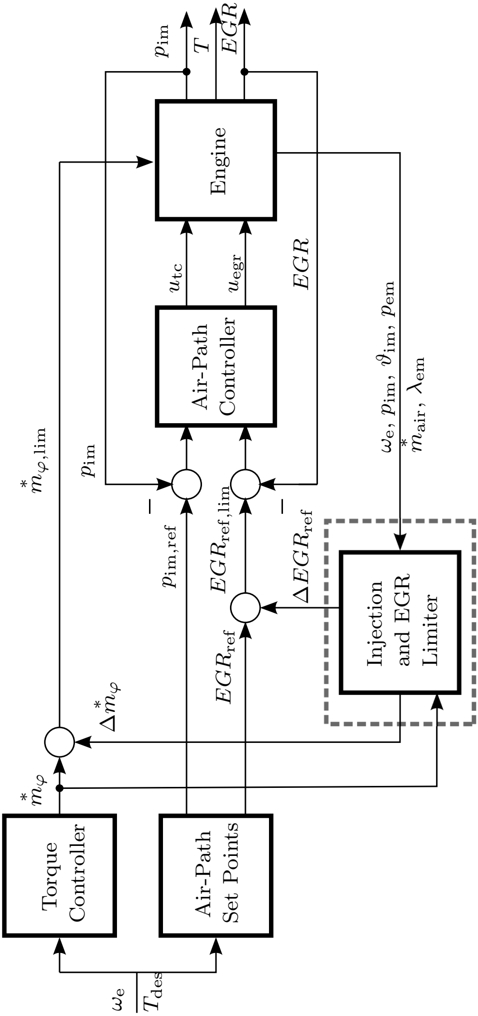

Figure 3.1: Simplified control structure of a diesel engine. The injection and EGR limiter is highlighted.

or a variable-geometry turbine. Figure 3.1 shows a simplified overview of the control structure. The control inputs for the turbo charger and the EGR valve (u_{tc} and u_{egr}) are provided by an air-path controller which controls the intake pressure p_{im} and the EGR to the given set points. The second feedback signal (EGR) is deliberately chosen to be unspecific. Almost all air-path controllers use the intake pressure as a first feedback variable, whereas different signals can be chosen for the second feedback variable. Among others, valid choices are the fresh-air mass flow [37], the AFR [49], the estimated fresh-air charge [44] or the estimated burnt-gas fraction [51, 28]. The torque controller calculates the injected fuel mass-flow $\overset{*}{m}_{\varphi}$ as a function of the desired torque T_{des} and the engine speed ω_{e}. The air-path controller, the associated set points and the torque controller are assumed to be available.

The goal of the injection and EGR limiter is to use the estimated cylinder charge to detect transients which are too fast for the air-path controller to follow. In that case, the fuel mass flow has to be reduced to the value $\overset{*}{m}_{\varphi,\mathrm{lim}}$ in order to prevent excessive PM emissions. Simultaneously, the EGR has to be reduced in order to improve the acceleration of the turbocharger. Because the air path of a diesel engine is highly nonlinear, coupled, and sensitive to operating-point changes, it is not advisable to manipulate the EGR valve directly. Furthermore, a direct manipulation of the EGR valve necessitates anti-windup and bumpless-transfer measures, which may require an adaptation of the air-path controller. Instead, the reference value for the EGR is reduced to the value $EGR_{\mathrm{ref,lim}}$. That way, the injection and EGR limiter can work independently of the air-path controller. This independence brings the benefit of a high flexibility to deal with various types of air-path controllers.

3.3 Experimental facility

The engine used for the measurements is a production-type automotive engine equipped with a VGT and high pressure EGR. An overview of the specifications of the engine is given in Table 3.1. For the experiments, the standard engine control unit (ECU) was partly bypassed using an ETAS ES910 rapid control prototyping module. The air-path controller of the ECU was fully bypassed. In its place, an experimental air-path controller was used (see chapter 2). It uses the intake pressure p_{im} and burnt-gas fraction x_{im} as feedback signals. The intake burnt-gas fraction is defined by

$$x_{\mathrm{im}} = \frac{m_{\mathrm{bg,im}}}{m_{\mathrm{bg,im}} + m_{\mathrm{air,im}}}, \tag{3.1}$$

Table 3.1: Specifications of the engine used for the experiments

Number of cylinders	6 cylinders
Displacement	2,987 cm^3
Power	160 kW
Turbocharging	Single stage VGT
EGR	High pressure

with the mass of burnt gas and air in the intake manifold, $m_{\text{bg,im}}$ and $m_{\text{air,im}}$, respectively. These feedback signals have been chosen because they are closely linked to the cylinder charge. The intake burnt-gas fraction cannot be measured and is estimated instead. The estimator used is presented in Sec. 3.4.3.
Furthermore, the torque controller was bypassed such that the ECU value of the desired injected fuel volume can be adapted before being sent to the injection controller. This bypass of the fuel injection was implemented in such a way that the synchronization of the data acquisition with the crank angle which is carried out by the ECU remains intact. All other ECU functionalities remained active. The NO_x emissions were measured using a Continental Smart NO_x Sensor. The PM emissions were measured using an AVL Micro Soot Sensor. Both sensors were located downstream of the turbine.

3.4 Controller description

The injection and EGR limiter is active during transients in which a lack of fresh air occurs because they are too fast for the air-path controller to follow. Using an estimate for the cylinder charge, the reduction of the injected fuel mass and the EGR can be determined. The injection limiter is described in Sec. 3.4.1. The EGR limiter is described in Sec. 3.4.2, while Sec. 3.4.3 explains the estimator for the intake burnt-gas fraction which is used to determine the cylinder charge.

3.4.1 Injection limiter

The injection limiter has to reduce the amount of fuel injected such that excessive PM emissions are prevented. The PM emissions are strongly linked to the normalized value of the AFR λ,

$$\lambda = \frac{m_{\text{air,comb}}}{m_{\text{fuel,comb}} \cdot \sigma_0}, \tag{3.2}$$

with the mass of air and fuel taking part in the combustion, $m_{\text{air,comb}}$ and $m_{\text{fuel,comb}}$, and the stoichiometric AFR σ_0,

$$\sigma_0 = \left.\frac{m_{\text{air,comb}}}{m_{\text{fuel,comb}}}\right|_{\text{stoich.}} . \tag{3.3}$$

Therefore, it is meaningful to define a fixed lower limit for the AFR[1]. Assuming the cylinder charge to be known, the maximum allowable amount of fuel to be injected for a given lower limit of the AFR can be calculated. In order to derive that equation, first the calculation of the AFR for a given cylinder charge and amount of fuel injected is considered.

The AFR can be calculated from the burnt-gas fraction after combustion x_{comb}, which is defined by

$$x_{\text{comb}} = \frac{m_{\text{bg,ac}}}{m_{\text{bg,ac}} + m_{\text{air,ac}}}, \tag{3.4}$$

with the mass of burnt gas and air after combustion, $m_{\text{bg,ac}}$ and $m_{\text{air,ac}}$, respectively. The burnt-gas fraction after combustion is linked to the normalized AFR λ and the stoichiometric AFR σ_0 by

$$x_{\text{comb}} = \frac{1 + \sigma_0}{1 + \lambda \cdot \sigma_0}. \tag{3.5}$$

This relationship can be inverted to yield

$$\lambda = \frac{1 - x_{\text{comb}} + \sigma_0}{\sigma_0 \cdot x_{\text{comb}}}. \tag{3.6}$$

Assuming a lean combustion, for a given intake burnt-gas fraction x_{im}, cylinder mass-flow $\overset{*}{m}_{\text{cyl}}$, and fuel mass-flow $\overset{*}{m}_{\varphi}$, the burnt-gas fraction after combustion is given by

$$x_{\text{comb}} = \frac{x_{\text{im}} \cdot \overset{*}{m}_{\text{cyl}} + (1 + \sigma_0) \cdot \overset{*}{m}_{\varphi}}{\overset{*}{m}_{\text{cyl}} + \overset{*}{m}_{\varphi}}. \tag{3.7}$$

[1]In the following, the term AFR refers to the normalized AFR unless indicated otherwise.

Using (3.7) and (3.6), the AFR λ can be calculated from the intake burnt-gas fraction, the cylinder mass-flow and the injected fuel mass-flow. This relationship can be inverted to yield the maximum allowable amount of fuel injected $\overset{*}{m}_{\varphi,\mathrm{lim}}$ for a given minimum allowable AFR λ_{min} and the current intake burnt-gas fraction and cylinder mass-flow,

$$x_{\mathrm{comb,max}} = \frac{1+\sigma_0}{1+\lambda_{\mathrm{min}}\cdot\sigma_0} \tag{3.8}$$

$$\overset{*}{m}_{\varphi,\mathrm{lim}} = \frac{\overset{*}{m}_{\mathrm{cyl}}\cdot(x_{\mathrm{comb,max}}-x_{\mathrm{im}})}{1+\sigma_0-x_{\mathrm{comb,max}}}. \tag{3.9}$$

The intake burnt-gas fraction x_{im} can be estimated (see Sec. 3.4.3), and the cylinder mass-flow $\overset{*}{m}_{\mathrm{cyl}}$ can be calculated using a model for the volumetric efficiency η_{vol} [22],

$$\overset{*}{m}_{\mathrm{cyl}} = \frac{p_{\mathrm{im}}}{R\vartheta_{\mathrm{im}}}\cdot\frac{V_d\cdot\omega_{\mathrm{e}}}{4\pi}\cdot\eta_{\mathrm{vol}}(\omega_{\mathrm{e}},p_{\mathrm{im}},p_{\mathrm{em}}). \tag{3.10}$$

Figure 3.2 shows several identical load steps using different values for λ_{min}. For every value of λ_{min}, the injected fuel volume is limited accordingly. The minimum values of the measured AFR are always slightly higher than the specified minimum value λ_{min}. This effect is caused by the fact that the AFR λ_{em} which is measured in the exhaust manifold is not equal to the AFR λ of the combustion. By measuring λ_{em} instead of λ, the time delay caused by the cyclic operation of the engine and the mixing dynamics of the exhaust manifold are added to the measurement result. Although the measured AFRs do not reach the allowed minimum, the actual AFRs of the combustion are lower and closer to the allowed limit.

3.4.2 EGR limiter

In order to improve the transient response of the turbocharger, the EGR can be reduced. Such an EGR reduction is only necessary when low AFRs are predicted. Therefore, the EGR reduction is activated when the injection reduction is active. The severity of the transient can be judged by the difference between the minimum allowable AFR λ_{min} and the AFR that is predicted to occur if the injection is not limited λ_{pred}. The latter can be calculated using (3.7) and (3.6). Because the second feedback variable of the air-path controller of the engine considered is the intake burnt-gas fraction, the reference value for this signal is adapted. The reduction of the

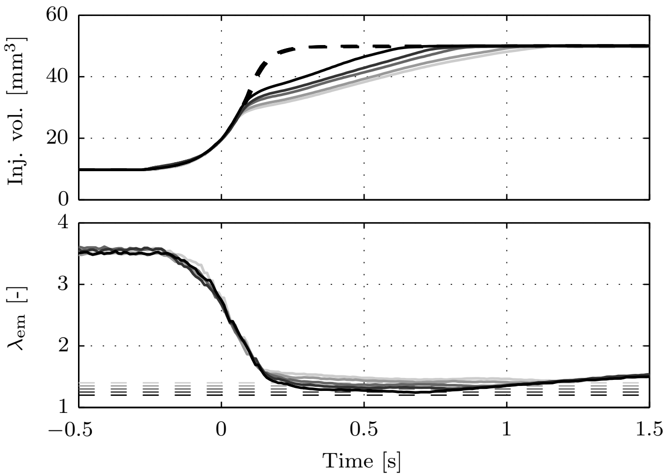

Figure 3.2: Transient behavior of the injection limiter for a load step using different values for λ_{min} (shown dashed in the lower plot).

reference value (if $\lambda_{\text{pred}} < \lambda_{\text{min}}$) is chosen to be proportional to the difference between the minimum allowable AFR and the AFR that is predicted without an injection reduction,

$$x_{\text{im,ref,lim}} = x_{\text{im,ref}} - K_{\text{egr}} \cdot (\lambda_{\text{min}} - \lambda_{\text{pred}}). \tag{3.11}$$

The parameter K_{egr} can be used to tune the level of intervention. For feedback variables other than the intake burnt-gas fraction, formulations similar to the linear form shown in (3.11) can be used.

3.4.3 Intake burnt-gas estimator

The injection and EGR limiter is only active during transients. It is thus crucial that a dynamic estimation of the cylinder charge is used. Because the cylinder charge is determined by the intake pressure and the burnt-gas fraction, it is sufficient to measure the former and estimate the latter. The burnt-gas fraction can be estimated using a measurement of the fresh-air mass-flow and the air-to-fuel ratio together with an estimate of the cylinder mass flow [74]. Assuming an isothermal receiver, the equations governing the dynamics of the intake-manifold pressure and burnt-gas fraction are

$$\frac{d}{dt}p_{\mathrm{im}} = \frac{R \cdot \vartheta_{\mathrm{im}}}{V_{\mathrm{im}}} \cdot [\overset{*}{m}_{\mathrm{air}} + \overset{*}{m}_{\mathrm{egr}} - \overset{*}{m}_{\mathrm{cyl}}] \tag{3.12}$$

$$\frac{d}{dt}x_{\mathrm{im}} = \frac{\vartheta_{\mathrm{im}} \cdot R}{p_{\mathrm{im}} \cdot V_{\mathrm{im}}} \cdot [\overset{*}{m}_{\mathrm{egr}} \cdot x_{\mathrm{egr}} - x_{\mathrm{im}} \cdot (\overset{*}{m}_{\mathrm{air}} + \overset{*}{m}_{\mathrm{egr}})]. \tag{3.13}$$

The dynamics of the estimator are given by

$$\frac{d}{dt}\widehat{p}_{\mathrm{im}} = \frac{R \cdot \vartheta_{\mathrm{im}}}{V_{\mathrm{im}}} \cdot [\overset{*}{m}_{\mathrm{air}} + \widehat{\overset{*}{m}}_{\mathrm{egr}} - \overset{*}{m}_{\mathrm{cyl}}] \tag{3.14}$$

$$\frac{d}{dt}\widehat{x}_{\mathrm{im}} = \frac{\vartheta_{\mathrm{im}} \cdot R}{p_{\mathrm{im}} \cdot V_{\mathrm{im}}} \cdot [\widehat{\overset{*}{m}}_{\mathrm{egr}} \cdot x_{\mathrm{egr}} - \widehat{x}_{\mathrm{im}} \cdot (\overset{*}{m}_{\mathrm{air}} + \widehat{\overset{*}{m}}_{\mathrm{egr}})] \tag{3.15}$$

$$\widehat{\overset{*}{m}}_{\mathrm{egr}} = K_P \cdot (p_{\mathrm{im}} - \widehat{p}_{\mathrm{im}}) + K_I \cdot \int (p_{\mathrm{im}} - \widehat{p}_{\mathrm{im}}) dt. \tag{3.16}$$

The estimated EGR mass flow $\widehat{\overset{*}{m}}_{\mathrm{egr}}$ is calculated using an input estimator [69]. It simulates the intake-pressure dynamics (3.14) and uses an aggressive PI controller (3.16) to control the amount of EGR mass flow needed in order match the simulated intake pressure $\widehat{p}_{\mathrm{im}}$ with the measured intake pressure p_{im}. The estimated EGR mass flow is then used to calculate the burnt-gas fraction (3.15). The fresh-air mass flow $\overset{*}{m}_{\mathrm{air}}$ is measured with a hot-film air-mass meter (HFM) mass-flow sensor. The intake temperature ϑ_{im} is also measured. The cylinder mass flow $\overset{*}{m}_{\mathrm{cyl}}$ can be calculated using (3.10). The intake volume V_{im} and the ideal gas constant of air R are assumed to be known. The burnt-gas fraction of the EGR x_{egr} can be approximated with the burnt-gas fraction in the exhaust manifold x_{em}. Assuming lean combustion, it can be calculated from the measured air-to-fuel ratio in the exhaust manifold λ_{em} using

$$x_{\mathrm{egr}} \approx x_{\mathrm{em}} = \frac{1 + \sigma_0}{1 + \lambda_{\mathrm{em}} \cdot \sigma_0}. \tag{3.17}$$

The estimator described by (3.14)-(3.16) is capable of dynamically estimating the intake burnt-gas fraction. It is thus well suited to air-path control. However, it is not suitable for the estimation of the intake burnt-gas fraction with the goal of a model-based injection reduction. The reason for this shortcoming is the following:

In steady-state conditions, the estimated burnt-gas fraction is

$$\widehat{x}_{\mathrm{im,ss}} = \frac{\widehat{\overset{*}{m}}_{\mathrm{egr}} \cdot x_{\mathrm{egr}}}{\overset{*}{m}_{\mathrm{cyl}}} \tag{3.18}$$

$$= \frac{\overset{*}{m}_{\mathrm{cyl}} - \overset{*}{m}_{\mathrm{air}}}{\overset{*}{m}_{\mathrm{cyl}}} \cdot \frac{1+\sigma_0}{1+\lambda_{\mathrm{em}} \cdot \sigma_0}. \tag{3.19}$$

Alternatively, (3.5) and (3.7) can be used to obtain a steady-state estimate. Assuming a steady state ($\lambda_{\mathrm{em}} = \lambda$) yields

$$\frac{1+\sigma_0}{1+\lambda_{\mathrm{em}} \cdot \sigma_0} = x_{\mathrm{comb}} = \frac{x_{\mathrm{im}} \cdot \overset{*}{m}_{\mathrm{cyl}} + (1+\sigma_0) \cdot \overset{*}{m}_{\varphi}}{\overset{*}{m}_{\mathrm{cyl}} + \overset{*}{m}_{\varphi}}. \tag{3.20}$$

Solving (3.20) for the intake burnt-gas fraction yields a second steady-state estimation for the burnt-gas fraction,

$$\widehat{x}_{\mathrm{im,ss},\varphi} = \frac{1+\sigma_0}{1+\lambda_{\mathrm{em}} \cdot \sigma_0} \cdot \left(1 + \frac{\overset{*}{m}_{\varphi}}{\overset{*}{m}_{\mathrm{cyl}}}\right) - (1+\sigma_0) \cdot \frac{\overset{*}{m}_{\varphi}}{\overset{*}{m}_{\mathrm{cyl}}}. \tag{3.21}$$

Ideally, (3.19) and (3.21) yield the same result. Both equations use the measurement data of the AFR λ_{em} and an estimate of the cylinder mass-flow $\overset{*}{m}_{\mathrm{cyl}}$. Equation (3.19) uses the fresh-air mass-flow $\overset{*}{m}_{\mathrm{air}}$ as a third variable, whereas (3.21) uses the injected fuel mass-flow $\overset{*}{m}_{\varphi}$. Equations (3.19) and (3.21) are equivalent because $\overset{*}{m}_{\mathrm{air}}$ and $\overset{*}{m}_{\varphi}$ are linked in steady state (ss) via λ_{em},

$$\lambda_{\mathrm{em}} \overset{ss}{=} \lambda = \frac{\overset{*}{m}_{\mathrm{air}}}{\sigma_0 \cdot \overset{*}{m}_{\varphi}}. \tag{3.22}$$

In reality, however, (3.22) cannot hold due to sensor inaccuracies. Thus there is an offset between the results of (3.19) and (3.21). The injection limiter is based on the same equations as (3.21). Therefore, if offset-free injection limitation is desired, the estimator has to reach the steady-state value defined by (3.21). This behavior can be achieved by extending the burnt-gas equation of the estimator (3.15) by a correction term that forces the steady-state value to converge to the value $\widehat{x}_{\mathrm{im,ss},\varphi}$,

$$\frac{d}{dt}\widehat{x}_{\mathrm{im}} = \frac{\vartheta_{\mathrm{im}} \cdot R}{p_{\mathrm{im}} \cdot V_{\mathrm{im}}} \cdot [\widehat{\overset{*}{m}}_{\mathrm{egr}} \cdot x_{\mathrm{egr}} - \widehat{x}_{\mathrm{im}} \cdot (\overset{*}{m}_{\mathrm{air}} + \widehat{\overset{*}{m}}_{\mathrm{egr}})] - L \cdot (\widehat{x}_{\mathrm{im}} - \widehat{x}_{\mathrm{im,ss},\varphi}). \tag{3.23}$$

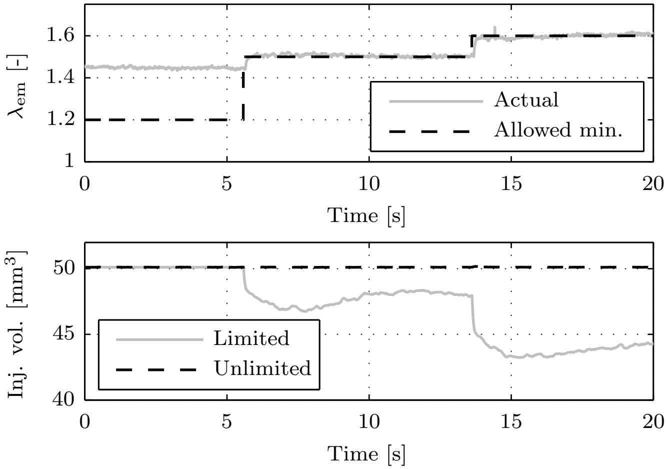

Figure 3.3: Stationary behavior of the injection limiter for step changes of $\lambda_{\min}$.

The parameter L can be used to adjust the speed with which the estimator converges to $\widehat{x}_{\mathrm{im,ss},\varphi}$. Using this correction term, the steady-state estimate of the burnt-gas fraction and the injection reduction are consistent. This fact can be checked by considering an injection limitation during steady-state conditions. Figure 3.3 shows the behavior of the injection limiter during steady-state operation. In that measurement, the minimum allowable value for the AFR $\lambda_{\min}$ is changed stepwise. Once $\lambda_{\min}$ exceeds the stationary AFR, the injected fuel volume is limited accordingly. Because the estimator and the injection reduction are consistent, the AFR is reached without offset by decreasing the fuel mass injected.

3.5 Experimental results

In order to validate the proposed method and to show the influence of the two tuning parameters $\lambda_{\min}$ and K_{egr} on the drivability and the transient pollutant emissions, the injection and EGR limiter has been implemented on an engine on a test bench. In the experiments, an exemplary load step is carried out for different values of these parameters. The nominal reference value for the intake burnt-gas fraction is set constant in order to

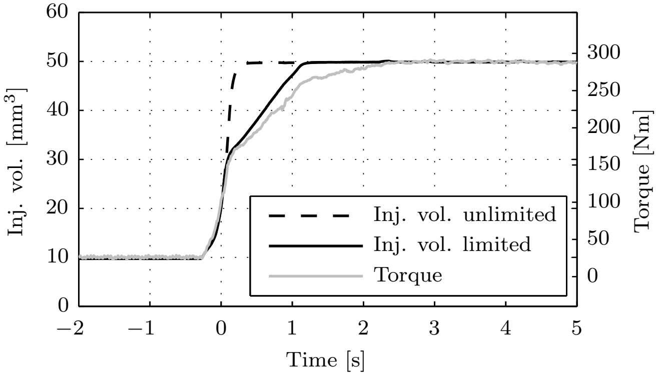

Figure 3.4: Comparison of the fuel quantity and the dynamometer torque during a load step with constant engine speed.

clarify the effect of the EGR reduction. The reference value of the intake pressure depends on the speed and load of the engine and it is taken from a lookup table.

In the following measurements, the drivability, which is the possibility to deliver the torque desired by the driver, is represented by the fuel quantity. Figure 3.4 shows a comparison of the fuel quantity and the torque[2] during a load step with injection limitation. The limitation of the fuel quantity translates directly into a degraded torque development, which is perceived as a reduction of the drivability. The torque development shows a behavior which is similar to the increase in fuel quantity. This result is not surprising if we consider that the torque is generated by combusting the fuel injected. It is therefore acceptable to consider the fuel quantity as a measure for the torque available and the drivability.

3.5.1 Influence of the injection limiter

Figure 3.5 shows the results for a variation of λ_{min} for a constant value of K_{egr}. As expected, the variation of λ_{min} has a large influence on the PM emissions and the drivability. The higher the value of λ_{min} is chosen, the less fuel is injected, which leads to degraded drivability, and the lower are

[2]The torque signal depicted in Fig. 3.4 is the dynamometer torque. The engine torque shows a similar development because the dynamometer was controlled to maintain a constant engine speed.

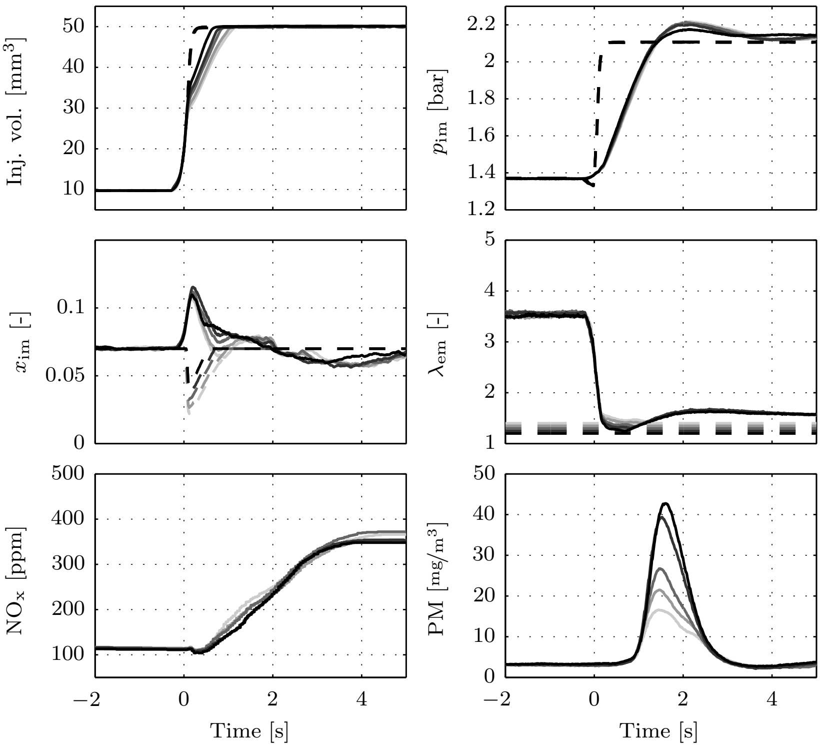

Figure 3.5: Load steps with a variation of λ_{min} and a constant value of $K_{egr} = 0.1$. Reference values are indicated by dashed lines, whereas actual values are indicated by solid lines. The different shadings correspond with increasing lightness to the values $\lambda_{min} = [1.2, 1.25, 1.3, 1.35, 1.4]$.

the amounts of PM emitted. Because the level of EGR reduction depends on the difference between the minimum allowable AFR and the predicted AFR, the variation of λ_{min} also influences the EGR reduction. However, the effect is small and the resulting effect on the NO_x emissions is small as well.

3.5.2 Influence of the EGR limiter

Figure 3.6 shows the results for a variation of K_{egr} for a constant value of λ_{min}. The EGR reduction leads to an improved acceleration of the tur-

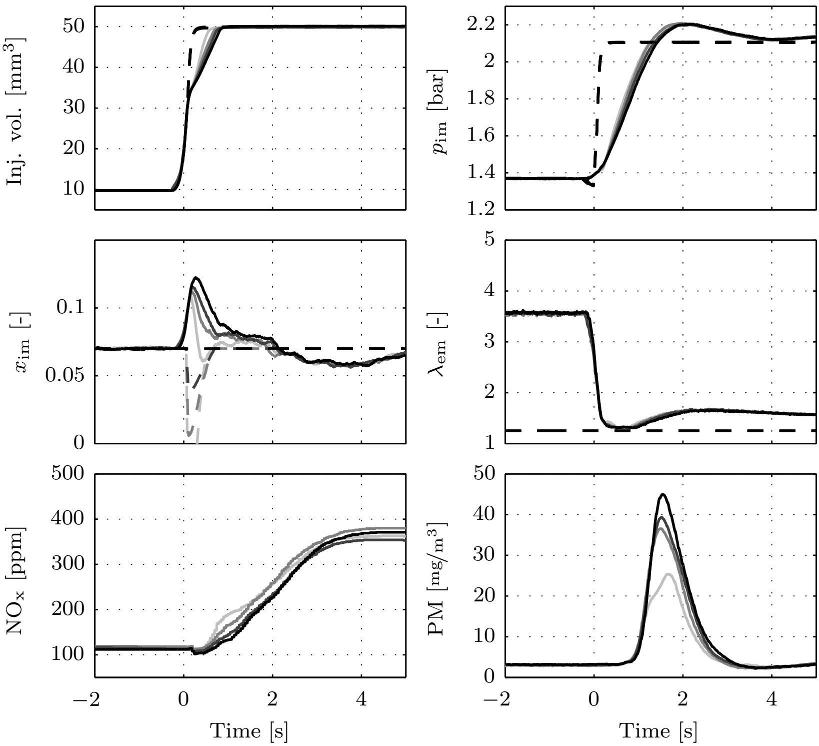

Figure 3.6: Load steps with a variation of K_{egr} and a constant value of $\lambda_{min} = 1.25$. Reference values are indicated by dashed lines, whereas actual values are indicated by solid lines. The different shadings correspond with increasing lightness to the values $K_{egr} = [0, 0.1, 0.2, 0.4]$.

bocharger and a faster buildup of the intake pressure. Together with the leaner gas mixture aspirated, it allows an increased fuel injection, thus improving the drivability. The increased fuel injection also causes increased combustion temperatures, which leads to an improved oxidation of soot and a concomitant reduction in PM emissions. But unless the EGR reduction is very strong, this effect is much smaller than the effect of the variations of λ_{min} (Fig. 3.5). Furthermore, the EGR reduction leads to a slight increase in NO_x emissions. However, the transient peak created by the EGR reduction is small compared to the steady-state value after the step. This effect is caused by the fact that the disturbance of the air-path controller by the load step leads to a temporary increase in EGR. Even with an EGR reduction, there is always sufficient EGR available to prevent a substantial NO_x peak from occurring. Under other circumstances, the NO_x peak could have been more pronounced.

3.5.3 Transient operating strategies

Using the two tuning parameters λ_{min} and K_{egr}, various transient operating strategies can be realized. The following three possible transient operating strategies are considered:

- **Low soot strategy:** This strategy has to avoid low air-to-fuel ratios while reducing the EGR strongly in order to realize low soot emissions. This behavior is achieved by using a high value for both λ_{min} and K_{egr}. Here, the parameters $\lambda_{\text{min}} = 1.4$ and $K_{\text{egr}} = 0.4$ are used.

- **Good drivability strategy:** This strategy has to allow low air-to-fuel ratios while reducing the EGR strongly in order to realize a good drivability by maximizing the fuel quantity injected. This behavior is achieved by using a low value for λ_{min} and a high value for K_{egr}. Here, the parameters $\lambda_{\text{min}} = 1.2$ and $K_{\text{egr}} = 0.4$ are used.

- **Low NO_x strategy:** This strategy may not reduce the EGR in order to realize low NO_x emissions. This behavior is achieved by using the parameter $K_{\text{egr}} = 0$. The minimum air-to-fuel ratio has little influence on the NO_x emissions. The value of λ_{min} should therefore be chosen such that a satisfying compromise between the drivability and the soot emissions is achieved. Here, the parameter $\lambda_{\text{min}} = 1.35$ is used.

Figure 3.7 shows the experimental results for these transient operating strategies. The results are in agreement with the objectives of the respective operating strategies.

3.6 Conclusion

In this chapter, a novel combined, model-based injection and EGR limiter has been described. It uses a model-based, dynamic estimation of the

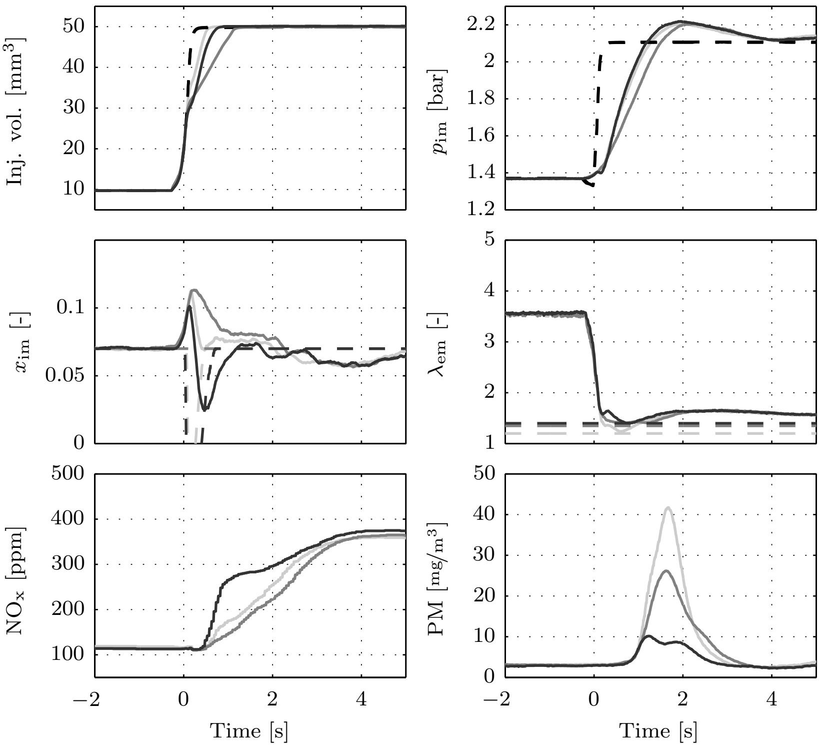

Figure 3.7: Load steps for different transient operating strategies: Low soot (dark grey), low NO_x (grey), and good drivability (light grey).

intake-manifold burnt-gas fraction. The estimator incorporates an extension to make the estimate suitable for offset-free control of the fuel injection. Based on that estimate, the injected fuel mass can be reduced such that the AFR does not fall below a specified minimum allowable AFR. This intervention reduces the PM emissions and the drivability. Furthermore, the severity of the predicted undershooting of the AFR can be used to activate a temporary decrease of the EGR reference value, forcing the air-path controller to close the EGR valve. This intervention leads to better drivability and increased NO_x emissions. Using the two tuning parameters of the two measures, the trade-off between transient emissions and drivability can be adjusted and various transient operating strategies can be realized. Future research could analyze the possibility to improve the performance of the EGR reduction by taking into account the structure of the air-path controller.

Chapter 4

Equivalent Emission Minimization Strategy

One of the main challenges during the development of operating strategies for modern diesel engines is the reduction of the CO_2 emissions while complying with ever more stringent limits for the pollutant emissions. The inherent trade-off between the emissions of CO_2 and pollutants renders a simultaneous reduction difficult. Therefore, an optimal operating strategy is sought that yields minimal CO_2 emissions while holding the cumulative pollutant emissions at the allowed level. Such an operating strategy can be obtained offline by solving a constrained optimal control problem. However, the final-value constraint on the cumulated pollutant emissions prevents this approach to be adopted for causal control. This chapter proposes a framework for causal optimal control of diesel engines. The optimization problem can be solved online when the constrained minimization of the CO_2 emissions is reformulated as an unconstrained minimization of the CO_2 emissions and the weighted pollutant emissions (i.e. equivalent emissions). However, the weighting factors are not known a priori. A method for the online calculation of these weighting factors is proposed. It is based on the HJB equation and a physically motivated approximation of the optimal cost-to-go. A case study shows that the causal control strategy defined by the online calculation of the equivalence factor and the minimization of the equivalent emissions is only slightly inferior to the non-causal offline optimization, while being applicable to online control.
The content of this chapter is based on [32]. One figure (Fig. 4.1) and a section discussing it (Sec. 4.3.3) have been added.

4.1 Introduction

Today, almost 17% of the carbon dioxide (CO_2) emissions are caused by road transportation [1]. By 2035, the global number of road transport vehicles is expected to have almost doubled compared to 2009 [2]. Given the impact of carbon dioxide emissions on the climate [3], it is clear that the improvement of the fuel efficiency of powertrains is crucial. Due to their high fuel efficiency, diesel engines are used in a wide range of applications. However, because of their lean combustion they cannot be equipped with a three-way catalyst to reduce the nitrogen oxide (NO_x) emissions, such as is the common practice with spark ignition engines. Furthermore, a large part of the combustion is diffusion combustion, which leads to the formation of particulate matter (PM). Since these pollutants are harmful to both humans and the environment, emission legislation is becoming increasingly stringent with the introduction of ever lower pollutant emission limits. These emission limits are usually defined as cumulative or cycle-averaged values for a given test cycle [7].
However, a reduction of the engine-out NO_x emissions usually increases the CO_2 emissions because the fast, high-temperature combustion required for a high combustion efficiency is also favorable for the production of NO_x [4]. On the other hand, a reduction of the tailpipe NO_x emissions using exhaust-gas aftertreatment also increases the CO_2 emissions. For example, lean NO_x traps require periods of rich exhaust gas for regeneration. Selective catalytic reduction (SCR) does not increase the CO_2 emissions directly, but urea consumption and fuel consumption (i.e. CO_2 emissions) are equivalent in the light of operating costs. Generally, there is a trade-off between lowering the CO_2 emissions and lowering the NO_x emissions of a diesel engine. At the same time, a similar trade-off exists between the CO_2 emissions and the PM emissions. For example, high injection pressures and post injections can be used to reduce the engine-out PM emissions. However, they may increase the fuel consumption. The use of exhaust-gas aftertreatment, such as diesel particulate filters, also increases the fuel consumption due to the requirement of high exhaust-gas temperatures for regeneration. As a result of these trade-offs, the optimal operating strategy is the one that achieves the lowest possible CO_2 emissions while staying below the upper limit for the respective cumulated pollutant emissions on a given cycle.

Optimal control theory [75, 76] can be used to determine the optimal control inputs for a diesel engine [27, 77, 78, 79]. However, those methods assume full knowledge of the future operating points. This lack of causality renders them not applicable to real-time control. A significant problem is posed especially by the handling of the final-state constraint, which is used to enforce the compliance with the pollutant emission limit. Because the cumulated pollutant emissions at the end of the cycle are constrained, it is always necessary to consider the full driving cycle in the optimization. This problem can be solved by removing the final state constraint and including the weighted pollutant emissions in the performance criterion. For example in [80], the weighted NO_x emissions are included in an optimization of the operating costs of a diesel engine. There, the weighting factor is considered a tuning parameter. Alternatively, the optimal weighting factor can be obtained by solving the non-causal optimal control problem. However, in both cases the control system is sensitive to disturbances and model errors. Furthermore, the driving cycle used for tuning or optimization may not accurately represent real driving situations. In order to comply with the pollutant emission limit even in the presence of disturbances, model errors, and situations not covered by the reference cycle, the weighting factor needs to be adapted online. So far, no method for the online adaptation of the weighting factor has been proposed.

This chapter proposes a generic framework for the causal minimization of the CO_2 emissions while keeping the pollutant emissions on a certain level. It is based on the minimization of the equivalent emissions, which are defined as the sum of the CO_2 emissions and the weighted pollutant emissions. A simple, yet effective method for the online adaptation of the weighting factors is derived. Using these weighting factors, the equivalent emissions can be minimized online to realize a causal optimal operating strategy. The approach is demonstrated in a case study where its performance is compared with that of the non-causal optimal solution. The proposed causal approach is shown to achieve CO_2 emissions that are only marginally larger than the non-causal optimum value while keeping the pollutant emissions very close to the legislative limit.

The framework presented in this chapter is deliberately of a generic nature such that a wide range of problems are covered. No assumption is made concerning the complexity of the optimization problem in which the equivalent emissions are minimized. In the case study, a simple, static

optimization is considered. The online solution of complex, dynamic optimization problems, especially on a series-production ECU, may not yet be feasible. However, once increased computational power and more efficient numerical algorithms render the solution of such problems feasible, the framework presented in this chapter can be applied.
Section 4.2 gives an overview of the optimal control problem and its solution using optimal control theory. In Sec. 4.3, the method used for the adaptation of the weighting factor is derived. Section 4.4 presents the case study and Sec. 4.5 concludes the chapter.

4.2 Optimal control of a diesel engine

This section describes the optimal control problem and its solution using Pontryagin's minimum principle. Section 4.2.1 describes the structure of the class of systems considered here. In Sec. 4.2.2 the optimization problem is defined, and the properties of the optimal solution are analyzed in Sec. 4.2.3.

4.2.1 System description

The engine is assumed to be described by a system of first-order ordinary differential equations (ODE),

$$\dot{\boldsymbol{x}}_{\text{eng}}(t) = \boldsymbol{f}_{\text{eng}}\big(\boldsymbol{x}_{\text{eng}}(t), \boldsymbol{u}(t)\big), \tag{4.1}$$

where $\boldsymbol{x}_{\text{eng}}$ is the state vector and $\boldsymbol{u}$ the control input vector. The subscript "eng" indicates the fact that the state variables are associated with the engine. These state variables may represent physical variables, such as pressures and temperatures, if a mean-value model [22] has been used. If a data-based, empirical model [81] is used, they do not necessarily have a physical meaning. The ODE formulation (4.1) also includes engines equipped with an exhaust-gas aftertreatment (EGA). The chemical processes taking place in an EGA are often described by partial differential equations. However, the EGA can be discretized spatially into a finite number of cells in order to obtain a set of ordinary differential equations. For example, in [82, 83] this technique is used to obtain a control-oriented model of an SCR.
Because the cumulated mass of the pollutant emissions is restricted by legislation, the engine model is extended by a set of artificial state variables

$\boldsymbol{x}_{\text{emis}}$ to track the cumulative emissions,

$$\boldsymbol{x} = \begin{bmatrix} \boldsymbol{x}_{\text{eng}} \\ \boldsymbol{x}_{\text{emis}} \end{bmatrix}, \qquad \boldsymbol{x}_{\text{emis}} = \begin{bmatrix} x_{\text{emis},1} \\ \vdots \\ x_{\text{emis},n} \end{bmatrix}. \tag{4.2}$$

The emission state vector $\boldsymbol{x}_{\text{emis}}$ consists of n elements, one for each of the n pollutant species to be tracked. It is a priori not clear how the elements of $\boldsymbol{x}_{\text{emis}}$ should be defined. The legislative emission limit is often defined in terms of brake specific emissions [7]. Therefore, a possible approach is to extend the engine model by a set of state variables, which represent the current brake specific emissions. The brake specific emissions are defined by

$$\overline{\boldsymbol{m}}_{\text{emis}} = \frac{\boldsymbol{m}_{\text{emis}}}{W}, \tag{4.3}$$

with the cumulated mass of the respective emissions $\boldsymbol{m}_{\text{emis}}$ and the total amount of mechanical work delivered to the crankshaft W. The time derivative of the brake specific emissions is

$$\begin{aligned} \dot{\overline{\boldsymbol{m}}}_{\text{emis}} &= \frac{\dot{\boldsymbol{m}}_{\text{emis}} \cdot W - \boldsymbol{m}_{\text{emis}} \cdot P}{W^2} \\ &= \frac{1}{W} \cdot (\dot{\boldsymbol{m}}_{\text{emis}} - \overline{\boldsymbol{m}}_{\text{emis}} \cdot P) \end{aligned} \tag{4.4}$$

with the power P and the time derivative of the cumulated emissions $\dot{\boldsymbol{m}}_{\text{emis}}$. Alternatively, the engine model can be extended by state variables which represent the absolute (i.e. not brake-specific) mass of the respective emissions $\boldsymbol{m}_{\text{emis}}$. The time derivative of such state variables is

$$\dot{\boldsymbol{m}}_{\text{emis}} = \overset{*}{\boldsymbol{m}}_{\text{emis}}, \tag{4.5}$$

with the instantaneous mass flow of the respective emissions $\overset{*}{\boldsymbol{m}}_{\text{emis}}$. It is important to note that the following equations hold for the derivative of the two potential choices of additional state variables:

$$\frac{\partial \dot{\overline{\boldsymbol{m}}}_{\text{emis}}}{\partial \overline{\boldsymbol{m}}_{\text{emis}}} = diag\Big(-\frac{P}{W}\Big) \neq 0 \tag{4.6a}$$

$$\frac{\partial \dot{\boldsymbol{m}}_{\text{emis}}}{\partial \boldsymbol{m}_{\text{emis}}} = 0. \tag{4.6b}$$

This difference is crucial. Choosing $\boldsymbol{x}_{\text{emis}} = \boldsymbol{m}_{\text{emis}}$ is preferable because then, the dynamics of $\boldsymbol{x}_{\text{emis}}$ are independent of the current value of $\boldsymbol{x}_{\text{emis}}$

and the derivative with respect to $\boldsymbol{x}_{\text{emis}}$ vanishes (4.6b). The advantage provided by this property will become apparent in the next section. The state variables of the extended system thus are

$$\boldsymbol{x} = \begin{bmatrix} \boldsymbol{x}_{\text{eng}} \\ \boldsymbol{m}_{\text{emis}} \end{bmatrix}, \tag{4.7}$$

and the extended state dynamics are

$$\dot{\boldsymbol{x}}(t) = \boldsymbol{f}\big(\boldsymbol{x}(t), \boldsymbol{u}(t)\big) = \begin{bmatrix} \boldsymbol{f}_{\text{eng}}\big(\boldsymbol{x}(t), \boldsymbol{u}(t)\big) \\ \boldsymbol{f}_{\text{emis}}\big(\boldsymbol{x}(t), \boldsymbol{u}(t)\big) \end{bmatrix} = \begin{bmatrix} \boldsymbol{f}_{\text{eng}}\big(\boldsymbol{x}(t), \boldsymbol{u}(t)\big) \\ \overset{*}{\boldsymbol{m}}_{\text{emis}}\big(\boldsymbol{x}(t), \boldsymbol{u}(t)\big) \end{bmatrix}. \tag{4.8}$$

The engine model was deliberately chosen to be very general. The approach described in this chapter is applicable to a wide range of systems, which is reflected by the choice of the model.

4.2.2 Problem formulation

The control task is to minimize the CO_2 emissions while staying below a cumulative limit for the pollutant emissions $\boldsymbol{m}_{\text{emis,lim}}$. Technically, CO_2 emissions are also pollutant emissions. But in this chapter, the term "pollutant emissions" and the emission state variables $\boldsymbol{x}_{\text{emis}}$ refer to the emission species which are limited by legislation (e.g. NO_x and PM). Adopting the notation introduced in [75], the problem can be described by an optimal control problem with a partially constrained final state.

$$\min_{\boldsymbol{u}(\cdot)} \Big\{ J(\boldsymbol{u}) = \int_0^T L\big(\boldsymbol{x}(t), \boldsymbol{u}(t)\big) dt = \int_0^T \overset{*}{m}_{CO_2}\big(\boldsymbol{x}(t), \boldsymbol{u}(t)\big) dt \Big\} \tag{4.9a}$$

s. t.

$$\boldsymbol{x}(0) = \boldsymbol{x}_0 \tag{4.9b}$$

$$\dot{\boldsymbol{x}}(t) = \boldsymbol{f}\big(\boldsymbol{x}(t), \boldsymbol{u}(t)\big) \qquad \text{for all } t \in 0, T \tag{4.9c}$$

$$\boldsymbol{x}_{\text{emis}}(T) \leq \boldsymbol{m}_{\text{emis,lim}} \tag{4.9d}$$

In addition to the constraints given above, the control input could be constrained. The engine state variables $\boldsymbol{x}_{\text{eng}}$ are assumed to be unconstrained because state constraints would complicate the solution presented in the next section substantially [75]. For the same reason, state-dependent constraints, such as constraints for the instantaneous emissions, are excluded too.

4.2.3 Solution using Pontryagin's minimum principle

The properties of the optimal solution are analyzed using Pontryagin's minimum principle [75]. The Hamiltonian is defined as

$$H\big(\boldsymbol{x}(t), \boldsymbol{u}(t), \boldsymbol{\lambda}(t)\big) = \overset{*}{m}_{\mathrm{CO}_2}\big(\boldsymbol{x}(t), \boldsymbol{u}(t)\big) + \boldsymbol{\lambda}^T(t) \cdot \boldsymbol{f}\big(\boldsymbol{x}(t), \boldsymbol{u}(t)\big). \quad (4.10)$$

According to Pontryagin's minimum principle, the following conditions must hold for the optimal solution, which is indicated by the superscript "o". The initial value and the equation governing the dynamics need to be satisfied.

$$\boldsymbol{x}(0) = \boldsymbol{x}_0 \quad (4.11a)$$

$$\dot{\boldsymbol{x}}^o(t) = \nabla_{\boldsymbol{\lambda}} H_{|o} = \boldsymbol{f}\big(\boldsymbol{x}^o(t), \boldsymbol{u}^o(t)\big) \quad (4.11b)$$

For the co-states, the following equation must hold:

$$\begin{aligned}\dot{\boldsymbol{\lambda}}^o(t) &= -\nabla_{\boldsymbol{x}} H_{|o} \\ &= -\nabla_{\boldsymbol{x}} \overset{*}{m}_{\mathrm{CO}_2}\big(\boldsymbol{x}^o(t), \boldsymbol{u}^o(t)\big) - \left[\frac{\partial \boldsymbol{f}}{\partial \boldsymbol{x}}\big(\boldsymbol{x}^o(t), \boldsymbol{u}^o(t)\big)\right]^T \boldsymbol{\lambda}^o(t) \quad (4.11c)\end{aligned}$$

The unconstrained final state of the engine state variables is represented by the condition

$$\boldsymbol{\lambda}^o_{\mathrm{eng}}(T) = 0, \quad (4.11d)$$

whereas the upper limit for the final state of the pollutant state variables is represented by the condition

$$\boldsymbol{\lambda}^o_{\mathrm{emis}}(T) \geq 0. \quad (4.11e)$$

For all admissible inputs $\boldsymbol{u}$, the Hamiltonian is minimized with respect to $\boldsymbol{u}$.

$$H\big(\boldsymbol{x}^o(t), \boldsymbol{u}^o(t), \boldsymbol{\lambda}^o(t)\big) \leq H\big(\boldsymbol{x}^o(t), \boldsymbol{u}, \boldsymbol{\lambda}^o(t)\big) \quad (4.12)$$

The dynamics of the co-states (4.11c) can be divided into co-states for the engine and co-states for the emissions. (For the sake of clarity, the dependencies on the input and the state are omitted.)

$$\begin{bmatrix} \dot{\boldsymbol{\lambda}}^o_{\mathrm{eng}}(t) \\ \dot{\boldsymbol{\lambda}}^o_{\mathrm{emis}}(t) \end{bmatrix} = \begin{bmatrix} -\nabla_{\boldsymbol{x}_{\mathrm{eng}}} \overset{*}{m}_{\mathrm{CO}_2} - \left[\frac{\partial \boldsymbol{f}}{\partial \boldsymbol{x}_{\mathrm{eng}}}\right]^T \boldsymbol{\lambda}^o(t) \\ -\nabla_{\boldsymbol{x}_{\mathrm{emis}}} \overset{*}{m}_{\mathrm{CO}_2} - \left[\frac{\partial \boldsymbol{f}}{\partial \boldsymbol{x}_{\mathrm{emis}}}\right]^T \boldsymbol{\lambda}^o(t) \end{bmatrix} \quad (4.13)$$

Because neither the system dynamics nor the CO_2 emissions depend on the cumulated pollutant emissions, the following relations hold:

$$\nabla_{\boldsymbol{x}_{\text{emis}}} \overset{*}{m}_{CO_2}\big(\boldsymbol{x}(t), \boldsymbol{u}(t)\big) = 0 \tag{4.14a}$$

$$\frac{\partial \boldsymbol{f}}{\partial \boldsymbol{x}_{\text{emis}}}\big(\boldsymbol{x}(t), \boldsymbol{u}(t)\big) = 0 \tag{4.14b}$$

The dynamics of the co-states are thus

$$\begin{bmatrix} \dot{\boldsymbol{\lambda}}^{o}_{\text{eng}}(t) \\ \dot{\boldsymbol{\lambda}}^{o}_{\text{emis}}(t) \end{bmatrix} = \begin{bmatrix} -\nabla_{\boldsymbol{x}_{\text{eng}}} \overset{*}{m}_{CO_2} - \left[\frac{\partial \boldsymbol{f}}{\partial \boldsymbol{x}_{\text{eng}}}\right]^T \boldsymbol{\lambda}^o(t) \\ 0 \end{bmatrix}. \tag{4.15}$$

The optimal co-state vector corresponding to the cumulated emissions $\boldsymbol{\lambda}^o_{\text{emis}}$ is constant. This result is a consequence of the choice $\boldsymbol{x}_{\text{emis}} = \boldsymbol{m}_{\text{emis}}$. If $\boldsymbol{x}_{\text{emis}} = \overline{\boldsymbol{m}}_{\text{emis}}$ had been chosen instead, the term $\frac{\partial \boldsymbol{f}}{\partial \boldsymbol{x}_{\text{emis}}}$ would not have vanished (4.6a). Considering the final value condition (4.11e), we obtain

$$\boldsymbol{\lambda}^o_{\text{emis}} = const. \geq 0. \tag{4.16}$$

Using (4.14a), (4.14b) and (4.16), we can rewrite the Hamiltonian (4.10) as

$$\begin{aligned} H\big(\boldsymbol{x}_{\text{eng}}, \boldsymbol{u}, \boldsymbol{\lambda}(t)\big) &= \overset{*}{m}_{CO_2}\big(\boldsymbol{x}_{\text{eng}}, \boldsymbol{u}\big) + \boldsymbol{\lambda}^T(t) \cdot \boldsymbol{f}\big(\boldsymbol{x}_{\text{eng}}, \boldsymbol{u}\big) \\ &= \overset{*}{m}_{CO_2}\big(\boldsymbol{x}_{\text{eng}}, \boldsymbol{u}\big) + \boldsymbol{\lambda}^T_{\text{emis}} \cdot \boldsymbol{f}_{\text{emis}}\big(\boldsymbol{x}_{\text{eng}}, \boldsymbol{u}\big) \\ &\qquad + \boldsymbol{\lambda}^T_{\text{eng}}(t) \cdot \boldsymbol{f}_{\text{eng}}\big(\boldsymbol{x}_{\text{eng}}, \boldsymbol{u}\big) \\ &= \overset{*}{m}_{CO_2}\big(\boldsymbol{x}_{\text{eng}}, \boldsymbol{u}\big) + \sum_{i=1}^{n} \lambda_{\text{emis},i} \cdot \overset{*}{m}_{\text{emis},i}\big(\boldsymbol{x}_{\text{eng}}, \boldsymbol{u}\big) \\ &\qquad + \boldsymbol{\lambda}^T_{\text{eng}}(t) \cdot \boldsymbol{f}_{\text{eng}}\big(\boldsymbol{x}_{\text{eng}}, \boldsymbol{u}\big). \end{aligned} \tag{4.17}$$

The time dependency of the inputs $\boldsymbol{u}$ and the states $\boldsymbol{x}$ has been omitted for clarity. The rewritten Hamiltonian (4.17) is equivalent to the Hamiltonian of the minimization of the CO_2 emissions and the weighted pollutant emissions with a free final state:

$$\min_{\boldsymbol{u}(\cdot)} \Big\{ \tilde{J}(\boldsymbol{u}) = \int_0^T \Big(\overset{*}{m}_{\mathrm{CO_2}}\big(\boldsymbol{x}_{\mathrm{eng}}(t), \boldsymbol{u}(t)\big) + \sum_{i=1}^{n} \lambda_{\mathrm{emis},i} \cdot \overset{*}{m}_{\mathrm{emis},i}\big(\boldsymbol{x}_{\mathrm{eng}}(t), \boldsymbol{u}(t)\big) \Big) dt \Big\} \tag{4.18a}$$

s. t.

$$\boldsymbol{x}_{\mathrm{eng}}(0) = \boldsymbol{x}_{\mathrm{eng},0} \tag{4.18b}$$

$$\dot{\boldsymbol{x}}_{\mathrm{eng}}(t) = \boldsymbol{f}_{\mathrm{eng}}\big(\boldsymbol{x}_{\mathrm{eng}}(t), \boldsymbol{u}(t)\big) \qquad \text{for all } t \in 0, T. \tag{4.18c}$$

In this case, the vector $\boldsymbol{\lambda}_{\mathrm{emis}} \geq 0$ is not a co-state vector but a set of parameters. They can be interpreted as the equivalence factors, which are used to calculate the equivalent CO_2 emissions for a certain amount of the respective pollutant emissions. A strategy that solves (4.18a)-(4.18c) is thus called an "equivalent emission minimization strategy" (EEMS). The unconstrained minimization of the equivalent emissions (4.18a)-(4.18c) is a reformulation of the original constrained minimization of the CO_2 emissions (4.9a)-(4.9d).

This reformulation of the problem is similar to the Karush-Kuhn-Tucker conditions for static optimization [84], where the constraints are represented by adjoining them to the performance criterion using Lagrange multipliers, which are also called the dual variables. The reformulated problem (4.18a)-(4.18c) is thus called the (partially) dual formulation.

When a causal solution of the optimal control problem is considered, the dual formulation has a crucial advantage. For model predictive control (MPC), a rule of thumb is to choose the length of the prediction horizon to be equal to approximately five times the relevant time constant of the system [85]. For the original constrained optimization problem the relevant time constant is infinity because the constrained state variables are integrators. Thus, the entire future driving cycle would have to be considered in order to obtain a meaningful solution[1]. For the reformulated dual optimization problem the relevant time constant is finite because the underlying model consists only of the engine. The slowest relevant dynamic of the engine is the acceleration of the turbo charger, which is in the order of one second. Therefore, a prediction horizon in the order of a few sec-

[1]Shorter horizons are possible if an appropriate end cost term is used. However, this term can only be determined when the entire driving cycle is known.

onds is sufficient, which enables causal online optimization strategies with relatively short prediction horizons.

4.3 Causal control strategies

The last section showed that a constrained minimization of the CO_2 emissions can be reformulated to an unconstrained minimization of the equivalent emissions. This reformulation enables the online solution of the dual optimal control problem with a limited time horizon. However, the equivalence factors, which yield the correct cumulated emissions, are not known a priori. They may be determined by iterative tuning or by solving the non-causal optimization problem (4.9a)-(4.9d). However, in order to realize a causal online optimization, which compensates for model errors, disturbances, and situations not covered by the reference cycle, an online calculation of the equivalence factors is required.
In Sec. 4.3.1, a method for the online calculation of the equivalence factors is derived. It is based on feedback control of the pollutant emissions. Section 4.3.2 describes the calculation of the corresponding reference values and Sec. 4.3.3 presents the overall causal control structure. Section 4.3.4 discusses the similarities between this approach and the one used for the causal optimal energy management of hybrid electric vehicles.

4.3.1 Calculation of the equivalence factors

The optimal equivalence factors $\lambda_{\text{emis},i}$ in (4.18a) can be calculated from the optimal cost-to-go function using the Hamilton-Jacobi-Bellman (HJB) equation [75, 76]. The optimal cost-to-go function is not known, but it can be approximated.
The starting point for this approach is the original optimization problem (4.9a)-(4.9d). Because the goal is to develop a causal strategy, the final state constraint (4.9d) has to be removed. Without knowledge of the future, the final state constraint cannot be evaluated. However, we need to ensure that the pollutant emissions do not exceed the limit. As in [86], this can be achieved by extending the performance criterion (4.9a) with a term that penalizes deviations of the cumulated pollutant emissions $\boldsymbol{x}_{\text{emis}}$

from the reference value $\boldsymbol{x}_{\mathrm{ref}}$,

$$\begin{aligned}\widehat{J}(\boldsymbol{u}) &= \int_0^T \widehat{L}\big(\boldsymbol{x}(t), \boldsymbol{u}(t)\big) dt \\ &= \int_0^T \left(\overset{*}{m}_{\mathrm{CO_2}}\big(\boldsymbol{x}(t), \boldsymbol{u}(t)\big) + \sum_{i=1}^{n} \alpha_i \cdot \Big(\frac{x_{\mathrm{ref},i}(t) - x_{\mathrm{emis},i}(t)}{\Delta x_{\mathrm{norm},i}} \Big)^{2q} \right) dt, \end{aligned} \tag{4.19}$$

with the weighting parameter α_i and the normalization of the deviation $\Delta x_{\mathrm{norm},i}$ of the respective pollutants, and the order of the penalty $q \in \mathbb{N}$. This leads to the extended Hamiltonian (the time dependency has been omitted)

$$\widehat{H}(\boldsymbol{u}) = \overset{*}{m}_{\mathrm{CO_2}}(\boldsymbol{x}, \boldsymbol{u}) + \sum_{i=1}^{n} \alpha_i \cdot \Big(\frac{x_{\mathrm{ref},i} - x_{\mathrm{emis},i}}{\Delta x_{\mathrm{norm},i}} \Big)^{2q} + \boldsymbol{\lambda}^T \cdot \boldsymbol{f}(\boldsymbol{x}, \boldsymbol{u}), \tag{4.20}$$

and the optimal input

$$\boldsymbol{u}^o = \mathrm{argmin}\big(\widehat{H}(\boldsymbol{u})\big). \tag{4.21}$$

The additional penalty term of the extended Hamiltonian does not depend explicitly on the control input $\boldsymbol{u}$. Therefore, the optimal control input $\boldsymbol{u}^o$, which minimizes the Hamiltonian $\widehat{H}$ of the unconstrained extended problem, also minimizes the Hamiltonian H of the original constrained problem.
Using the optimal cost-to-go function

$$\widehat{\mathcal{J}}^o(\boldsymbol{x}, t) = \min_{\boldsymbol{u}(\cdot)} \Big\{ \int_t^T \widehat{L}\big(\boldsymbol{\xi}(\tau), \boldsymbol{u}(\tau)\big) d\tau \ \Big| \ \boldsymbol{\xi}(t) = \boldsymbol{x} \Big\}, \tag{4.22}$$

the equivalence factors corresponding to the cumulated pollutant emissions can be calculated using the HJB equation [75, 76],

$$\boldsymbol{\lambda}^o(\boldsymbol{x}, t) = \frac{\partial \widehat{\mathcal{J}}^o(\boldsymbol{x}, t)}{\partial \boldsymbol{x}} \qquad \Longrightarrow \qquad \boldsymbol{\lambda}^o_{\mathrm{emis}}(\boldsymbol{x}, t) = \frac{\partial \widehat{\mathcal{J}}^o(\boldsymbol{x}, t)}{\partial \boldsymbol{x}_{\mathrm{emis}}}. \tag{4.23}$$

The optimal cost-to-go function $\widehat{\mathcal{J}}^o(\boldsymbol{x}, t)$ in (4.23) is not known. But a suboptimal cost-to-go function can be approximated by

$$\widehat{\mathcal{J}}(\boldsymbol{x}) = \underbrace{\widehat{\mathcal{J}}_{\mathrm{nom}}(\boldsymbol{x}) + \widehat{\mathcal{J}}_{\mathrm{emis}}(\boldsymbol{x})}_{\mathrm{CO_2}} + \underbrace{\widehat{\mathcal{J}}_{\mathrm{pen}}(\boldsymbol{x})}_{\text{Penalty}}. \tag{4.24}$$

As indicated, the first two terms correspond to the CO_2 emissions in the extended cost function (4.19), whereas the last term corresponds to the penalty term. More precisely, the terms correspond to:

- Nominal cost $\widehat{\mathcal{J}}_{\text{nom}}(\boldsymbol{x})$: The CO_2 emissions caused by driving the rest of the cycle with optimal instantaneous pollutant emissions.

- Emissions-saving cost $\widehat{\mathcal{J}}_{\text{emis}}(\boldsymbol{x})$: The additional CO_2 emissions caused by bringing the cumulated pollutant emissions to their respective reference level.

- Penalty cost $\widehat{\mathcal{J}}_{\text{pen}}(\boldsymbol{x})$: The penalty imposed for the deviation of the respective cumulated pollutant emissions from their reference value.

The following sections will describe the three terms in detail.

Nominal cost $\widehat{\mathcal{J}}_{\text{nom}}(x)$

The term $\widehat{\mathcal{J}}_{\text{nom}}(\boldsymbol{x})$ describes the CO_2 emissions that are produced by running the rest of the cycle with optimal instantaneous pollutant emissions. This term is independent of the current cumulated pollutant emissions,

$$\frac{\partial \widehat{\mathcal{J}}_{\text{nom}}(\boldsymbol{x})}{\partial \boldsymbol{x}_{\text{emis}}} = 0. \tag{4.25}$$

Since we are only interested in the derivative of the cost with respect to the state variables $\boldsymbol{x}_{\text{emis}}$ (4.23), the term $\widehat{\mathcal{J}}_{\text{nom}}(\boldsymbol{x})$ does not have to be calculated.

Emissions-saving cost $\widehat{\mathcal{J}}_{\text{emis}}(x)$

The term $\widehat{\mathcal{J}}_{\text{emis}}(\boldsymbol{x})$ describes the CO_2 emissions that are produced in addition to the nominal CO_2 emissions described by $\widehat{\mathcal{J}}_{\text{nom}}(\boldsymbol{x})$. They are caused by bringing the cumulated pollutant emissions to the reference level. The time horizon considered for this process is in the order of minutes or hours. The time constants of the state variables of the engine are much shorter than this horizon. On such a long timescale, the current value of the engine state variables has a negligible influence on the total future CO_2 emissions. It can thus be assumed that the term $\widehat{\mathcal{J}}_{\text{emis}}(\boldsymbol{x})$ depends only on the state variables corresponding to the pollutant emissions $\boldsymbol{x}_{\text{emis}}$. Assuming that for the horizon considered, the average value K_i of additional CO_2 emissions caused by the saving of the respective pollutant emissions is known, the CO_2 penalty is

$$\widehat{\mathcal{J}}_{\text{emis}}(\boldsymbol{x}) = \Delta m_{\text{CO}_2} = \sum_{i=1}^{n} K_i \cdot \Delta m_{\text{emis},i} = \sum_{i=1}^{n} K_i \cdot (x_{\text{emis},i} - x_{\text{ref},i}). \quad (4.26)$$

Penalty cost $\widehat{\mathcal{J}}_{\text{pen}}(x)$

The term $\widehat{\mathcal{J}}_{\text{pen}}(\boldsymbol{x})$ describes the penalty that is imposed for the control error between the actual cumulated pollutant emissions and their reference values. In order to calculate this term, the estimated future control error is required. The controller is assumed to decrease the control error of the respective pollutant emissions linearly with time, such that after the time $T_{h,i}$ it has vanished:

$$x_{\text{ref,fut},i}(\tau) - x_{\text{emis,fut},i}(\tau) = \Big(x_{\text{ref},i}(t) - x_{\text{emis},i}(t)\Big) \cdot \Big(1 - \frac{\tau}{T_{h,i}}\Big) \quad (4.27)$$

The total penalty for the deviation of the actual values from the reference values can be calculated by integration of the future trajectories.

$$\begin{aligned} \widehat{\mathcal{J}}_{\text{pen}}(\boldsymbol{x}) &= \sum_{i=1}^{n} \int_0^{T_{h,i}} \alpha_i \cdot \Big(\frac{x_{\text{ref,fut},i}(\tau) - x_{\text{emis,fut},i}(\tau)}{\Delta x_{\text{norm},i}}\Big)^{2q} d\tau \\ &= \sum_{i=1}^{n} \frac{\alpha_i \cdot T_{h,i}}{2q+1} \Big(\frac{x_{\text{ref},i}(t) - x_{\text{emis},i}(t)}{\Delta x_{\text{norm},i}}\Big)^{2q} \end{aligned} \quad (4.28)$$

Total cost and resulting equivalence factor

The approximated (suboptimal) cost-to-go function is

$$\begin{aligned} \widehat{\mathcal{J}}(\boldsymbol{x}) = \widehat{\mathcal{J}}_{\text{nom}}(\boldsymbol{x}) + \sum_{i=1}^{n} \Bigg(& K_i \cdot (x_{\text{emis},i} - x_{\text{ref},i}) \\ & + \frac{\alpha_i \cdot T_{h,i}}{2q+1} \Big(\frac{x_{\text{ref},i}(t) - x_{\text{emis},i}(t)}{\Delta x_{\text{norm},i}}\Big)^{2q} \Bigg), \end{aligned} \quad (4.29)$$

and the resulting co-states are

$$\lambda_{\text{emis},i}(x_{\text{emis},i}) = \frac{\partial \widehat{\mathcal{J}}(\boldsymbol{x})}{\partial x_{\text{emis},i}} = 0 + K_i + \widetilde{\alpha}_i \cdot \big(x_{\text{emis},i}(t) - x_{\text{ref},i}(t)\big)^{2q-1}, \quad (4.30)$$

with the substitution

$$\widetilde{\alpha}_i = \frac{2q \cdot \alpha_i \cdot T_{h,i}}{(2q+1) \cdot \Delta x_{\mathrm{norm},i}^{2q}}. \tag{4.31}$$

The average additional CO_2 emissions for a given saving of a pollutant K_i varies with the driving profile. Since the instantaneous value of K_i depends on the operating point, the average value of K_i depends on the operating points occurring during the period considered. Therefore, it needs to be adapted during operation in order to maintain the correct level of emissions. An integrator with integration time T_{int} can be used to achieve this goal,

$$\begin{aligned}\lambda_{\mathrm{emis},i}\big(x_{\mathrm{emis},i}(t)\big) = K_{i,0} + \int_0^t \frac{x_{\mathrm{emis},i}(\tau) - x_{\mathrm{ref},i}(\tau)}{T_{\mathrm{int},i}} d\tau \\ + \widetilde{\alpha}_i \cdot \big(x_{\mathrm{emis},i}(t) - x_{\mathrm{ref},i}(t)\big)^{2q-1}.\end{aligned} \tag{4.32}$$

Assuming a quadratic penalty for the pollutant control error ($q = 1$), this equation corresponds to a PI controller for every one of the pollutant emission species, using the respective equivalence factor as the control input. When tuning the PI controller, it has to be ensured that the adaptation of K_i is carried out slowly[2]. The pollutant emissions can be measured using a sensor. The reference values can be calculated using the methods described in the next section. The equivalence factors calculated using (4.32) are then used for the minimization of the equivalent emissions (4.18a)-(4.18c).

4.3.2 Calculation of the reference values

The method for calculating the equivalence factors (4.32) requires the pollutant reference values to be known. One possible approach is to assume that the respective reference values for the instantaneous pollutant emissions $\overset{*}{m}_{\mathrm{emis,ref},i}$ depend on the operating point, which is defined by the engine speed ω_{e} and the torque T,

$$x_{\mathrm{ref},i}(t) = \int_0^t \overset{*}{m}_{\mathrm{emis,ref},i}\big(\omega_{\mathrm{e}}(\tau), T(\tau)\big) d\tau. \tag{4.33}$$

[2]One previous assumption was that the time horizon considered for bringing the pollutant emissions to the reference level is much longer than the time constants of the engine dynamics.

These reference values can be stored in a lookup table. They may represent the steady-state calibration of the engine. If a non-causal optimal solution has been obtained for the reference cycle, the pollutant emissions of the optimal solution can also be used to parametrize the lookup table.

Alternatively, a simpler approach is to consider a constant brake-specific reference value $\overline{m}_{\text{emis,ref},i}$ for the pollutant emissions. For heavy-duty engines, the cycle-averaged limit imposed by legislation is usually defined as a brake-specific value, which can be used as the reference value. Together with the power of the engine, the evolution of the reference value of the pollutant emissions can be calculated,

$$x_{\text{ref},i}(t) = \overline{m}_{\text{emis,ref},i} \cdot \int_0^t \omega_{\text{e}}(\tau) \cdot T(\tau) d\tau. \tag{4.34}$$

For passenger-car applications, where it is common to specify the emission limit in g/km, the integral in equation (4.34) can be replaced by the integration of the vehicle speed.

Clearly, the assumption of a constant $\overline{m}_{\text{emis,ref},i}$ is a strong simplification and the resulting reference trajectories may be unrealistic at times. For example, in an operating point where the brake-specific emissions are always considerably higher than the average value of the cycle, it is not possible to operate the engine such that the reference value can be followed. However, the advantage of that strategy is that it requires no information except for the reference brake-specific emissions.

4.3.3 Overall control structure

Figure 4.1 shows the structure of the overall EEMS controller. The reference values for the pollutant emissions are generated according to (4.33) or (4.34). For every pollutant species, a PI controller is used to adapt the corresponding equivalence factor according to (4.32). These equivalence factors are then used in the minimization of the equivalent emissions (4.18a)-(4.18c). The resulting optimal control inputs are applied to the engine and the pollutants emitted are measured. The cumulated mass of the pollutants emitted is calculated and fed back in the control loop.

4.3.4 Comparison to ECMS for hybrid vehicles

The equivalent emission minimization strategy (EEMS) presented in Secs. 4.2.3 and 4.3.1 is similar to the equivalent consumption minimization strat-

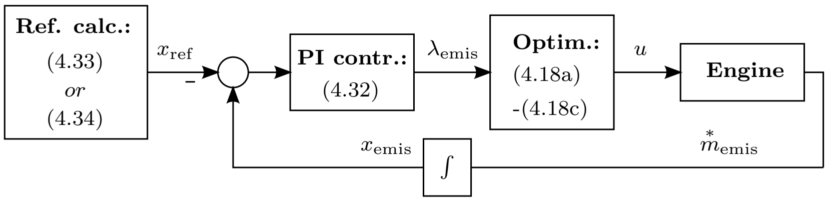

Figure 4.1: Structure of the EEMS controller with the calculation of the reference values (Ref. calc.), the PI controllers for the adaptation of the equivalence factors (PI contr.), the minimization of the equivalent emissions (Optim.), and the cumulation of the measured pollutant emissions. The corresponding equation numbers are given in the respective blocks.

egy (ECMS) used for the online optimal energy management of hybrid electric drivetrains [87]. This is caused by the fact that both problems are structurally similar. In this chapter, the goal is the minimization of the CO_2 emissions while maintaining a certain pollutant emission level. The goal of optimal energy management is the minimization of the fuel consumption while sustaining the battery charge. For both problems, the final state constraint(s) can be represented by an extension of the performance criterion. This approach results in a minimization of the equivalent emissions and the equivalent consumption, respectively. In both cases, the unknown optimal equivalence factor(s) is/are constant and an estimate can be calculated using feedback in order to allow a causal online optimization. Due to the similarity of the two problems, the calculation of the equivalence factors using the HJB equation and the approximated cost-to-go (Sec. 4.3.1) was inspired by [86]. The main structural difference between the two problems concerns the reference value. For ECMS, the reference state of charge is constant or bounded[3]. For EEMS, the reference value for the cumulated pollutant emissions is constantly increasing (see Sec. 4.3.2). Another difference is the fact that for ECMS, the state of charge of the battery is constrained throughout the entire cycle, whereas when EEMS is used, the cumulated pollutant emissions are constrained only at the end of the cycle.

The similarity between the two problems is also likely to lead to future

[3]There exist approaches where the reference value for the state of charge is adapted [88]. However, because the state of charge always lies in the interval $[0, 1]$, the reference value is expected to do so as well.

combinations of the EEMS approach with the ECMS approach. Clearly, the NO_x and PM emissions are a concern for diesel electric hybrid drivetrains. In [89, 90, 91, 92, 93, 94, 95, 96, 97, 98, 99, 100], the NO_x emissions are included in the performance criterion of the ECMS problem. However, there the equivalence factor for the NO_x emissions is only a tuning parameter and it is not adapted actively in order to maintain a certain NO_x emission level, as it is proposed in this chapter.

4.4 Case study

This section presents a case study in which the performance of the EEMS on a driving cycle is studied. The optimal solution obtained with dynamic programming (DP) is used as a benchmark for various versions of EEMS. The case study is carried out in simulation using a validated model of a diesel engine. Section 4.4.1 defines the control problem and describes the different controllers to be compared. Section 4.4.2 presents and discusses the results of the comparison. Due to reasons of confidentiality, all emissions data have been normalized.

4.4.1 Problem setting

We consider a 8.7 l turbocharged, heavy-duty diesel engine running a driving cycle lasting 1800 s. It consists of five repetitions of a section of the urban part of the World Harmonized Transient Cycle (WHTC). Figure 4.2 shows one repetition of that section. The goal is the minimization of the CO_2 emissions while keeping the NO_x emissions below the final value constraint $m_{\mathrm{NO_x,lim}}$. The control input is the deviation of the crank angle for the start of injection (SOI) from its nominal value,

$$u = \delta\varphi_{\mathrm{SOI}}. \tag{4.35}$$

In order to determine the optimal SOI and to simulate the engine on the driving cycle, an engine model is required which reproduces the influence of the SOI on the CO_2 and NO_x emissions. Because we are considering time scales in the order of entire driving cycles, the dynamics of the engine can be neglected and the engine may be represented by a steady-state model

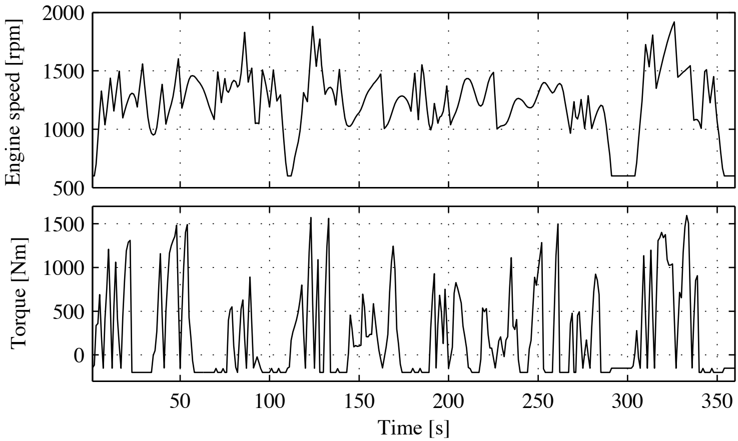

Figure 4.2: Section of the WHTC used in the case study.

with the inputs engine speed ω_e, torque T, and control input u,

$$\overset{*}{m}_{\mathrm{CO_2}} = f\big(\omega_{\mathrm{e}}, T, u\big) \tag{4.36}$$

$$\overset{*}{m}_{\mathrm{NO_x}} = f\big(\omega_{\mathrm{e}}, T, u\big). \tag{4.37}$$

The steady-state engine model (4.36)-(4.37) is realized as a lookup table, which was derived from a validated dynamic engine model [101].
The driving cycle prescribes the engine speed ω_{e} and the torque T. It is sampled with the step size $\Delta t = 1\,\mathrm{s}$ and it consists of $N = 1800$ samples. The dynamics of the sole state variable $x = m_{\mathrm{NO_x}}$ are discretized using the Euler forward integration scheme, such that a discrete-time optimal control problem is obtained.

$$\min_{u(\cdot)} \Big\{ \sum_{n=0}^{N-1} \overset{*}{m}_{\mathrm{CO_2}}\big(\omega_{\mathrm{e}}(n), T(n), u(n)\big) \Big\} \tag{4.38a}$$

s. t.

$$x(0) = 0 \tag{4.38b}$$

$$x(n+1) = x(n) + \overset{*}{m}_{\mathrm{NO_x}}\big(\omega_{\mathrm{e}}(n), T(n), u(n)\big) \cdot \Delta t \quad , \quad n = 0, ..., N-1 \tag{4.38c}$$

$$x(N) \leq m_{\mathrm{NO_x,lim}} \tag{4.38d}$$

This is an optimization problem of the structure (4.9a)-(4.9d). Because it is time-discrete, it can be solved using dynamic programming (DP) [76]. That approach is guaranteed to find the optimal solution of the discretized problem. It can thus be used as a benchmark for the other approaches. As shown in Sec. 4.2.3, the dual formulation of the optimization can be solved alternatively,

$$\min_{u(\cdot)}\left\{\sum_{n=0}^{N-1} \overset{*}{m}_{\mathrm{CO_2}}\big(\omega_{\mathrm{e}}(n), T(n), u(n)\big) + \lambda_{\mathrm{NO_x}}(n)\cdot \overset{*}{m}_{\mathrm{NO_x}}\big(\omega_{\mathrm{e}}(n), T(n), u(n)\big)\right\}. \tag{4.39}$$

This optimization problem has the same structure as (4.18a)[4] and, given the optimal equivalence factor, it will produce the same solution as the DP. It can be solved online by minimizing the instantaneous equivalent emissions at every time step,

$$\begin{aligned} u(n) = \underset{u(n)}{\operatorname{argmin}}\Big\{ &\overset{*}{m}_{\mathrm{CO_2}}\big(\omega_{\mathrm{e}}(n), T(n), u(n)\big) \\ &+ \lambda_{\mathrm{NO_x}}(n)\cdot \overset{*}{m}_{\mathrm{NO_x}}\big(\omega_{\mathrm{e}}(n), T(n), u(n)\big)\Big\}. \end{aligned} \tag{4.40}$$

In the following, three different versions of EEMS are compared to the optimal solution obtained by DP. All three versions solve the minimization of the instantaneous equivalent emissions (4.40). They only differ in the way the equivalence factor is determined. The following three methods for determining the equivalence factor are considered:

- **EEMS with constant equivalence factor (CEF):** This method applies EEMS using the constant equivalence factor which yields the correct final cumulated $\mathrm{NO_x}$ emissions. This equivalence factor can be obtained by an iterative simulation of the closed loop consisting of the engine model (4.36)-(4.37) and the control law (4.40). Because the optimal control problems (4.38a)-(4.38d) and (4.39) are equivalent, this method yields the same solution as the DP when the optimal equivalence factor is used. However, it is not applicable for causal control because the optimal equivalence factor generally is not known.

[4] Equations (4.18b)-(4.18c) are not necessary, because in this case the engine model has no state variables.

- **EEMS with operating-point dependent reference NO_x emissions (OPdep):** This method applies EEMS using (4.32) to adapt the equivalence factor and (4.33) to calculate the reference NO_x emissions. The reference NO_x mass flow is calculated as a quadratic function of the operating point,

$$\overset{*}{m}_{\mathrm{NO_x,ref}}(\omega_\mathrm{e}, T) = a_0 + a_1 \cdot \omega_\mathrm{e} + a_2 \cdot T + a_3 \cdot \omega_\mathrm{e}^2 + a_4 \cdot T^2 + a_5 \cdot \omega_\mathrm{e} \cdot T. \quad (4.41)$$

The parameters $a_0 \ldots a_5$ are obtained by a least-squares fit of the NO_x emissions of the optimal solution obtained by DP. Figure 4.3 shows a comparison of the optimal NO_x emissions resulting from the DP and the fitted quadratic function. The quadratic model is a good approximation of the optimal values. However, this approach requires the availability of an optimal solution.

- **EEMS with constant brake-specific reference NO_x emissions (BSconst):** This method also applies EEMS using (4.32) to adapt the equivalence factor; however, it uses (4.34) to calculate the reference NO_x emissions. The reference value for the brake-specific NO_x emissions is equal to the average value, which was demanded for the DP solution:

$$\overline{m}_{\mathrm{NO_x,ref}} = \frac{m_{\mathrm{NO_x,lim}}}{W} = \frac{m_{\mathrm{NO_x,lim}}}{\sum_{n=0}^{N-1} \omega_\mathrm{e}(n) \cdot T(n) \cdot \Delta t}. \quad (4.42)$$

The two causal EEMS approaches OPdep and BSconst use the adaptation law (4.32) with identical tuning parameters $\widetilde{\alpha}$ and T_{int} for the adaptation of the equivalence factor. The tuning parameters were tuned manually.

4.4.2 Simulation results

Figure 4.4 shows the simulation results of the non-causal DP and the three EEMS approaches when applied to the engine model (4.36)-(4.37). The section of the WHTC is repeated five times. The optimal solution is a repetition of the optimal solution of the single section. The reason for this result is the fact that the only state variable represents the cumulated NO_x emissions, while the rest of the model does not depend on that state variable.

The first plot in Fig. 4.4 shows the cumulated NO_x emissions of the different solutions. The NO_x mass has been normalized with the final value

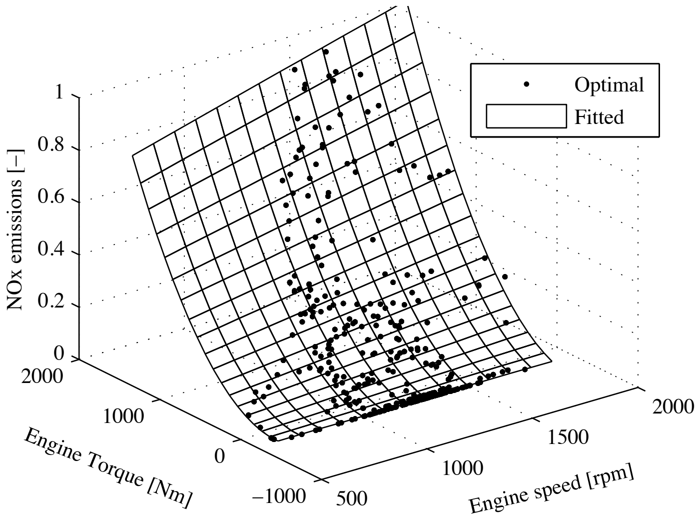

Figure 4.3: Normalized NO_x emissions of the optimal solution (dotted) and the quadratic model (4.41).

of the NO_x mass of the DP solution. The plot also shows the full range of attainable NO_x emissions, the upper limit corresponding to $\lambda_{NO_x} = 0$, and the lower limit corresponding to $\lambda_{NO_x} = \infty$. The cumulated NO_x emissions of all approaches are very similar such that on the given scale the respective lines cannot even be discerned. Therefore, the second plot shows the NO_x error

$$\Delta NO_x = m_{NO_x} - m_{NO_x,dp} \tag{4.43}$$

between the NO_x mass of the DP solution $m_{NO_x,dp}$ and the respective EEMS solution m_{NO_x}. Since the NO_x mass has been normalized, the NO_x error is normalized as well.

As the results of the CEF approach show, the online solution of the dual problem (4.40) is equal to the offline solution of the constrained problem (4.38a)-(4.38d) when the optimal constant equivalence factor is used. This result confirms the theoretical result which showed that the optimal equivalence factor of the cumulated pollutant emissions is always constant (4.15). Both causal EEMS approaches maintain the correct NO_x emission

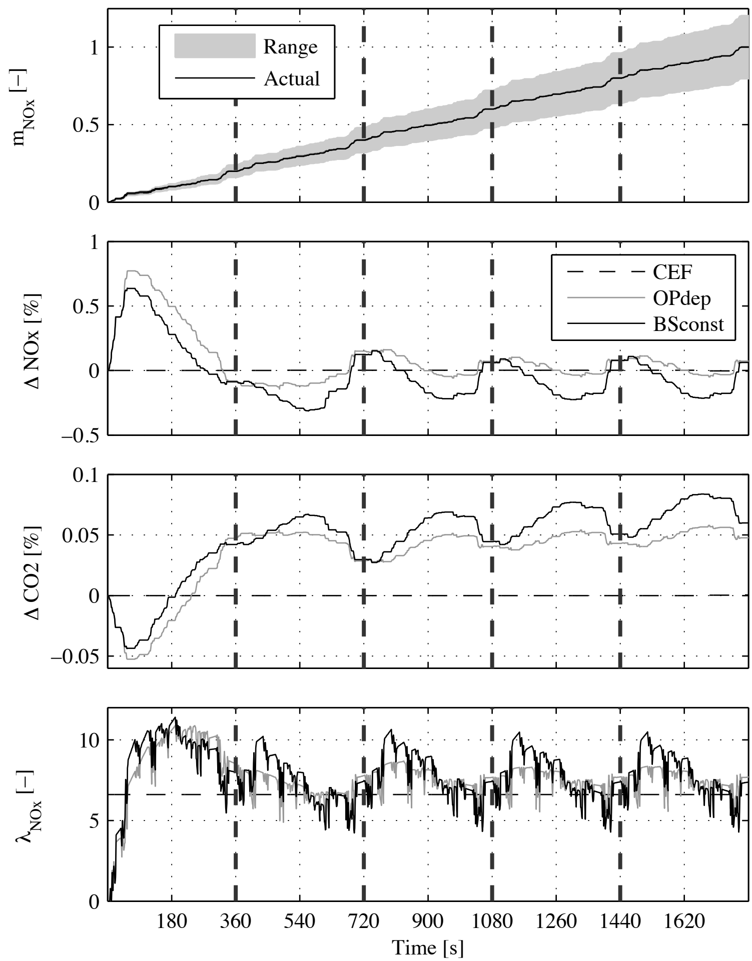

Figure 4.4: Normalized comparison of the optimal DP solution and the EEMS approaches. It shows the feasible range (light grey area) and the actual values of the cumulated NO_x emissions m_{NO_x}, the NO_x error ΔNO_x, the CO_2 error ΔCO_2, and the respective equivalence factor λ_{NO_x} of the EEMS approaches. The vertical lines indicate the beginning of a new section. The terms CEF, OPdep, and BSconst refer to the EEMS strategies with a constant equivalence factor, operating-point dependent reference emissions, and constant brake-specific reference emissions, respectively.

level by following the reference value for the NO_x emissions using feedback control. The cumulated NO_x emissions are kept within less than one percent of the final value.
The initial value K_0 for the equivalence factor in (4.32) was chosen to be zero. After the second repetition of the section, the two controllers have converged to a limit cycle, and the behavior for all subsequent sections remains the same. The OPdep approach keeps both the equivalence factor and the emissions closer to the DP solution. This result is caused by the fact that the assumption of operating-point dependent reference emissions is more realistic than the constant brake specific emissions.
The third plot of Fig. 4.4 shows the CO_2 error

$$\Delta CO_2 = m_{CO_2} - m_{CO_2,dp} \tag{4.44}$$

between the CO_2 mass of the DP solution $m_{CO_2,dp}$ and the respective EEMS solution m_{CO_2}. The CO_2 mass and the CO_2 error have been normalized with the final CO_2 mass of the DP solution. The plot clearly shows the trade-off between NO_x and CO_2 emissions. When the NO_x error increases, the CO_2 error decreases and vice versa. A large part of the CO_2 error is generated during the first two repetitions of the section before the EEMS controller has reached its limit cycle. In the beginning of the cycle, the equivalence factor is very low and the engine is operated with a very high fuel efficiency, thus emitting large amounts of NO_x. Then, the NO_x emissions have to be reduced at a later point when the CO_2 penalty is larger than the amount saved in the beginning. However, once the controller has reached the limit cycle after two repetitions of the section, the CO_2 penalty of the causal EEMS controllers is small.
The performance of the various strategies can be compared by considering the cumulative emissions at the end of the cycle. In order to obtain a fair comparison and to eliminate the influence of the initial value of the equivalence factor, only the last three sections shown in Fig. 4.4 are taken into account. Table 4.1 shows the normalized results. Both causal EEMS approaches have only slightly higher CO_2 emissions than the DP solution. The NO_x emissions are even slightly lower for both strategies. The OPdep approach has both lower CO_2 and NO_x emissions than the BSconst approach because the more realistic reference value leads to an equivalence factor that is closer to the optimal value. Generally, the performance of the causal EEMS approaches is very close to the non-causal, theoretical

Table 4.1: Normalized difference Δ between the various strategies and the optimal DP strategy for the last three sections.

Strategy	ΔCO_2 [%]	ΔNO_x [%]
DP	0	0
EEMS OPdep	+0.032	–0.129
EEMS BSconst	+0.050	–0.104

optimum.

Finally, the performance of the various approaches for different reference NO_x emission levels is compared. Figure 4.5 shows the normalized trade-off between the cumulated CO_2 emissions and the cumulated NO_x emissions for the DP solution and the two causal EEMS approaches. The optimal trade-off can be obtained by varying the constant equivalence factor of the dual problem (4.39) or by varying the NO_x limit value of the original problem (4.38a)-(4.38d). The causal trade-off is obtained by setting the reference values for the causal EEMS controllers accordingly. Throughout the entire range, the Pareto front of the causal EEMS solutions is very close to the optimal Pareto front. These results show that the EEMS approach is well suited to an online optimization of the CO_2 and pollutant emissions of a diesel engine.

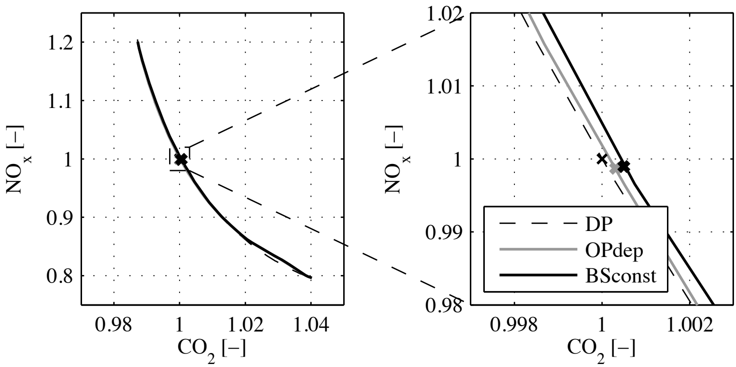

Figure 4.5: Normalized Pareto front of the cumulated NO_x and CO_2 emissions for the last three sections. Shown are the optimal DP solution and the two causal EEMS solutions. The solution shown in Fig. 4.4 and Table 4.1 is indicated by crosses.

4.5 Conclusion and outlook

This chapter presented a generic framework for the minimization of the CO_2 emissions of a diesel engine while maintaining a certain pollutant emission level. It consists of an online adaptation of the equivalence factors in combination with a minimization of the equivalent emissions. First, it was shown that the constrained state variables associated with the pollutant emissions can be eliminated by minimizing the equivalent emissions instead. The optimal equivalence factors, which weigh pollutant emissions versus CO_2 emissions, are constant for a given cycle and emission limit. A method for the online adaptation of the equivalence factors was then derived using the HJB equation and a physically motivated approximation of the optimal cost-to-go function. Finally, a case study combined this adaptation method with an online minimization of the equivalent emissions. The performance of the proposed causal control strategies was very close to the theoretical non-causal optimum, which was determined using dynamic programming. This result confirmed that the EEMS framework is well suited to causal optimal control of the CO_2 and pollutant emissions of a diesel engine.

The case study considered a static minimization of the equivalent emissions in combination with an adaptation of the equivalence factor. The results are very encouraging. In a next step, the EEMS framework could be applied to a more complex optimization problem. For example, additional control inputs, such as the injection pressure or additional injections, could be considered. In that case, the steady-state engine model (4.36)-(4.37) has to be extended in order to cover these inputs as well. The optimization carried out in every time step (4.40) gains additional arguments. Its solution becomes computationally somewhat more expensive, however, it remains straightforward. Furthermore, the method used for the adaptation of the equivalence factor (4.32) remains the same.

Another topic worth pursuing is the realization of an EEMS with multiple pollutant emission limits. The implementation is straightforward; In addition to the weighted NO_x emissions, the dual formulation of the control problem (4.39) and the optimization carried out in every time step (4.40) contain terms for the other weighted pollutant mass-flows. However, the solution of (4.40) does not become more complex. The additional equivalence factors are each adapted by an additional PI controller for the respective emission species (see (4.32)). It may prove advantageous to take into account the interaction among the various equivalence factors and the pollutant emissions by using a centralized multivariable controller instead of the individual PI controllers.

Furthermore, instead of the steady-state model (4.36)-(4.37), a dynamic engine model could be used for the optimization. The static optimization solved in every time step (4.40) is then replaced by a dynamic optimization of the structure (4.18a)-(4.18c). The solution of such dynamic optimization problems for diesel engines is currently under research [27]. The computational cost is significantly higher than for the solution of a static optimization, such as (4.40). However, the method used for the adaptation of the equivalence factor (4.32) remains the same.

Finally, future research could aim at the combination of EEMS and ECMS for hybrid vehicles. As discussed in Sec. 4.3.4, the goal would be to achieve a fuel-optimal, charge-sustaining operation while respecting the legislative limit for the pollutant emissions.

Chapter 5

Conclusion and Outlook

5.1 Conclusion

This thesis presents three main contributions to the research and development of model-based control strategies for diesel engines. First, a cascaded control structure for air-path control is presented. It is derived on the basis of a system analysis. It handles the disadvantageous properties of the plant well, while being applicable to a wide range of engine types. The calibration of its two controllers is straightforward because they can be tuned sequentially. The control performance of this control structure is superior to that of a conventional control structure, which is shown in an experimental comparison using two test-bench engines. With its combination of versatility, ease of tuning, and good performance, the cascaded control structure represents a solid framework for air-path control of diesel engines.

Then, a model-based method to adapt the fuel injection and the EGR during transients is presented. It can be used to adjust the trade-off between the transient pollutant emissions (NO_x and PM) and the drivability. The effectiveness of the controller is shown in experiments. Due to the model-based implementation, only two easily interpretable tuning parameters are required to realize various transient operating strategies. This ability to adjust the transient operation of the engine using only two tuning parameters renders it a valuable add-on feature for existing engine control systems.

Finally, a generic framework for causal optimal control of diesel engines is presented. It can be used to find an online solution to the inherently non-causal optimal control problem of operating a diesel engine with minimum fuel consumption while complying with an upper limit for the cumulative pollutant emissions. A case study shows that the performance of the proposed causal controller is only marginally inferior to that of the non-causal, optimal solution obtained by dynamic programming, while being applicable to online control. This promising first result and its generic nature suggest that the proposed framework is an important step towards an online optimization of diesel engines.

The findings of this thesis lead to a better understanding of existing systems, they introduce new degrees of freedom, and they pave the way for future control algorithms. They therefore contribute to the research and development of model-based control strategies for diesel engines.

5.2 Outlook

All three topics discussed in this thesis show the potential for further research. Further analyses could show how the cascaded air-path controller has to be adapted in order to operate with more complex air-path configurations including more than two turbo chargers or a low-pressure EGR. The injection and EGR limiter could be adapted to take into account the structure of the air-path controller to improve the performance of the EGR reduction. The framework for causal optimal control could be applied to a dynamic optimization using several inputs and emission species.

More generally, future research should continue to seek improvements in the control of the subsystems air path, combustion, and exhaust-gas aftertreatment. The constant development of the hardware of these subsystems necessitates a simultaneous development of the corresponding control systems. At the same time, the computational power of engine control units continues to increase. As a result, computationally expensive control algorithms, such as the solution of an optimization problem or the simulation of a detailed model, become feasible. Furthermore, new sensors, such as sensors for the pollutant emissions or the cylinder pressure, introduce new possibilities for control. This simultaneous development of the demands and the possibilities for the control systems of these subsystems ensures a continued need for research in these fields.

Finally, there still lies some untapped potential in the coordinated control of the three subsystems air path, combustion, and exhaust-gas aftertreatment. Although they may be controlled separately, an optimal operation of the engine can only be achieved if they are being coordinated by a supervisory controller. Such a supervisory controller could adapt the reference values of the underlying control systems such that the performance of the overall system is optimized. The EEMS approach presented in chapter 4 would be suited well to carry out such an online optimization of the overall system. In the case of an application in a hybrid vehicle, this supervisory controller could also carry out the energy management. To this end, a combination of the EEMS approach with the ECMS approach could be considered. Such a development would be a step toward a global power-train controller, which could help unlock the full potential of complex power trains combining various prime movers.

Bibliography

[1] "CO_2 emissions from fuel combustion – highlights," IEA Publications, International Energy Agency, Paris, France, 2012.

[2] "World energy outlook," IEA Publications, International Energy Agency, Paris, France, 2011.

[3] IPCC 2007, *Climate Change 2007: Synthesis Report. Contribution of Working Groups I, II and III to the Fourth Assessment Report of the Intergovernmental Panel on Climate Change*, [Core Writing Team, Pachauri, R.K and Reisinger, A.], Ed. IPCC, Geneva, Switzerland, 2007.

[4] J. Heywood, *Internal combustion engine fundamentals.* McGraw-Hill, 1988.

[5] J. Kagawa, "Health effects of diesel exhaust emissions – a mixture of air pollutants of worldwide concern," *Toxicology*, vol. 181–182, pp. 349–353, December 2002.

[6] A. C. Lloyd and T. A. Cackette, "Diesel engines: Environmental impact and control," *Journal of the Air & Waste Management Association*, vol. 51, no. 6, pp. 809–847, June 2001.

[7] C. D. Rakopoulos and E. G. Giakoumis, *Diesel Engine Transient Operation – Principles of Operation and Simulation Analysis.* Springer, 2009.

[8] N. Watson and M. S. Janota, *Turbocharging the Internal Combustion Engine.* The Macmillan Press Ltd., 1982.

[9] J. Galindo, J. Serrano, X. Margot, A. Tiseira, N. Schorn, and H. Kindl, "Potential of flow pre-whirl at the compressor inlet of automotive engine turbochargers to enlarge surge margin and overcome

packaging limitations," *International Journal of Heat and Fluid Flow*, vol. 28, no. 3, pp. 374–387, June 2007.

[10] Robert Bosch GmbH, *Diesel-Engine Management – Systems and Components*, 4th ed. Wiley, 2006.

[11] H. Bosch and F. Janssen, "Catalytic reduction of nitrogen oxides: A review on the fundamentals and technology," *Catalysis Today*, vol. 2, no. 4, pp. 369–531, 1988.

[12] J.-M. Kang, I. Kolmanovsky, and J. W. Grizzle, "Dynamic optimization of lean burn engine aftertreatment," *Journal of Dynamic Systems, Measurement, and Control*, vol. 123, no. 2, pp. 153–160, June 2001.

[13] E. Kladopoulou, S. Yang, J. Johnson, G. Parker, and A. G. Konstandopoulos, "A study describing the performance of diesel particulate filters during loading and regeneration – A lumped parameter model for control applications," in *SAE Technical paper 2003-01-0842*, 2003.

[14] L. Guzzella and A. Amstutz, "Control of diesel engines," *IEEE Control Systems Magazine*, vol. 18, no. 5, pp. 53–71, Oct. 1998.

[15] R. Johansson, P. Tunestål, and A. Widd, "Modeling and model-based control of homogeneous charge compression ignition (HCCI) engine dynamics," in *Automotive Model Predictive Control – Models, Methods and Applications*, L. del Re, F. Allgöwer, L. Glielmo, C. Guardiola, and I. Kolmanovsky, Eds. Springer, May 2010, vol. LNCIS 402, ch. 6, pp. 89—104.

[16] T. Ott, F. Zurbriggen, C. H. Onder, and L. Guzzella, "Cylinder individual feedback control of combustion in a dual fuel engine," in *Proceedings of the 7th IFAC Symposium on Advances in Automotive Control, Tokyo, Japan*, 2013.

[17] F. Tschanz, S. Zentner, C. H. Onder, and L. Guzzella, "Cascaded control of combustion and pollutant emissions in diesel engines," *Control Engineering Practice, available online*, 2014.

[18] F. Tschanz, "Control of particulate matter and nitrogen oxide emissions in diesel engines," Ph.D. dissertation, ETH Zurich, no. 20785, 2012.

[19] C. Schär, C. Onder, and H. P. Geering, "Control of an SCR catalytic converter system for a mobile heavy-duty application," *IEEE Transactions on Control Systems Technology*, vol. 14, no. 4, pp. 641–653, July 2006.

[20] S. Nakagawa, T. Hori, and M. Nagano, "A new feedback control of a lean NO_x trap catalyst," in *SAE Technical paper 2004-01-0527*, 2004.

[21] S. Skogestad and I. Postlethwaite, *Multivariable Feedback Control: Analysis and Design*, 2nd ed. John Wiley & Sons, 2005.

[22] L. Guzzella and C. Onder, *Introduction to Modeling and Control of Internal Combustion Engine Systems.* Springer, 2010.

[23] U. Christen, "Engineering aspects of H_∞ control," Ph.D. dissertation, ETH Zurich, no. 11433, 1996.

[24] B. D. O. Anderson and J. B. Moore, *Optimal Control – Linear Quadratic Methods.* Prentice Hall, 1989.

[25] M. Hafner and R. Isermann, "Multiobjective optimization of feedforward control maps in engine management systems towards low consumption and low emissions," *Transactions of the Institute of Measurement and Control*, vol. 25, no. 1, pp. 57–74, March 2003.

[26] J. Wahlström, L. Eriksson, and L. Nielsen, "EGR-VGT control and tuning for pumping work minimization and emission control," *IEEE Transactions on Control Systems Technology*, vol. 18, no. 4, pp. 993–1003, July 2010.

[27] J. Asprion, O. Chinellato, and L. Guzzella, "Optimal control of diesel engines: Numerical methods, applications, and experimental validation," *Accepted for publication in Mathematical Problems in Engineering*, 2014.

[28] S. Zentner, E. Schäfer, G. Fast, C. H. Onder, and L. Guzzella, "A cascaded control structure for air-path control of diesel engines," *Proceedings of the Institution of Mechanical Engineers, Part D: Journal of Automobile Engineering, available online*, 2014.

[29] E. Schäfer, T. Kreissig, G. Fast, S. Zentner, L. Guzzella, and C. Onder, "Method and device for operating an internal combustion engine with supercharging and exhaust-gas recirculation," Patent Nr. WO/2013/159899, October 2013.

[30] E. Schäfer, S. Zentner, and G. Fast, "Model-based development of a multi-variable control strategy for large diesel engines," in *Proceedings of the 6th Emission Control Conference, Dresden, Germany*, 2012.

[31] S. Zentner, E. Schäfer, C. Onder, and L. Guzzella, "Model-based injection and EGR adaptation and its impact on transient emissions and drivability of a diesel engine," in *Proceedings of the 7th IFAC Symposium on Advances in Automotive Control, Tokyo, Japan*, 2013, pp. 89–94.

[32] S. Zentner, J. Asprion, C. Onder, and L. Guzzella, "An equivalent emission minimization strategy for causal optimal control of diesel engines," *Energies*, vol. 7, no. 3, pp. 1230–1250, March 2014.

[33] F. Tschanz, S. Zentner, E. Özatay, C. H. Onder, and L. Guzzella, "Cascaded multivariable control of the combustion in diesel engines," in *Proceedings of the 2012 IFAC Workshop on Engine and Powertrain Control, Simulation and Modeling, Paris, France*, 2012, pp. 25–32.

[34] J. Asprion, G. Mancini, S. Zentner, C. H. Onder, N. Cavina, and L. Guzzella, "A framework for the iterative dynamic optimisation of diesel engines: numerical methods, experimental setup, and first results," in *WIT Transactions on Ecology and the Environment*, C. Brebbia, E. Magaril, and M. Khodorovsky, Eds. WIT Press, Southampton, 2014, vol. 190.

[35] I. Kolmanovsky, P. Moraal, M. Van Nieuwstadt, and A. Stefanopoulou, "Issues in modelling and control of intake flow in variable geometry turbocharged engines," in *Proceedings of the 18th*

IFIP Conference on System Modeling and Optimization, Detroit, MI, 1997.

[36] M. J. van Nieuwstadt, I. V. Kolmanovsky, P. E. Moraal, A. Stefanopoulou, and M. Jankovic, "EGR–VGT control schemes: experimental comparison for a high-speed diesel engine," *IEEE Control Systems Magazine*, vol. 20, no. 3, pp. 63–79, June 2000.

[37] A. G. Stefanopoulou, I. Kolmanovsky, and J. S. Freudenberg, "Control of variable geometry turbocharged diesel engines for reduced emissions," *IEEE Transactions on Control Systems Technology*, vol. 8, no. 4, pp. 733–745, July 2000.

[38] A. Schwarte, D. Schneider, M. Nienhoff, R. Kopold, A. Kornienko, I. Koops, and C. Birkner, "Physical model based control of the airpath of diesel engines for future requirements," *at - Automatisierungstechnik*, vol. 55, no. 7, pp. 346–351, July 2007.

[39] J. Wahlström and L. Eriksson, "Nonlinear input transformation for EGR and VGT control in diesel engines," *SAE International Journal of Engines, Paper 2010-01-2203*, vol. 3, no. 2, pp. 288–305, December 2010.

[40] B. Oh, M. Lee, Y. Park, K. Lee, and M. Sunwoo, "An exhaust gas recirculation control strategy for passenger car diesel engines using an inverse valve model," *Proceedings of the Institution of Mechanical Engineers, Part D: Journal of Automobile Engineering*, vol. 226, no. 3, pp. 362–371, March 2012.

[41] M. Jankovic and I. Kolmanovsky, "Constructive Lyapunov control design for turbocharged diesel engines," *IEEE Transactions on Control Systems Technology*, vol. 8, no. 2, pp. 288–299, March 2000.

[42] M. Larsen, M. Jankovic, and P. Kokotovic, "Indirect passivation design for a diesel engine model," in *Proceedings of the 2000 IEEE International Conference on Control Applications, Anchorage, AK*, 2000, pp. 309–314.

[43] V. Utkin, H.-C. Chang, I. Kolmanovsky, and J. Cook, "Sliding mode control for variable geometry turbocharged diesel engines," in *Proceedings of the 2000 American Control Conference, Chicago, IL*, vol. 1, no. 6, September 2000, pp. 584–588.

[44] M. Ammann, N. P. Fekete, L. Guzzella, and A. H. Glattfelder, "Model-based control of the VGT and EGR in a turbocharged common-rail diesel engine: Theory and passenger car implementation," in *SAE Technical paper 2003-01-0357*, 2003.

[45] S. Bengea, R. DeCarlo, M. Corless, and G. Rizzoni, "A polytopic system approach for the hybrid control of a diesel engine using VGT/EGR," *Journal of Dynamic Systems, Measurement, and Control*, vol. 127, no. 1, pp. 13–21, March 2005.

[46] J. Wang, "Hybrid robust air-path control for diesel engines operating conventional and low temperature combustion modes," *IEEE Transactions on Control Systems Technology*, vol. 16, no. 6, pp. 1138–1151, November 2008.

[47] J. Wahlström and L. Eriksson, "Robust nonlinear EGR and VGT control with integral action for diesel engines," in *Proceedings of the 17th IFAC World Congress, Seoul, Republic of Korea*, vol. 17, 2008, pp. 2057–2062.

[48] A. Amstutz and L. R. Del Re, "EGO sensor based robust output control of EGR in diesel engines," *IEEE Transactions on Control Systems Technology*, vol. 3, no. 1, pp. 39–48, March 1995.

[49] E. Alfieri, A. Amstutz, C. Onder, and L. Guzzella, "Model-based feedback control of the air-to-fuel ratio in diesel engines based on an empirical model," in *Proceedings of the 2006 IEEE International Conference on Control Applications, Munich, Germany*, October 2006, pp. 509–514.

[50] P. Moulin, O. Grondin, and L. Fontvieille, "Control of a two stage turbocharger on a diesel engine," in *Proceedings of the 48th IEEE Conference on Decision and Control, Shanghai, China*, December 2009, pp. 5200–5206.

[51] J. Chauvin, G. Corde, N. Petit, and P. Rouchon, "Motion planning for experimental airpath control of a diesel homogeneous charge-compression ignition engine," *Control Engineering Practice*, vol. 16, no. 9, pp. 1081–1091, September 2008.

[52] R. Wijetunge, J. Hawley, and N. Vaughan, "Application of alternative EGR and VGT strategies to a diesel engine," in *SAE Technical Paper 2004-01-0899*, 2004.

[53] M. Jung and K. Glover, "Calibratable linear parameter-varying control of a turbocharged diesel engine," *IEEE Transactions on Control Systems Technology*, vol. 14, no. 1, pp. 45–62, January 2006.

[54] X. Wei and L. del Re, "Gain scheduled H_∞ control for air path systems of diesel engines using LPV techniques," *IEEE Transactions on Control Systems Technology*, vol. 15, no. 3, pp. 406–415, May 2007.

[55] J. Mohammadpour, K. Grigoriadis, M. Franchek, Y.-Y. Wang, and I. Haskara, "LPV decoupling and input shaping for control of diesel engines," in *Proceedings of the 2010 American Control Conference, Baltimore, MD*, 2010, pp. 1477–1482.

[56] M. Lee and M. Sunwoo, "Modelling and H_∞ control of diesel engine boost pressure using a linear parameter varying technique," *Proceedings of the Institution of Mechanical Engineers, Part D: Journal of Automobile Engineering*, vol. 226, no. 2, pp. 210–224, February 2012.

[57] M. Hilsch, J. Lunze, R. Nitsche, and T. Arndt, "Fault-tolerant internal model control of a diesel engine air path," in *Proceedings of the 6th IFAC Symposium on Advances in Automotive Control, Munich, Germany*, 2010, pp. 572–577.

[58] P. Kotman, M. Bitzer, and A. Kugi, "Flatness-based feedforward control of a diesel engine air system with EGR," in *Proceedings of the 6th IFAC Symposium on Advances in Automotive Control, Munich, Germany*, 2010, pp. 598–603.

[59] P. Kotman, M. Bitzer, and A. Kugi, "Flatness-based feedforward control of a two-stage turbocharged diesel air system with EGR," in *Proceedings of the 2010 IEEE International Conference on Control Applications, Yokohama, Japan*, 2010, pp. 979–984.

[60] Y.-Y. Wang, I. Haskara, and O. Yaniv, "Quantitative feedback design of air and boost pressure control system for turbocharged diesel

engines," *Control Engineering Practice*, vol. 19, no. 6, pp. 626–637, June 2011.

[61] P. Ortner and L. del Re, "Predictive control of a diesel engine air path," *IEEE Transactions on Control Systems Technology*, vol. 15, no. 3, pp. 449–456, May 2007.

[62] H. J. Ferreau, P. Ortner, P. Langthaler, L. Del Re, and M. Diehl, "Predictive control of a real-world diesel engine using an extended online active set strategy," *Annual Reviews in Control*, vol. 31, no. 2, pp. 293–301, 2007.

[63] G. Stewart and F. Borrelli, "A model predictive control framework for industrial turbodiesel engine control," in *Proceedings of the 47th IEEE Conference on Decision and Control, Cancun, Mexico*, December 2008, pp. 5704–5711.

[64] M. Karlsson, K. Ekholm, P. Strandh, R. Johansson, and P. Tunestål, "Multiple-input multiple-output model predictive control of a diesel engine," in *Proceedings of the 6th IFAC Symposium on Advances in Automotive Control, Munich, Germany*, 2010, pp. 131–136.

[65] M. Herceg, T. Raff, R. Findeisen, and F. Allgöwer, "Nonlinear model predictive control of a turbocharged diesel engine," in *Proceedings of the 2006 IEEE International Conference on Control Applications, Munich, Germany*, October 2006, pp. 2766–2771.

[66] A. Murilo, M. Alamir, and P. Ortner, "Experimental validation of a parameterized NMPC for a diesel engine," in *Proceedings of the 2009 IFAC Workshop on Engine and Powertrain Control, Simulation and Modeling, Paris, France*, 2009, pp. 175–182.

[67] G. Zamboni and M. Capobianco, "Experimental study on the effects of HP and LP EGR in an automotive turbocharged diesel engine," *Applied Energy*, vol. 94, pp. 117–128, June 2012.

[68] F. Chiara, M. Canova, and Y.-Y. Wang, "An exhaust manifold pressure estimator for a two-stage turbocharged diesel engine," in *Proceedings of the 2011 American Control Conference, San Francisco, CA*, 2011, pp. 1549–1554.

[69] A. Stotsky and I. Kolmanovsky, "Application of input estimation techniques to charge estimation and control in automotive engines," *Control Engineering Practice*, vol. 10, no. 12, pp. 1371–1383, December 2002.

[70] L. Guzzella, *Analysis and Synthesis of Single-Input Single-Output Control Systems*, 3rd ed. vdf Hochschulverlag, 2011.

[71] J. Doyle and G. Stein, "Multivariable feedback design: Concepts for a classical/modern synthesis," *IEEE Transactions on Automatic Control*, vol. 26, no. 1, pp. 4–16, February 1981.

[72] P. Apkarian, P. Gahinet, and G. Becker, "Self-scheduled H_∞ control of linear parameter-varying systems: A design example." *Automatica*, vol. 31, no. 9, pp. 1251–1261, September 1995.

[73] T. Eidenböck, K. Mayr, W. Neuhauser, and P. Staub, "Der neue Sechszylinder-Dieselmotor von BMW mit drei Turboladern – Teil 1: Triebwerk und Aufladesystem," *MTZ – Motortechnische Zeitschrift*, vol. 73, no. 10, pp. 754–760, October 2012.

[74] J. Chauvin, N. Petit, P. Rouchon, G. Corde, and C. Vigild, "Air path estimation on diesel HCCI engine," in *SAE Technical Paper 2006-01-1085*, 2006.

[75] H. P. Geering, *Optimal Control with Engineering Applications.* Springer, 2007.

[76] D. P. Bertsekas, *Dynamic Programming and Optimal Control*, 3rd ed. Athena Scientific, 2005.

[77] M. Grahn, "Model-based diesel engine management system optimization – A strategy for transient engine operation," Ph.D. dissertation, Chalmers University of Technology, 2013.

[78] M. Benz, M. Hehn, C. H. Onder, and L. Guzzella, "Model-based actuator trajectories optimization for a diesel engine using a direct method," *Journal of Engineering for Gas Turbines and Power*, vol. 133, no. 3, pp. 032 806–1 – 032 806–11, March 2011.

[79] I. Kolmanovsky, M. Van Nieuwstadt, and J. Sun, "Optimization of complex powertrain systems for fuel economy and emissions," in

Proceedings of the 1999 IEEE International Conference on Control Applications, Kohala Coast, HI, vol. 1, 1999, pp. 833–839.

[80] R. Cloudt and F. Willems, "Integrated emission management strategy for cost-optimal engine-aftertreatment operation," in *SAE Technical paper 2011-01-1310*, 2011.

[81] M. Hafner, M. Schüler, O. Nelles, and R. Isermann, "Fast neural networks for diesel engine control design," *Control Engineering Practice*, vol. 8, no. 11, pp. 1211–1221, November 2000.

[82] C. M. Schär, C. H. Onder, H. P. Geering, and M. Elsener, "Control-oriented model of an SCR catalytic converter system," in *SAE Technical paper 2004-01-0153*, 2004.

[83] M. Devarakonda, G. Parker, J. H. Johnson, V. Strots, and S. Santhanam, "Adequacy of reduced order models for model-based control in a urea-SCR aftertreatment system," in *SAE Technical paper 2008-01-0617*, 2008.

[84] S. Boyd and L. Vandenberghe, *Convex Optimization.* New York, NY: Cambridge University Press, 2004.

[85] A. Bemporad, M. Morari, and N. L. Ricker, *Model predictive control toolbox – User's guide*, Mathworks.

[86] D. Ambühl, "Energy management strategies for hybrid electric vehicles," Ph.D. dissertation, ETH Zurich, no. 18435, 2009.

[87] A. Sciarretta and L. Guzzella, "Control of hybrid electric vehicles," *IEEE Control Systems Magazine*, vol. 27, no. 2, pp. 60–70, April 2007.

[88] D. Ambühl and L. Guzzella, "Predictive reference signal generator for hybrid electric vehicles," *IEEE Transactions on Vehicular Technology*, vol. 58, no. 9, pp. 4730–4740, November 2009.

[89] V. H. Johnson, K. B. Wipke, and D. J. Rausen, "HEV control strategy for real-time optimization of fuel economy and emissions," in *SAE Technical paper 2000-01-1543*, 2000.

[90] C.-C. Lin, H. Peng, J. W. Grizzle, and J.-M. Kang, "Power management strategy for a parallel hybrid electric truck," *IEEE Transactions on Control Systems Technology*, vol. 11, no. 6, pp. 839–849, November 2003.

[91] C.-C. Lin, H. Peng, and J. W. Grizzle, "A stochastic control strategy for hybrid electric vehicles," in *Proceedings of the 2004 American Control Conference, Boston, MA*, vol. 5, 2004, pp. 4710–4715.

[92] C. Musardo, B. Staccia, S. Midlam-Mohler, Y. Guezennec, and G. Rizzoni, "Supervisory control for NO_x reduction of an HEV with a mixed-mode HCCI/CIDI engine," in *Proceedings of the 2005 American Control Conference, Portland, OR*, vol. 6, 2005, pp. 3877–3881.

[93] G.-Q. Ao, J.-X. Qiang, H. Zhong, X.-J. Mao, L. Yang, and B. Zhuo, "Fuel economy and NO_x emission potential investigation and trade-off of a hybrid electric vehicle based on dynamic programming," *Proceedings of the Institution of Mechanical Engineers, Part D: Journal of Automobile Engineering*, vol. 222, no. 10, pp. 1851–1864, October 2008.

[94] H. Sagha, S. Farhangi, and B. Asaei, "Modeling and design of a NO_x emission reduction strategy for lightweight hybrid electric vehicles," in *Proceedings of the 35th Annual Conference of IEEE on Industrial Electronics, Porto, Portugal*, 2009, pp. 334–339.

[95] F. Willems, S. Spronkmans, and J. Kessels, "Integrated powertrain control to meet low CO_2 emissions for a hybrid distribution truck with SCR-denox system," in *Proceedings of the ASME 2011 Dynamic Systems and Control Conference, Arlington, VA*, 2011, pp. 907–912.

[96] R. Johri, A. Salvi, and Z. Filipi, "Optimal energy management for a hybrid vehicle using neuro-dynamic programming to consider transient engine operation," in *Proceedings of the ASME 2011 Dynamic Systems and Control Conference, Arlington, VA*, 2011, pp. 279–286.

[97] O. Grondin, L. Thibault, P. Moulin, A. Chasse, and A. Sciarretta, "Energy management strategy for diesel hybrid electric vehicle," in *Proceedings of the 2011 IEEE Vehicle Power and Propulsion Conference, Chicago, IL*, 2011, pp. 1–8.

[98] T. Nüesch, M. Wang, C. Voser, and L. Guzzella, "Optimal energy management and sizing for hybrid electric vehicles considering transient emissions," in *Proceedings of the 2012 IFAC Workshop on Engine and Powertrain Control, Simulation and Modeling, Paris, France*, 2012, pp. 278–285.

[99] F. Millo, C. V. Ferraro, and L. Rolando, "Analysis of different control strategies for the simultaneous reduction of CO_2 and NO_x emissions of a diesel hybrid passenger car," *International Journal of Vehicle Design*, vol. 58, no. 2–4, pp. 427–448, June 2012.

[100] L. Serrao, A. Sciarretta, O. Grondin, A. Chasse, Y. Creff, D. Di Domenico, P. Pognant-Gros, C. Querel, and L. Thibault, "Open issues in supervisory control of hybrid electric vehicles: A unified approach using optimal control methods," *Oil Gas Sci. Technol. – Rev. IFP Energies nouvelles*, vol. 68, no. 1, pp. 23–33, January-February 2013.

[101] J. Asprion, O. Chinellato, and L. Guzzella, "Optimisation-oriented modelling of the NO_x emissions of a Diesel engine," *Energy Conversion and Management*, vol. 75, pp. 61–73, November 2013.

Curriculum Vitae

Personal data

Name	Stephan Zentner
Date of birth	January 10, 1983
Place of birth	Tübingen, Germany
Nationality	German

Education

2009 – 2014	Doctoral student and teaching assistant at the Institute for Dynamic Systems and Control, Department of Mechanical and Process Engineering, ETH Zurich
2007 – 2009	MSc ETH in Mechanical Engineering degree at the Department of Mechanical and Process Engineering, ETH Zurich
2003 – 2006	BSc ETH in Mechanical Engineering degree at the Department of Mechanical and Process Engineering, ETH Zurich
2002 – 2003	Social service at Deutsches Rotes Kreuz Kreisverband Tübingen e.V., Germany
1993 – 2002	Wildermuth-Gymnasium Tübingen, Germany

Journal articles

- S. Zentner, E. Schäfer, G. Fast, C. H. Onder, and L. Guzzella, "A cascaded control structure for air-path control of diesel engines," *Proceedings of the Institution of Mechanical Engineers, Part D: Journal of Automobile Engineering, available online*, 2014
- S. Zentner, J. Asprion, C. Onder, and L. Guzzella, "An equivalent emission minimization strategy for causal optimal control of diesel engines," *Energies*, vol. 7, no. 3, pp. 1230–1250, March 2014
- F. Tschanz, S. Zentner, C. H. Onder, and L. Guzzella, "Cascaded control of combustion and pollutant emissions in diesel engines," *Control Engineering Practice, available online*, 2014

Conference articles

- S. Zentner, E. Schäfer, C. Onder, and L. Guzzella, "Model-based injection and EGR adaptation and its impact on transient emissions and drivability of a diesel engine," in *Proceedings of the 7th IFAC Symposium on Advances in Automotive Control, Tokyo, Japan*, 2013, pp. 89–94
- E. Schäfer, S. Zentner, and G. Fast, "Model-based development of a multi-variable control strategy for large diesel engines," in *Proceedings of the 6th Emission Control Conference, Dresden, Germany*, 2012
- F. Tschanz, S. Zentner, E. Özatay, C. H. Onder, and L. Guzzella, "Cascaded multivariable control of the combustion in diesel engines," in *Proceedings of the 2012 IFAC Workshop on Engine and Powertrain Control, Simulation and Modeling, Paris, France*, 2012, pp. 25–32
- J. Asprion, G. Mancini, S. Zentner, C. H. Onder, N. Cavina, and L. Guzzella, "A framework for the iterative dynamic optimisation of diesel engines: numerical methods, experimental setup, and first results," in *WIT Transactions on Ecology and the Environment*, C. Brebbia, E. Magaril, and M. Khodorovsky, Eds. WIT Press, Southampton, 2014, vol. 190

Patents

- E. Schäfer, T. Kreissig, G. Fast, S. Zentner, L. Guzzella, and C. Onder, "Method and device for operating an internal combustion engine with supercharging and exhaust-gas recirculation," Patent Nr. WO/2013/159899, October 2013